The Pennsylvania State University

The Graduate School

College of Engineering

FATIGUE OF CORD-RUBBER COMPOSITES FOR TIRES

A Thesis in

Engineering Science and Mechanics

by

Jaehoon Song

Submitted in Partial Fulfillment
of the Requirements
for the Degree of

Doctor of Philosophy

May 2004

The thesis of Jaehoon Song was reviewed and approved* by the following:

F. Costanzo
Associate Professor of Engineering Science and Mechanics
Thesis Co-Advisor
Chair of Committee

A. E. Segall
Associate Professor of Engineering Science and Mechanics
Thesis Co-Advisor

B. R. Tittmann
Schell Professor of Engineering Science and Mechanics

M. F. Amateau
Professor of Engineering Science and Mechanics

G. A. Lesieutre
Professor of Aerospace Engineering

J. A. Todd
Professor of Engineering Science and Mechanics
P. B. Breneman Department Head Chair of Engineering Science and Mechanics

*Signatures are on file in the Graduate School.

ABSTRACT

Fatigue behaviors of cord-rubber composite materials forming the *belt* region of radial pneumatic tires have been characterized to assess their dependence on *stress*, *strain* and *temperature history* as well as *materials composition and construction*. Using actual tires, it was found that interply shear strain is one of the crucial parameters for damage assessment from the result that higher levels of interply shear strain of actual tires reduce the fatigue lifetime. Estimated at various levels of load amplitude were the fatigue life, the extent and rate of resultant strain increase ("dynamic creep"), cyclic strains at failure, and specimen temperature. The interply shear strain of 2-ply 'tire belt' composite laminate under circumferential tension was affected by twisting of specimen due to tension-bending coupling. However, a critical level of interply shear strain, which governs the gross failure of composite laminate due to the delamination, appeared to be independent of different lay-up of 2-ply vs. symmetric 4-ply configuration. Reflecting their matrix-dominated failure modes such as cord-matrix debonding and delamination, composite laminates with different cord reinforcements showed the same S-N relationship as long as they were constructed with the same rubber matrix, the same cord angle, similar cord volume, and the same ply lay-up. Because of much *lower* values of *single cycle strength* (in terms of gross fracture load per unit width), the composite laminates with larger cord angle and the 2-ply laminates exhibited exponentially shorter fatigue lifetime, at a given stress amplitude, than the composite laminates with smaller cord angle and 4-ply symmetric laminates, respectively. The increase of interply rubber thickness lengthens their fatigue lifetime at an intermediate level of stress amplitude.

However, the increase in the fatigue lifetime of the composite laminate becomes less noticeable at very low stress amplitude. Even with small compressive cyclic stresses, the fatigue life of belt composites is predominantly influenced by the magnitude of maximum stress. Maximum cyclic strain of composite laminates at failure, which measures the total strain accumulation for gross failure, was independent of stress amplitude and close to the level of static failure strain. For all composite laminates under study, a linear correlation could be established between the temperature rise rate and dynamic creep rate which was, in turn, inversely proportional to the fatigue lifetime. Using the acoustic emission (AE) initiation stress value, better prediction of fatigue life was available for the fiber-reinforced composites having fatigue limit. The accumulation rate of AE activities during cyclic loading was linearly proportional to the maximum applied load and to the inverse of the fatigue life of cord-rubber composite laminates. Finally, a modified fatigue modulus model based on combination of power-law and logarithmic relation was proposed to predict the fatigue lifetime profile of cord-rubber composite laminates.

Table of Contents

LIST OF FIGURES

LIST OF TABLES

ACKNOWLEDGEMENTS

The author would like to thank the following people who have been instrumental in the progression of this dissertation:

- Dr. Francesco Costanzo for presenting problems to me, and allowing me the freedom to work on many of them at the same time, often with little or no progress.
- Dr. Albert E. Segall for his helpful input and advice during the generation of this dissertation.
- Drs. Bernhard R. Tittmann, Maurice F. Amateau, and George A. Lesieutre for their constant supports and critical reviews of my work.
- Pirelli Pneumatici, S.P.A., Dr. Almonacil Celine and Dr. Syed K. Mowdood for supplying the cord-rubber composite material for this study, in addition to financial support.
- National Highway Traffic Safety Administration (NHTSA) for supplying the actual tires for this work.
- Dr. Byung-Lip (Les) Lee for giving me a start in research and, more importantly, his friendship throughout the years I have known him.
- Han-Soon Cho and Cheol-Hun Song: My parents. I would not be here now without your sacrifice and love. Thank you!
- Kyung-Ah (Gia) Shin: My wife. Your motivation and support are without words.
- Sungho, Yerin (Julie), and David Minho Song: My kids. This research would not have been possible without your love and faith.

Chapter 1

INTRODUCTION

1.1 Background

Compared with other load-carrying structures, pneumatic tires are subjected to extreme loading conditions of high cyclic frequency and large deflections (Bono, 1988; Gough, 1982). As confirmed by field experience, such as the massive recall of Firestone tires which were involved in accidents with more than 250 people killed and hundreds more injured (New York Times, 2002), these combinations can cause fatigue damage in critical regions of tires which may eventually develop into catastrophic failures of whole tires. In the radial tires used for passenger vehicles, trucks, or aircraft, the most critical regions for fatigue damage and failures are reported to be the edge of working belts and around the endings of carcass ply near the bead (Figure 1.1).

As can be seen in Figures 1.2 and 1.3, the belt-leaving-belt tread separations begin as belt-edge separation at the edge of the second belt (NHTSA, 2001; Popper et al., 1986). This is the area of highest strain in a steel belted radial tire, primarily due to the structural discontinuity created by the abrupt change in modulus from steel to rubber. It is also a region with relatively poor cord-to-rubber adhesion because bare steel is exposed at the cut ends of the cords. The crack growth characteristics of the belt rubber evolve over time from the effects of aging.

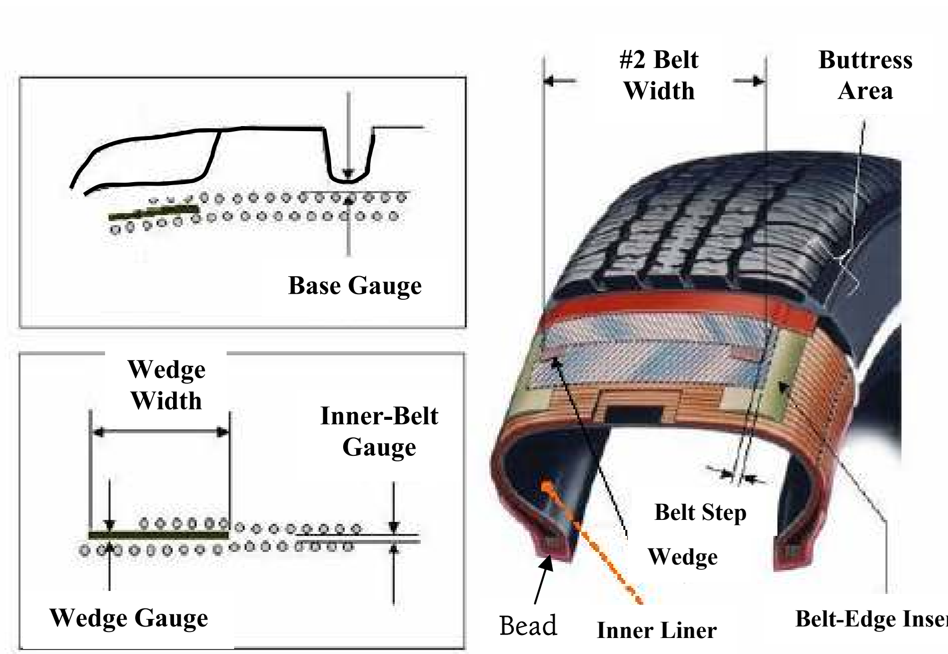

Figure 1.1 Radial tire construction (NHTSA, 2001)

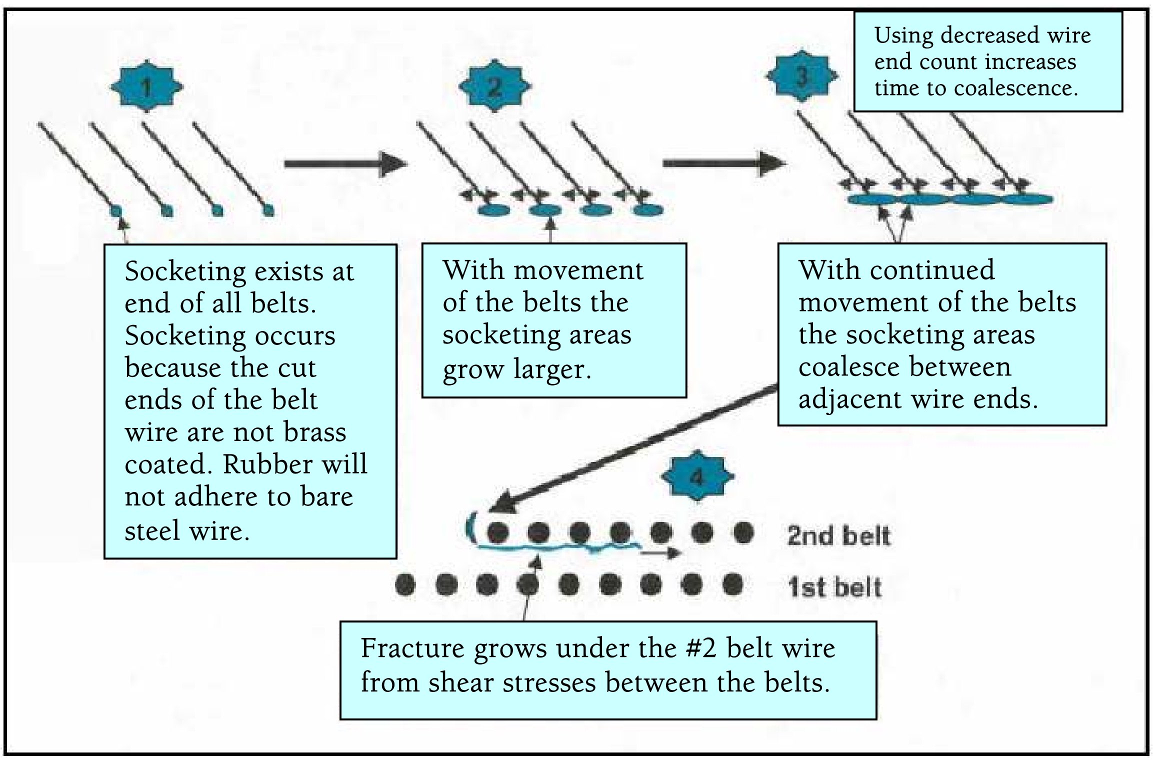

Figure 1.2 Belt-leaving-belt failure mechanism of actual tires (NHTSA, 2001)

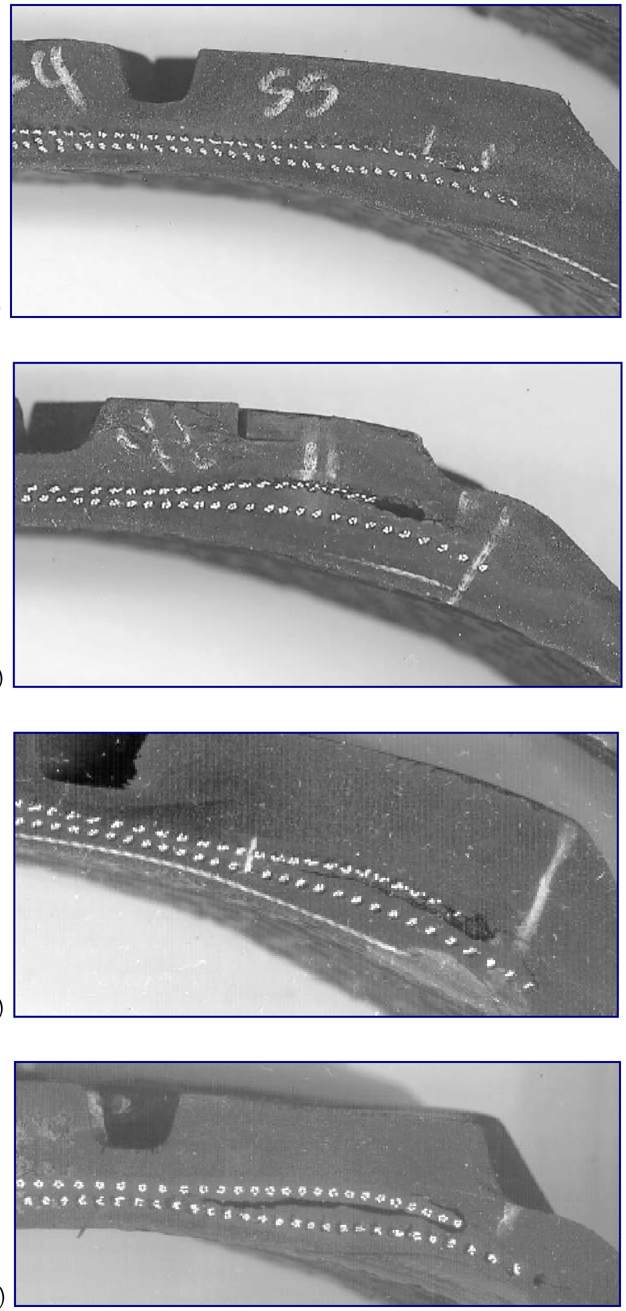

(a)

(b)

(c)

(d)

Figure 1.3 Separation progression patterns of Belt-leaving-belt failure: (a) single cord end (b) incipient separation (socketing) (c) lateral crack growth (d) accelerated crack growth (pockets) (NHTSA, 2001)

There are many factors controlling this evolution, including base operating temperature, oxygen content, compound type, usage conditions, and manufacturing variance. The strain state of the belt rubber is determined by various factors, including tire design, belt design, manufacturing variance, and usage conditions. Product life may be lengthened by design of the laminate construction to reduce the strain energy release rate. For example, the use of a belt edge filler element which increases the interply laminate distance at the edges may be useful in reducing the strain-energy density locally at the cord ends (Figure 1.1), thus suppressing the initiation and retarding propagation of the penny-shaped cracks (Huang and Yeoh, 1989). Once belt-edge separations have initiated, they can grow circumferentially and laterally along the edge of the second belt and develop into cracks growing between the belts. Such cracks can form areas of separation at one or more locations around the circumference of the tire. The rate of crack propagation, and the size of separation at which catastrophic belt-leaving-belt failure can occur, are dependent on the evolved (i.e., aged) state of the belt rubber. The areas of separation develop in crescent, or semi-elliptical, shaped patterns at various locations around one or both shoulders of the tire. If they grow large enough, they can result in catastrophic tread detachment (Figure 1.4), particularly at high speeds, when the centrifugal forces acting on the tire are greatest.

Distinct from ply separation, the so-called *ply ending separation* also involves crack propagation in the rubber matrix around the carcass ply endings. The process of damage accumulation in the belt-edge and carcass ply ending regions is attributed to a combination of localized mechanical overloading and heat generation along with the resultant deterioration of the constituent materials.

(a)

(b)

Figure 1.4 Belt-leaving-belt failure pattern of a failed tire; (a) on the tire carcass (b) on the tread (NHTSA, 2001)

As discussed so far, a basic understanding of tire failure mechanisms exists at least in a qualitative sense. However, the tasks of quantifying critical operating conditions such as speed, load, underinflation, and tire deflection responsible for the fatigue failures and predicting the useful life expectancy of a passenger, truck, or aircraft tire in a quantitative manner remains daunting. Accelerated testing using *dynamometers* provides a valuable means of evaluating the structural durability and life expectancy of the tires. However, it is too costly to rely exclusively on dynamometer test results for specifying the mileage or critical speed a tire may endure before replacement. The problem of cost-effectiveness involving dynamometer tests is further compounded when new materials have to be evaluated such as new matrices and/or reinforcements for tires. Moreover, the results of dynamometer tests merely reflect the sensitivity of each tire design and construction to a specific combination of test conditions, but they do not allow for the identification of the underlying mechanisms of material property degradation and damage accumulation.

In addition to the dynamometer tests just discussed, the property degradation profile of tire materials can be assessed by utilizing coupon specimens cut from the critical regions (Popper et al., 1986; Clark, 1986). This type of durability analysis provides useful information on failures caused by the deterioration of material properties. Some estimates may assume that tire failure occurs at a certain percentage reduction in strength of material elements. However, the validation of such hypothesis requires an understanding of how the deterioration of material properties leads to fatigue damage accumulation and eventual structural failure of tires.

1.2 Objectives

This research program will investigate and measure the response of angle-plied cord-rubber composite specimens as a way to study degradation and failure mechanisms in the *belt* region of radial truck tires. Specifically, the objectives of this project are:

(a) to characterize and model the dependence of fatigue lifetime of composites on *stress*, *strain* and *temperature history*;

(b) to investigate the mechanisms of local damage accumulation, material property degradation and structural failure;

(c) to establish the measurement of local strain change, heat generation and acoustic emission (AE) as a viable experimental technique for real-time monitoring of the damage accumulation process; and

(d) to establish an empirical model for the prediction of fatigue life for cord-rubber composites.

1.3 Literature Review

The mechanics of fatigue and related failures of composite laminates are complicated and quite different from those of isotropic materials. Compared with composite materials with rigid matrices, a relatively limited amount of research has been reported on the fatigue behavior and fracture mechanisms of cord-rubber composites. A comprehensive literature review of composite materials and tires is now presented, and it is organized in the following fashion:

(a) Deformation of cord-rubber composites;

(b) Failure of cord-rubber composites;

(c) Cumulative fatigue damage and life prediction of fiber-reinforced composites; and

(d) Acoustic emission behavior during fatigue loading.

1.3.1 Deformation of Cord-Rubber Composites

The cord-rubber composite is a common laboratory specimen for the study of the tire belt region because it resembles the structural belts of a tire, as well as conveyer belts and other similar systems. Comprehensive research into the stress-strain response of cord-rubber composites has been conducted by a number of investigators (Patel et al., 1976; Walter, 1978; Vorachek, 1979; Kumar and Berk, 1982; Tabaddor, 1985; Pidaparti, 1992). In these studies, there has been a keen interest in the application of analytical techniques to predict the stress-strain response of the cord-rubber composite as a structural component of pneumatic tires. Unfortunately, modeling the nonlinear, viscoelastic, heterogeneous, and anisotropic characteristics of cord-rubber composites is very difficult. However, within certain limitations, it was found that the use of a linear-elastic, homogeneous, orthotropic material model for these composites is acceptable (Patel et al., 1976; Walter, 1978; Vorachek, 1979), with theoretical predictions of elastic moduli of unidirectional lamina of cord-rubber composite showing a reasonable agreement with experimental data.

In the case of angle-plied cord-rubber composite laminates, the primary concerns were interply shear deformation as well as axial stress-strain response. In particular, interply shear deformation, which eventually leads to delamination type failure, was extensively analyzed by investigators such as Pipes and Pagano (1970), Lou and Walter (1979), Breidenbach and Lake (1979, 1981), Stalnaker et al. (1980), Ford et al. (1982), Deeskinazi and Cembrola (1984), and Cembrola and Dudek (1985). These studies have shown that interply shear strain develops in any composite laminate consisting of opposite-angle plies. Upon extension, the constituent plies exhibit in-plane shear deformation of opposite direction with a tendency toward an increase of reinforcement angle. However, this action is prevented by mutual constraint due to interply bonding (Figures 1.5 and 1.6). For composites with relatively rigid matrices, Pipes and Pagano (1970) used classical elasticity theory to describe the interlaminar behavior of a symmetric angle-plied laminate under uniform axial extension. Finite-difference solution techniques were employed to estimate stresses and displacements throughout the region. Results indicated that significant interlaminar shear-stresses are required to allow shear transfer between the layers of the laminate and high stresses in the neighborhood of the free edge cause delamination of the laminate, in particular under fatigue loadings.

In addition to measuring the axial modulus and Poisson's ratio, Walter (1978) and Lou and Walter (1979) experimentally determined the variation of interply shear strain with cord angle for nylon cord-rubber composite laminate (Figure 1.7). Furthermore, these researchers expanded the stress-strain equations of the classical laminated plate theory to accommodate interply shear-strain. Stalnaker et al. (1980) developed an effective finite-element model to simulate the experimentally measured response. This modeling included the interply shear-strain effect, by treating the composite structure as a torsional axi-symmetric layered cylinder. The predicted circumferential deformation in the axi-symmetric hoop agreed well with experimentally measured axial deformation in the flat laminate. In follow-up work, Ford et al. (1982) developed a straight pin-test technique to allow visualization of interlaminar shear strain in both cord-rubber composite laminates and radial tire belts (Figure 1.8).

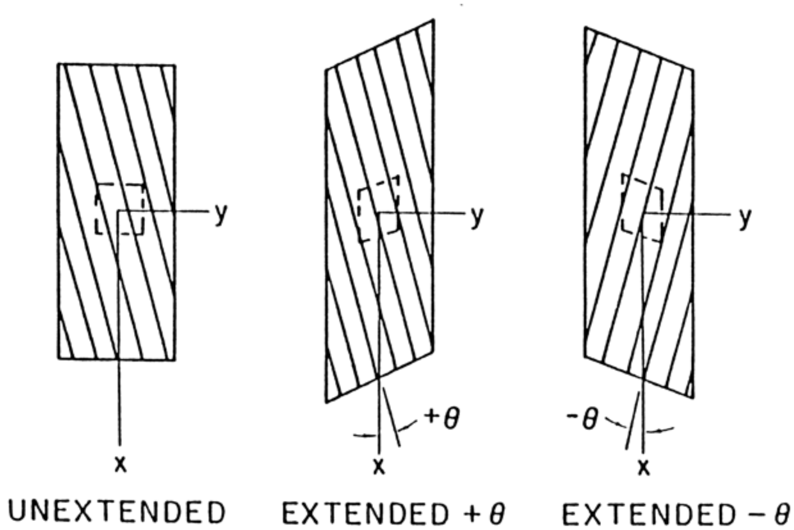

Figure 1.5 Single-ply shear-coupling behavior of actual cord-rubber specimens

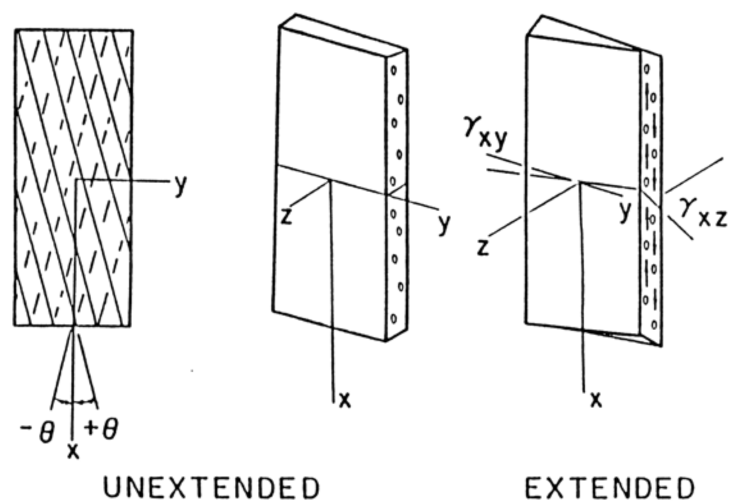

Figure 1.6 Behavior of two-ply $\pm\theta$ laminate under uniaxial tensile loading (Stalnaker et al., 1980)

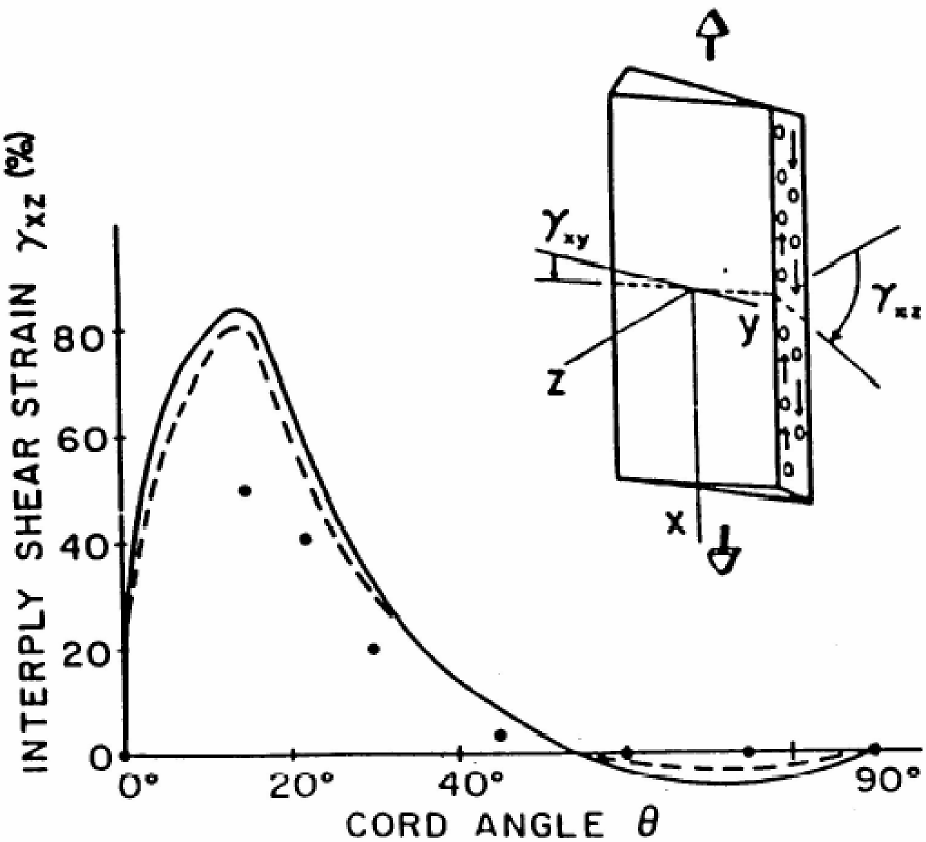

Figure 1.7 Comparison between theoretically predicted (—, ---) and experimentally measured (●) values of interply shear strain γ_{xz} as a function of cord angle $\boldsymbol{\theta}$ for two-ply 110/2 polyester-rubber laminates at 10% specimen extension (Walter, 1978)

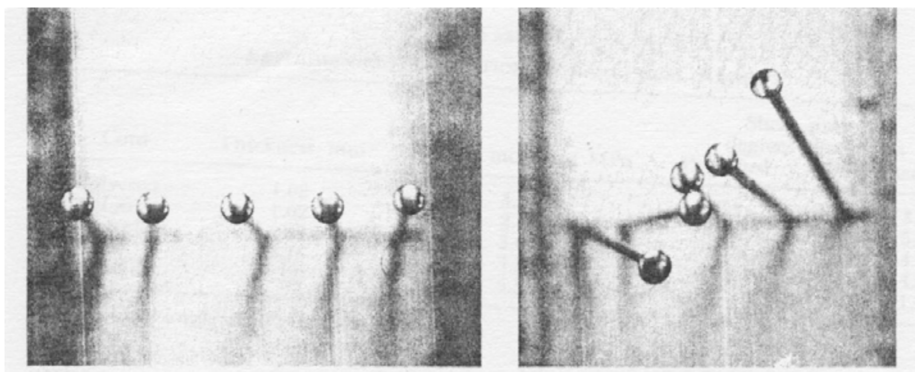

Figure 1.8 Illustration of interply shear strains using the pin test; before (a) and after (b) inflation (Deeskinazi and Cembrola, 1983)

In particular, Ford et al. (1982) used the standard pin test to measure interlaminar shear deformation patterns and successfully verified the results using finite element analyses.

Later, Deeskinazi and Cembrola (1984) studied the effect of different design variables used in the construction of tire belts on the interply shear strain using a belted cylinder structure. The authors found that the belt cord angle, interply rubber thickness, modulus of the interply rubber, and belt width all had a very strong influence on interply shear. Finally, Cembrola and Dudek (1985) developed a finite element model which included an interply rubber layer to account for the interlaminar shear deformation. The results of the finite element analysis based on a three-layer model showed excellent agreement with experimental data for cord angles greater than 10°.

1.3.2 Failure of Cord-Rubber Composites

In general, failure modes of composites materials are complicated and markedly different from those of homogeneous and isotropic materials. For instance, fiber-matrix debonding, matrix cracking, and fiber fracture are commonly observed in fiber-reinforced composites with relatively rigid matrices. In addition to the above failure modes, delamination is often observed in composite laminates. The initiation and propagation of local damage in angle-plied cord-rubber composite laminates was first investigated in detail by Breidenbach and Lake (1979). Their composite laminate system contained two layers of symmetrically disposed nylon cords. Using a model cord-rubber composite with exposed cords, Breidenbach and Lake examined the mechanics of propagation of interply cracks. The researchers assumed that the initiation process, during which an interply crack was formed, was relatively short and excluded the process from their study. The specimens were partitioned into three deformation regions: a central region where deformations were relatively uniform and approximately obeyed a pantographic model, and two regions along the free edges where deformations varied in a complex manner. In these edge regions, shear-strains up to 1000% can occur due to an overall extension of roughly 5%. These high shear strains created stress concentrations at the edge and eventually lead to the initiation of penny-shaped cracks at the cord ends. Local damage induced in the form of cord-matrix debonding around the cut ends of cords was referred to as "socketing". Under continued loading, a damage zone was developed from the socketing sites along the edge. These damage zones were observed to propagate between the plies both along the length and across the width of a laminate. It was found that the interply cracks propagated until delamination aroused and led to laminate's failure. The same sequence of fatigue failure modes was observed by Lee et al. (1990, 1993a, 1993b, 1994, 1998, 2000), Liu and Lee (1996), Ku (1996), and Ku et al. (1998) for various types of cord-rubber composite laminate reinforced with steel wire, as well as nylon cord at a range of reinforcement angle from ±19° to ±38°.

The initiation of penny shaped cracks has been investigated by Gent et al. (1981) and Huang and Yeoh (1988). Gent et al. (1981) assumed that the energy necessary to create a penny shaped crack needed to be greater than the sum of the energy required to fracture the cord-rubber interface and any increase in the strain energy of the rubber itself. Deformation in the cord was assumed to be negligible. Huang and Yeoh (1988), knowing that the two plies in a cord-rubber composite are rarely identical, demonstrated that cracks typically developed in the narrower ply. Huang and Yeoh (1988) also showed that the fatigue life of the composite was a linearly decreasing function of the dynamic amplitude, load and maximum interlaminar shear strain. Additional research into cord-rubber composites has focused on finite-element modeling of the structure to determine areas of high stress concentration and to model the three-dimensional dynamic response of the composite (Pidaparti, 1996; Pidaparti and Liu, 1996; Martin, 2000).

1.3.3 Fatigue Damage and Life Prediction of Fiber-Reinforced Composites

The prediction of fatigue damage and fatigue life for composite materials has been the subject of many investigations during the last three decades. In fact, the very definition of "cumulative damage" is a very complicated problem for fiber-reinforced composites in general. Both static and dynamic loadings contribute to the accumulation of damage in these heterogeneous materials in the form of fiber-matrix debonding, matrix cracking, delamination, and fiber fracture. Although one can disregard fiber fracture while studying the failure of angle-plied fiber-reinforced composite laminates, the task of defining matrix-dominated damage is still complicated. In this situation, one must deal with the number of debonding sites, crack lengths, crack density, delamination length, and delamination width as damage parameters. These types of damage can be detected through microscopy and other non-destructive testing (NDT) methods.

Numerous experimental techniques have been developed to detect and monitor fatigue damage in composites. For instance, Chang and co-workers (1976) observed the damage initiation and growth followed by structural failure of graphite fiber-reinforced epoxy composite laminates from a sequence of X-ray pictures recorded during testing. Using more conventional means, Qwen and Howe (1972) observed the development of damage at several sites of the polished edge of a chopped, glass-fiber matrix-reinforced polyester resin composite during tensile fatigue loading. Kaczmarek (1995) used ultrasonic technique to measure matrix crack density and delamination size in carbon fiber-reinforced epoxy resin composites.

The observed accumulation of fatigue damage in composites depends on the applied stress level, frequency, number of fatigue cycles, etc. Originally, a number of cumulative damage theories developed for metals were applied to the case of fiber-reinforced composites to describe the relative importance of stress interactions and the amount of damage induced under fatigue loading. The first example was the use of Palmgren-Miner's linear damage rule (1945) in Broutman et al's work (1972) for glass-epoxy composites. In Palmgren-Miner's model, fatigue damage is defined as a ratio of the number of cycles under fatigue loading, n, to the number of cycles to failure, N. In this model, the amount of damage accumulation is independent of load sequence. However the experimental data generally contradicts the Palmgren-Miner's damage model. Hence, extensive efforts have been made to develop more accurate damage models.

Various theories proposed to characterize the damage state of metals and composite materials under fatigue loading were thoroughly reviewed by Hwang and Han (1986a). Hwang and Han proposed four requirements to establish a universal fatigue damage model:

a. The model should explain fatigue phenomena at an applied stress level.
b. The model should explain fatigue phenomena for an overall applied stress range.
    i. During a cycle at a high applied-stress level, the material should sustrain more damage than that caused by a low applied stress level.
    ii. If it is true that failure occurs at each maximum applied stress level, then the final damage (accumulated damage just before failure) at a

low applied stress level should be larger than that of a high applied stress level.

c. The model should incorporate multi-stress level fatigue phenomena.

d. It is desirable to establish the fatigue damage model without an S-N curve.

Hwang and Han also proposed three different damage models based on the resultant strain and introduced the term “fatigue modulus” to characterize this relation (Figure 1.9).

There are several empirical relations for predicting fatigue life such as Basquin’s relation (power law), straight line in S-N curve, and the Coffin and Manson’s relation. The S-N curve still appears to be the most popular method of characterizing the fatigue behavior of composite materials. While most empirical equations are based on the classical power law, one of the simpler equations used to describe the fatigue behavior of several composite materials is as follows:

$$\sigma_a = \sigma_0 - b \log N \tag{1.1}$$

where σ_a is the maximum applied stress, σ_o is the single cycle maximum stress, b is a positive constant, and N is the number of cycles to failure.

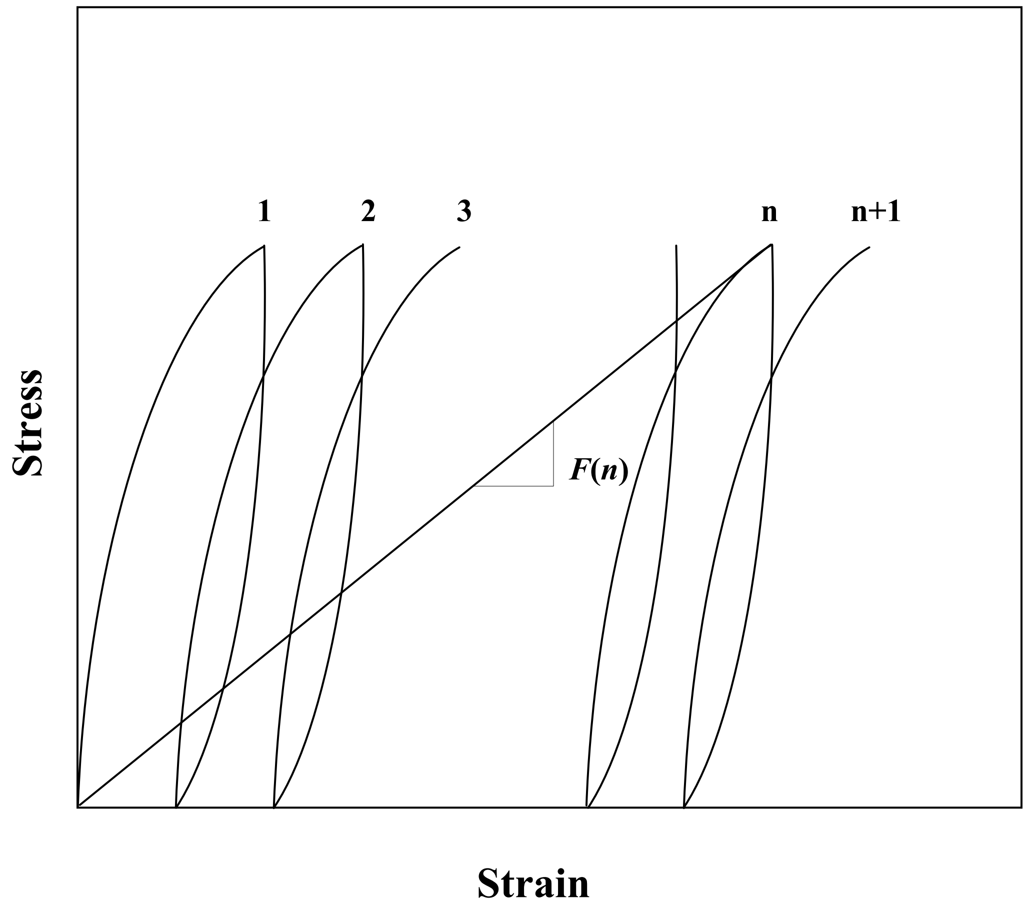

Figure 1.9 Definition of fatigue modulus, $F(n)$ (Hwang and Han, 1986b)

Other theories have been formulated for the characterization of the fatigue behavior of composite materials. There are three basic models used to predict fatigue life: residual strength degradation, modulus degradation, and damage tolerance approaches. An excellent review of work in this area of fatigue life predictions has been given by Liu and Lessard (1994). In addition to reviewing earlier models, they proposed an analytical approach for evaluating the growth of fatigue damage in terms of the fatigue life of general laminated composites containing 0° plies based on a minimum number of experimental measurements. According to Huston (1994), most of the life prediction methods for polymeric composite materials are based on the residual strength degradation. However, he suggested that theories for fatigue failure based on the reduction of stiffness have one significant advantage over the remaining strength theories: remaining life can be assessed by non-destructive techniques. In addition, Huston suggested that less testing is required for stiffness-degradation-based models.

One such analysis based upon stiffness degradation was proposed by Poursartip et al. (1982). In their analysis, it was assumed that the stiffness reduction could be related in a linear manner to the damage that was present due to fatigue. By making arguments based on the global stiffness reduction due to cracks in composite materials, they were able to linearly relate the measured stiffness reduction to damage. The damage parameter could then be integrated from its initial value to some final (critical) value using the experimentally measured stiffness reduction. Failure was predicted to occur at the point where the damage parameter reached the critical value.

In the residual strength degradation approach, fatigue failure is typically assumed to occur when the residual strength becomes equal to the applied maximum stress amplitude. Such an approach was used by Broutman and Sahu (1972) who were able to make predictions for the residual strengths of laminates subjected to two-stress level cumulative fatigue damages. Using this approach, the agreement between predicted and experimentally measured residual strengths for glass reinforced plastics (GRP) was found to be good.

Hashin and Rotem (1978) proposed a cumulative fatigue damage theory in which the damage during cyclic loading may be represented by the residual lifetime under subsequent constant amplitude cycling. The theory was based upon the concept of damage curve families which are defined in terms of residual lifetimes for two-stage loading. The damage in two components due to different histories was considered to be equivalent if it gave the same remaining life under subsequent loading at the same stress level. The researchers compared their analytical results to those of Miner's rule for multi-stage loading programs and found that there was considerable difference. In contrast, their results compared favorably to the experimental data obtained on both soft and hard steels.

In Hwang and Han's work (1986), the concept of fatigue modulus was further extended to derive a model which can predict the fatigue life of composites based on the resultant strain as follows:

$$N = [B(1-r)]^{1/c} \tag{1.2}$$

where r = the applied stress level/static tensile strength,
B is a material constant,
c is a material constant.

Using Equation (1.2), the fatigue life of materials, measured in terms of the number of load cycles N, can be predicted if the applied stress level/static tensile strength, r, material constants B and c are known. Hwang and Han successfully verified their theory by comparing the calculated values of fatigue life with experimental data for the case of glass-epoxy composite laminate. However, a realistic trend of fatigue lifetime profiles for the case of cord-rubber composite could not be predicted from Hwang and Han's equation even with the same minimum stress (Ku, 1996). Ku established two empirical models for the prediction of fatigue life using dynamic creep data of cord-rubber composites as follows:

$$N_f = \frac{\varepsilon_f - \varepsilon_0'}{a} \ , \tag{1.3}$$

$$N_f = \frac{\varepsilon_f - \varepsilon_0^*}{10^{\alpha}(\Delta\sigma)^{\beta}} \ , \tag{1.4}$$

where a is a dynamic creep rate in the steady state region, ε_0' extrapolated initial strain, ε^* strain in static unloading curve, $\Delta\sigma$ stress range, σ and β material constants.

In recent work, South (2001) predicted the fatigue lifetime of unaged and thermally aged 2-ply cord-rubber composite laminates using generated master curves and mechanical property data. The predictions were discretized into crack initiation and crack propagation phases. The crack initiation phase utilized a residual strength approach while the crack propagation phase employed a fracture mechanics approach.

In this project, and as will be discussed in Chapter 5, the fatigue life of cord-rubber composite laminates will be calculated by using the above equations (Hwang and Han, 1986; Ku, 1996) in conjunction with a modified model of fatigue failure based on fatigue modulus developed herein. The predicted results will be then compared with the experimentally measured lives.

1.3.4 Acoustic Emission Behavior during fatigue loading

The characteristic failure response of composites is different from that of metals under static as well as dynamic loads. Roughly speaking, metals exhibits one failure mode that typically consists of the nucleation and growth of a single dominant flaw. By contrast, composites exhibit a number of co-existing damage mechanisms such as fiber breaks, matrix cracking, delamination, and interface failure. Identification of these damage mechanisms and the study of their influence on residual properties becomes important for an economical and reliable engineering design. Real-time monitoring of damage accumulation processes becomes extremely helpful to this study due to the complex fatigue failure mechanisms of cord-rubber composite laminates. A particular feature of composites is that when they are subjected to mechanical loading, microcracks may develop long before the final failure of the structure (Bader et al., 1979). The effects of these microcracks, which are mainly due to matrix cracking, delamination and fiber breakage, are that the stiffness of the structure will decrease (Adolfsson and Gudmundson, 1995). Moreover, moisture or other chemicals may diffuse into the material and cause the structure to leak and/or trigger an earlier failure. It is therefore of great importance to have access to experimental methods which can assess the initiation and growth of these damage related processes. Within this context, the current investigation explored the use of acoustic emission (AE) analysis for real-time monitoring of the damage accumulation process in cord-rubber composite laminates.

Acoustic emissions are the result of elastic stress waves that travel through a material after a nonconservative event occurs. As confirmed in many different materials

(Pollock, 1988; Spanner, 1974), the source of AE is a sudden release of energy induced by microcracks, friction, plastic deformation, or other non-conservative events. AE monitoring involves the detection and conversion of these mechanical stress waves released by specific damage events in the material into electrical voltage signals by piezoelectric transducers that are mounted on the specimen surface. Signal amplification and electronic processing of these transmitted waves are then translated into an acoustic signature.

The damage accumulation under cyclic loading as well as static tensile loading is therefore characterized by AE often accompanied by sudden release of energy (Lenain, 1979). Past studies on various structural materials have shown that different failure modes generate distinctly different acoustic signatures (Rotem, 1979; Harris et al., 1979; Carsson and Norrbom, 1983; Ghorbel et al, 1991; Wevers et al., 1991; Ghaffari and Awerbush, 1991). Therefore, the use of AE analysis as a NDE tool for real-time monitoring of structural integrity could prove quite successful and valuable, particularly if the acoustic signature of the failure mode is known. However, scant research has been done with cord-rubber composite laminates using AE analysis (Gray and Summerscales, 1984; Lee and Hippo, 1991; Ku, 1996) even though it is a promising technique used for other structural materials such as metal and advanced fiber composites (Rotem, 1979; Harris et al., 1979; Carsson and Norrbom, 1983; Ghorbel et al, 1991; Wevers et al., 1991; Ghaffari and Awerbush, 1991). Interestingly, Ku (1996) observed that there is a clear trend showing that the fatigue life is linearly proportional to the AE increase rate.

Unfortunately, the use of AE for damage monitoring has several shortcomings that can limit its effectiveness. Since the AE transducer picks up surface elastic waves that were originated by the energy released from the defect zone, when the stress field is changed, it would be a straightforward assumption that the AE wave would carry all the information about its original source. However, the acoustic wave when propagating passes through many obstacles, which can alter its shape and frequency. The composite material is heterogeneous and nonisotropic, and therefore the propagation speed differs in different directions. Also, the layered media as well as the fiber-matrix interfaces cause some changes in the wave form. The coupling between the material surface and the transducer as well as the transducer response itself, also change the final output signal. Nevertheless, the information about the AE source is present in the transducer output signal, but the difficulty lies in canceling the interrupting effects. In addition, external sources of noise such as gripping and sliding may interfere with analysis and generally cannot be fully filtered. Often, a proper selection of the frequency range or threshold amplitude settings on the AE instrument will minimize unwanted information.

Nevertheless, the AE technique has been used to monitor damage processes during proof testing, and based on this AE data. Many thousands of fiberglass tanks and lift booms have been instpected and accepted or rejected based on the AE data (Fowler, 1984; Hamstad, 1986b). The reasons that lead to the usefulness of AE data for these purposes are:

a. real-time monitoring of damage processes as a function of changes in other variables (e.g., time and load level);

b. high sensitivity (e.g., individual filament fractures, individual filament debonding, as well as matrix cracking and delamination can all be monitored);

c. total volume sensitivity to the regions of the test sample which are stressed; and

d. location of regions in the sample in which damage is accumulating.

One of the four criteria used to accept or reject composite tanks is commonly called the Felicity ratio (FR) which is the ratio between the applied load at which the acoustic emission reappears during the next application of loading and the previous maximum applied load (Figure 1.10). Fowler (1977; 1979) was the first to introduce the term. Other researchers (e.g., Bunsell, 1977) had observed the same phenomenon and called it a violation of the Kaiser effect. The basic observation is that upon a successive load cycle to a sufficiently high load level, AE is observed to begin to occur at a load level that is less than the previous maximum load. This Felicity effect is quantified as the Felicity ratio. As can be clearly seen, a FR < 1 is directly related to damage and/or frictional processes on repeated load cycles to the same load level. Hull and Golaski (1980) studied the Felicity effect on glass/polymer filament-wound pipe loaded in two different modes. For hoop loading they found the FR was < 1 for all load levels. For combined hoop and axial loading the FR was ≥ 1 for low load levels and the FR was ≤ 1 at higher load levels. Fowler and Gray (1979) stated that the Felicity effect is a measure of the total amount of damage and that the effect is related to the redistribution of residual stresses during the unload time. Bunsell (1977) attributed the FR < 1 to be due to the fact that on unloading, the matrix goes into compression such that to reach the same overall load on the next load cycle the fibers have to be stressed further thus leading to more fiber breaks with the resulting AE. Tao and Gao (1982) derived an expression related the FR less than unity to the effective reduction in cross-sectional area which results on unload due to a redistribution of stress and consequently new AE on reloading.

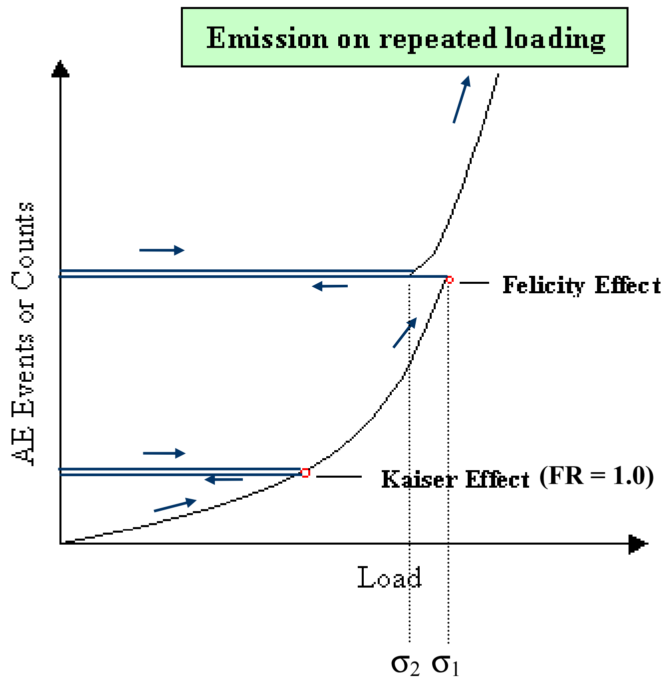

$$\textbf{Felicity ratio, FR} = \frac{\sigma_2}{\sigma_1}$$

Figure 1.10 Felicity effect and Kaiser effect

Even though the basic physics of the Felicity effect has not yet been clarified, this effect has been a valuable tool for nondestructive inspection of certain composite structures.

Unfortunately, despite these literature reviews provides all aspects of the research that has been conducted on cord-rubber composite materials for vehicle tires, there is no simple test methodology for the laboratory simulation of belt-leaving-belt failure processes of two working belts of vehicle tires.

1.4 Approach

The current research program has been pursued to clarify the many issues just discussed in the case of radial passenger or truck tires by investigating the mechanisms of local damage accumulation, material property degradation, and structural failure for the cord-rubber composite specimens representing the *belt-edge* region. These various degradation mechanisms have been examined under laboratory loading conditions of cyclic tension so as to simulate circumferential tension (Figure 1.11), which is the most important element of the complex loading of actual tires.

The present research effort used an experimental method, with an emphasis on the failure modes in the shoulder area of bias aircraft tires, developed by Lee et al. (1990) to study the *delamination* process in the flat coupon specimens of angle-plied cord-rubber composites reinforced with nylon cords. Under cyclic loading with constant stress amplitude simulating the dynamic state of circumferential tension in the footprint region of the tires, the angle-plied composites exhibited extensive interply shear deformation eventually leading to delamination type failures (Figures 1.7 and 1.12). In addition, the use of the coupon specimens with free edges allowed the direct observation of the damage accumulation preceding the delamination. The dependence of fatigue lifetime of the tire belt on the stress, strain, and temperature history was examined to establish valid failure criteria by using flat coupon specimens with steel wire cables. An empirical model was formulated to predict the fatigue life of cord-rubber composite laminate.

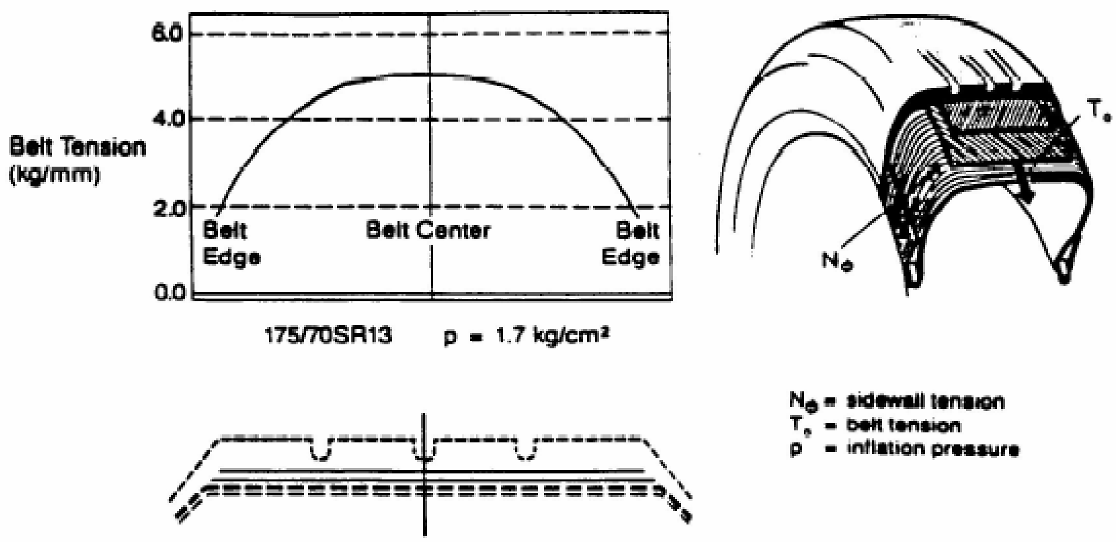

(a)

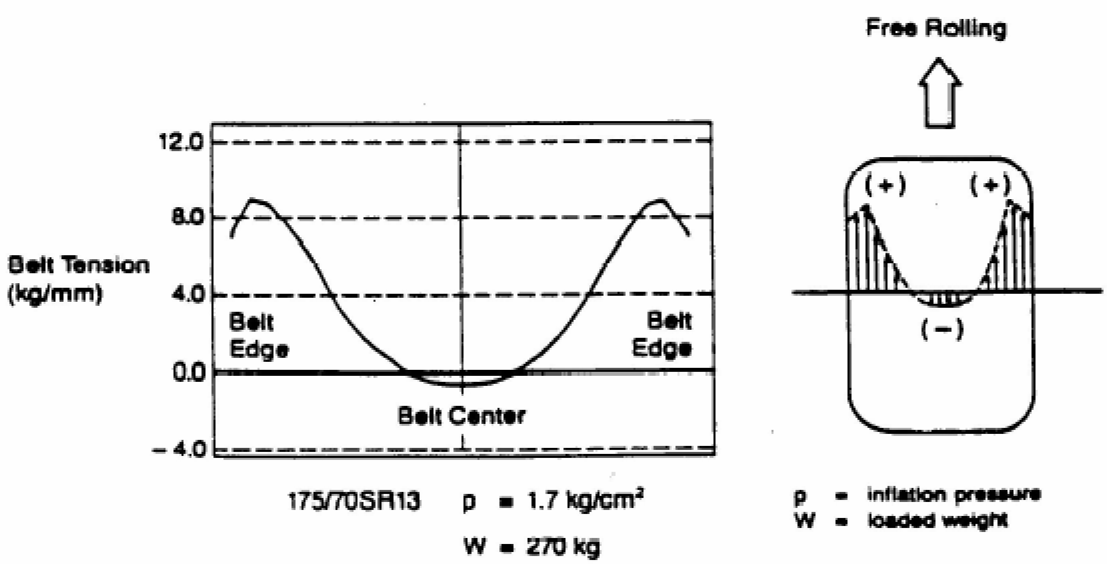

(b)

Figure 1.11 Belt tension (a) by inflation pressure and (b) in free rolling

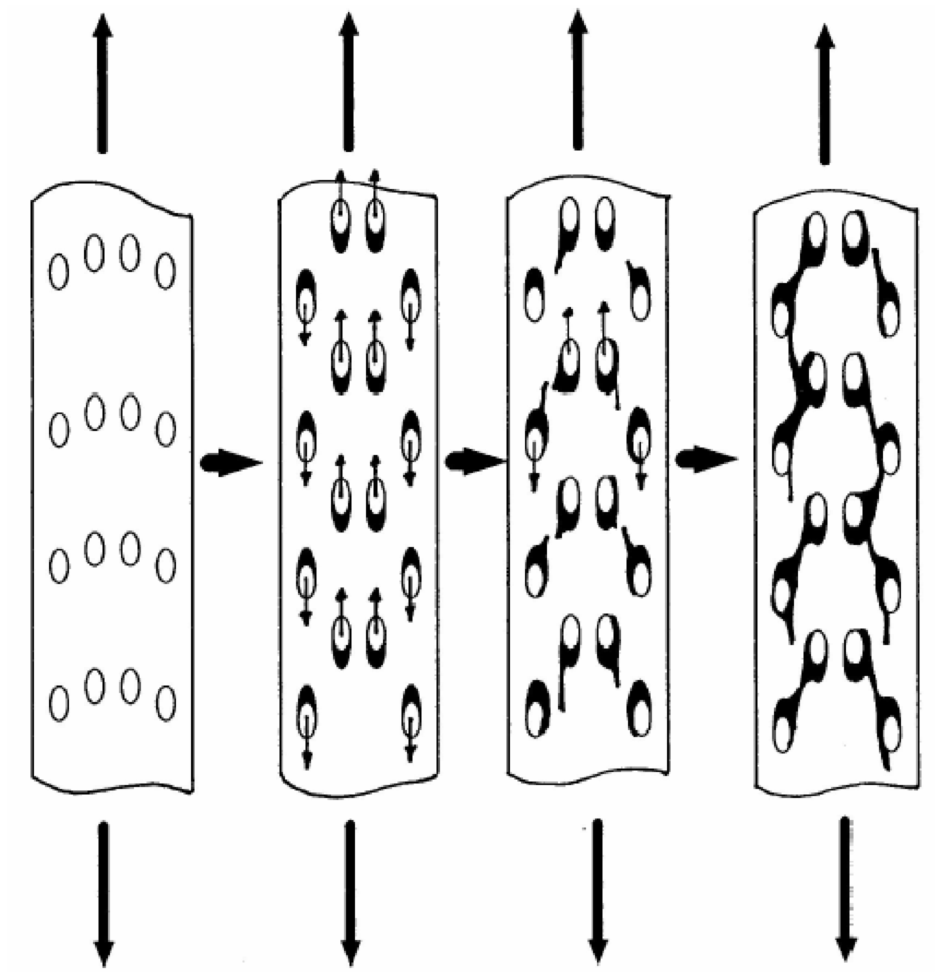

Figure 1.12 Schematic diagram for the cord-matrix debonding, matrix cracking and delamination process (Lee et al., 1998)

Chapter 2

INTERPLY SHEAR DEFORMATION OF ACTUAL TIRES

The interply shear measurement technique has been used to determine the shear strain at the belt edge of a tire (Cembrola and Dudek, 1985). As a preliminary test of coupon specimen testing, interply shear strain in the belt edge region of actual tires was measured (Lee et al., 2002).

2.1 Experimental Techniques

2.1.1 Actual Tire Preparation

Various types of unused spare or new tires (235/75R15) have been provided by the Office of Defects Investigation at the National Highway Traffic Safety Administration (NHTSA). The collection of tires in question included:

ATX '92 through '96

'96 ATX vs. '96 Wilderness AT

'97 Wilderness AT from Wilson vs. '97 Wilderness AT from Decatur

'97 Wilderness AT vs. '99 Wilderness AT after the design change

'96/'97 Wilderness AT vs. '96/'97 Goodyear Wrangler

These tires underwent *no* prior mechanical loading, but might have experienced prior environmental aging.

2.1.2 Interply Shear Measurement

The actual tire tests were conducted at room temperature using an Instron servo-hydraulic test frame fitted with a MTS controller (Figure 2.1) In-situ measurement of interply shear strain of two belt plies was performed after exposing the belt edge region of tire by local cuts and subjecting each inflated tire to a constant level of static footprint load (Figure 2.2). At a given level of footprint load, the relative displacement of two belt plies was measured by photographing the movement of the grid line drawn initially through the ply thickness at a 90° angle (Figure 2.3). A cyclic range of relative displacement of two belt plies was defined by performing the measurements when the exposed belt edge region was within as well as out of footprint, based on 3 readings at 0°, 45°, and 90° rotation for each tire.

The values of interply shear strain range were determined by dividing the values of cyclic range of *relative displacement* of two belt plies with the average values of *interply rubber thickness* in the exposed region (Figure 2.4). Here the interply rubber thickness is defined as the distance from the center of tire cord cross-section in upper belt ply to the center of tire cord cross-section in lower belt ply (which includes the belt wedge plus belt skim coats for one-half of upper and lower belt plies respectively).

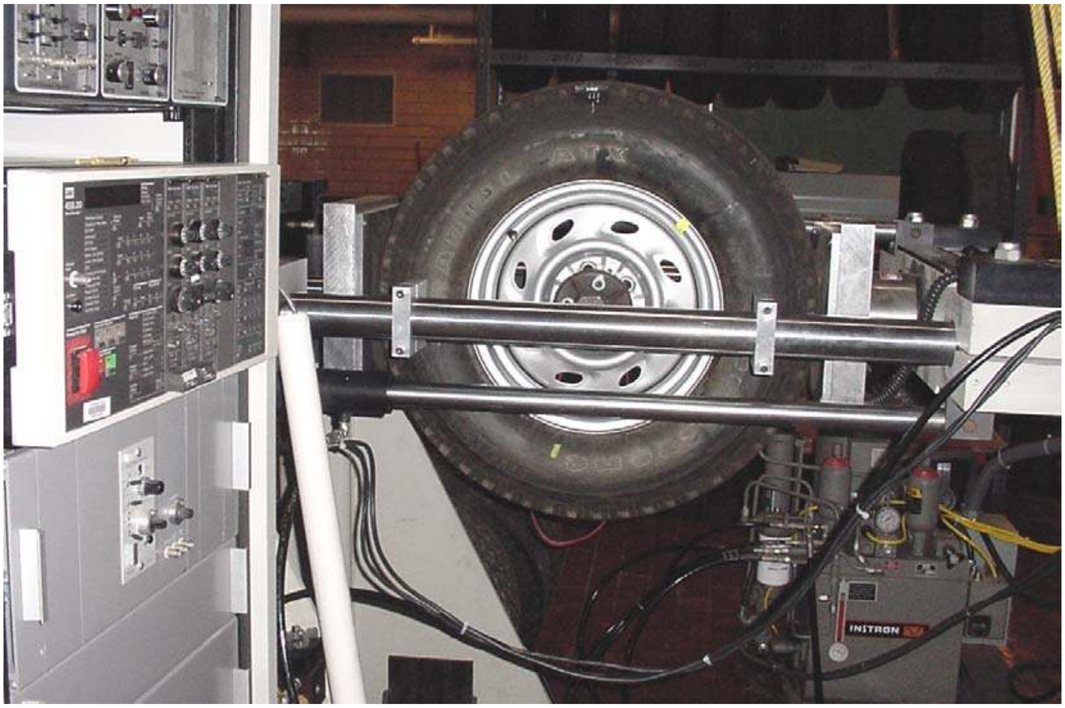

Figure 2.1 Static Loading Arrangement for Pneumatic Tires

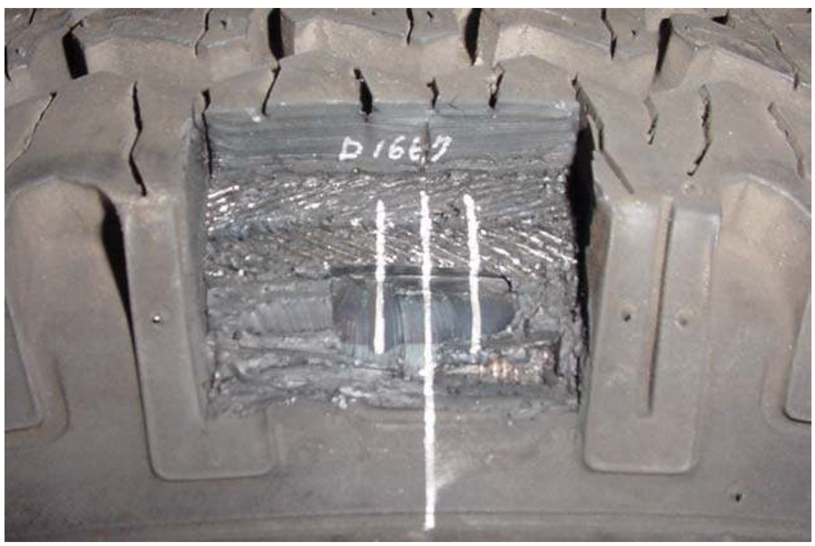

Figure 2.2 Belt edge region exposed and grid lines drawn for strain measurement

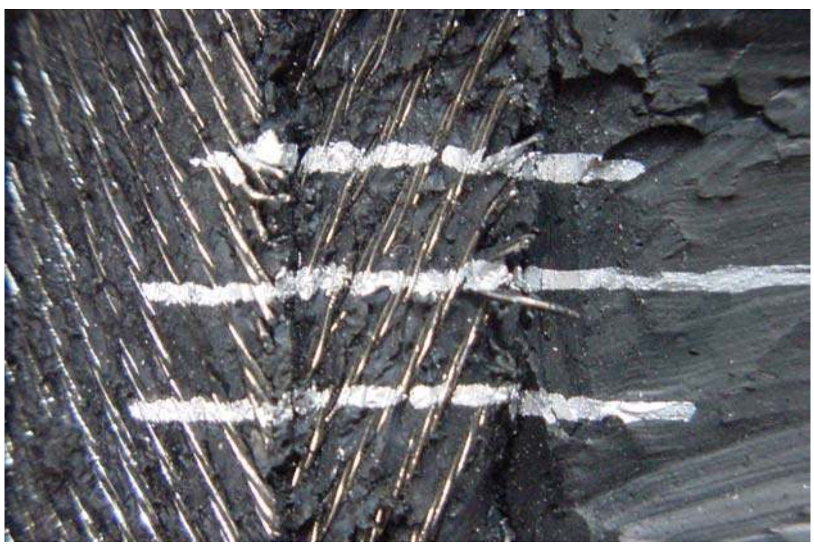

Figure 2.3 Top view of exposed upper belt (wires at 20° left) and lower belt (20° right) in relative displacement under moderate footprint load

$$\text{Interply Shear Strain} = \frac{\text{"X" (relative displacement)}}{\text{Interply rubber thickness}}$$

Figure 2.4 Interply shear strain measurement of an actual tire

The measurements of interply shear strain were performed at a standard inflation pressure of 26 psi under the following three levels of footprint load: 1400 lb, 1500 lb (one-half of Rear Axle Gross Axle Weight Rating (GAWR) for Ford Explorer XLT model), and 1600 lb. In addition, the measurements were carried out under the footprint load of 1500 lb using the inflation pressure of 22 psi (below the standard) and 28 psi (above the standard) respectively.

2.2 Experimental Results and Discussion

A total of 26 tires were available for in-situ measurement of interply shear strain and the results of interply shear strain at the belt edge region of actual tires were reasonably reproducible. The dependence of this test results on the footprint load, inflation pressure, types of source tire and their year of manufacturing was examined through a series of graphic plots (Figures 2.5 through 2.9).

In comparison with the Goodyear tires, the Firestone tires manufactured prior to their '98 design change exhibit not only higher levels of local belt edge strain (cyclic range of interply shear strain) but also a greater sensitivity of local strain to the vehicle load (Figures 2.5 through 2.9). A greater sensitivity of local belt edge strain to the vehicle load in the case of Firestone tires means increased chances for debonding of belt wire ends from the rubber ("socketing") and ensuing delamination of belt plies with higher cargo weight. As can be seen in Figures 2.5 and 2.6, the design change for the Firestone tires in '98 reduced the levels of interply shear strain between two belts making them comparable to those of the Goodyear tires.

Therefore, it can be concluded that higher levels of interply shear strain reduce the fatigue lifetime, and interply shear strain is one of the crucial parameters for damage assessment. However, this interply shear strain measurement for actual tires has some limitations. First of all, in order to predict fatigue behaviors of any tire designs, actual tire samples should be manufactured and prepared appropriately for interply shear strain measurement.

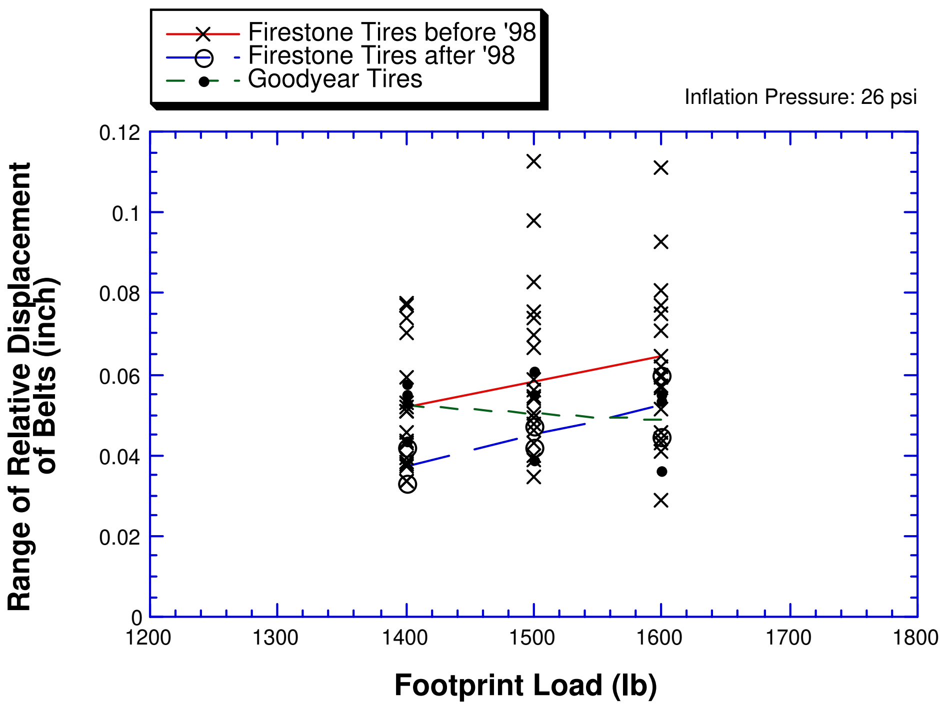

Figure 2.5 Range of relative displacement of belts vs. footprint load

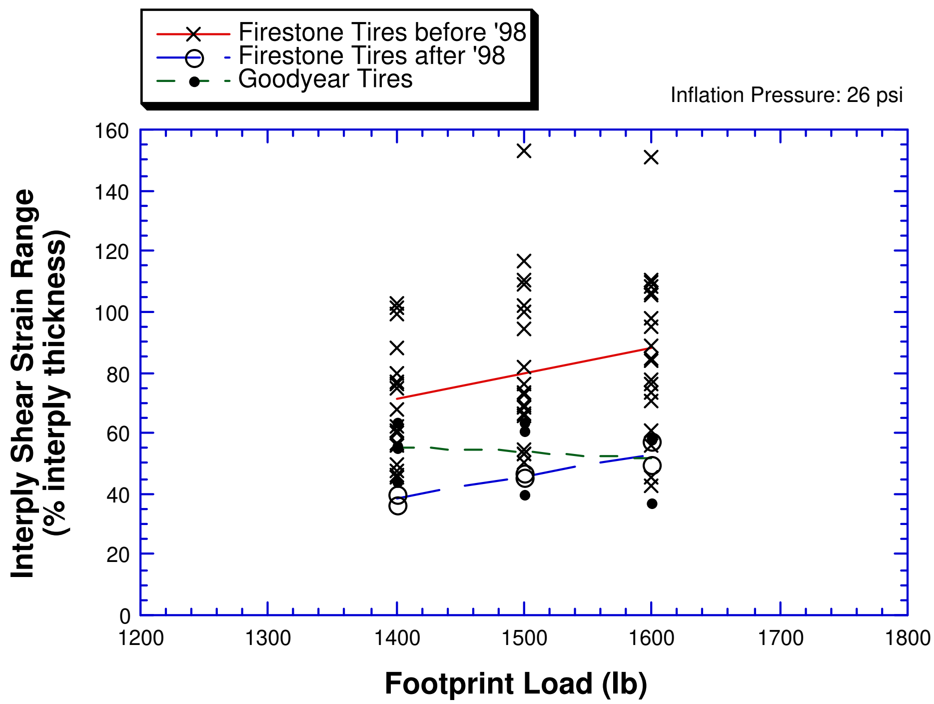

Figure 2.6 Interply shear strain range (% interply thickness) vs. footprint load

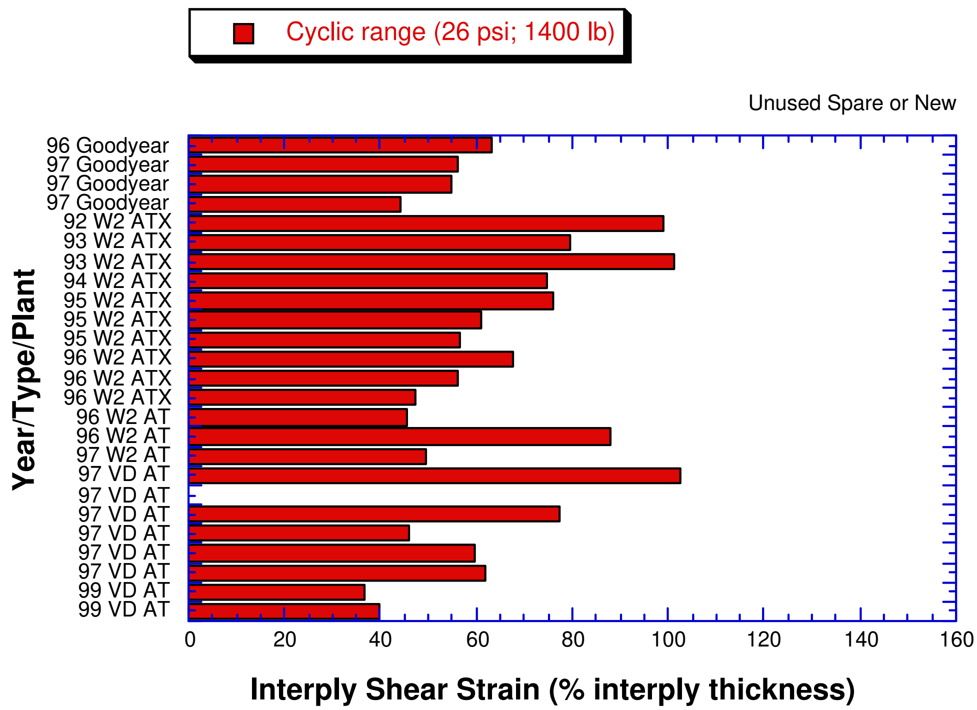

Figure 2.7 Interply shear strain range (% interply thickness) at inflation pressure 26psi and footprint load 1,400lb

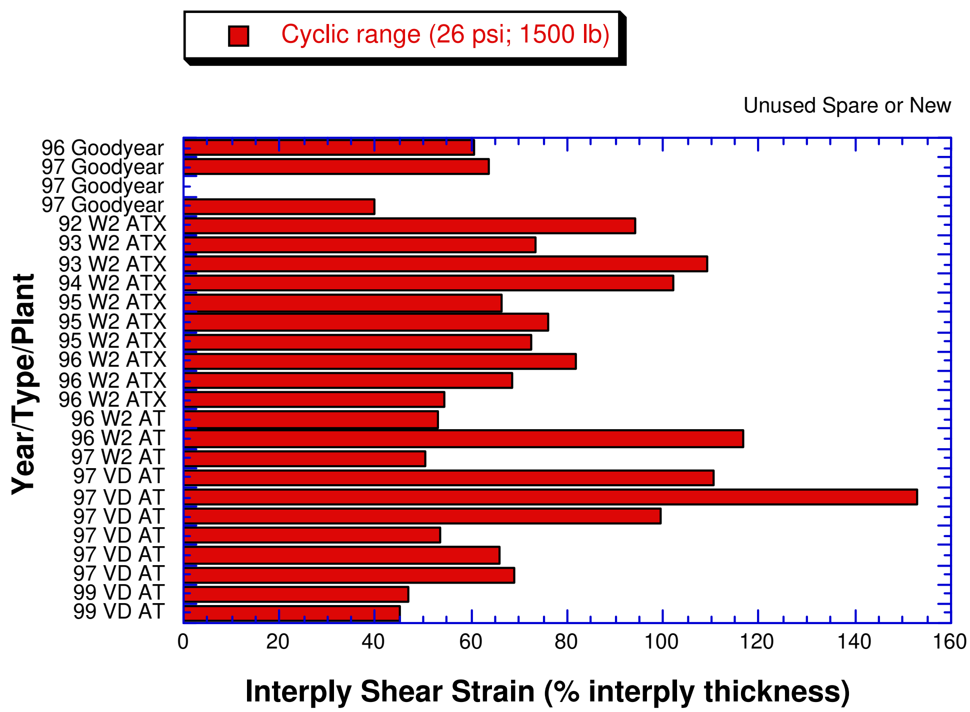

Figure 2.8 Interply shear strain range (% interply thickness) at inflation pressure 26psi and footprint load 1,500lb

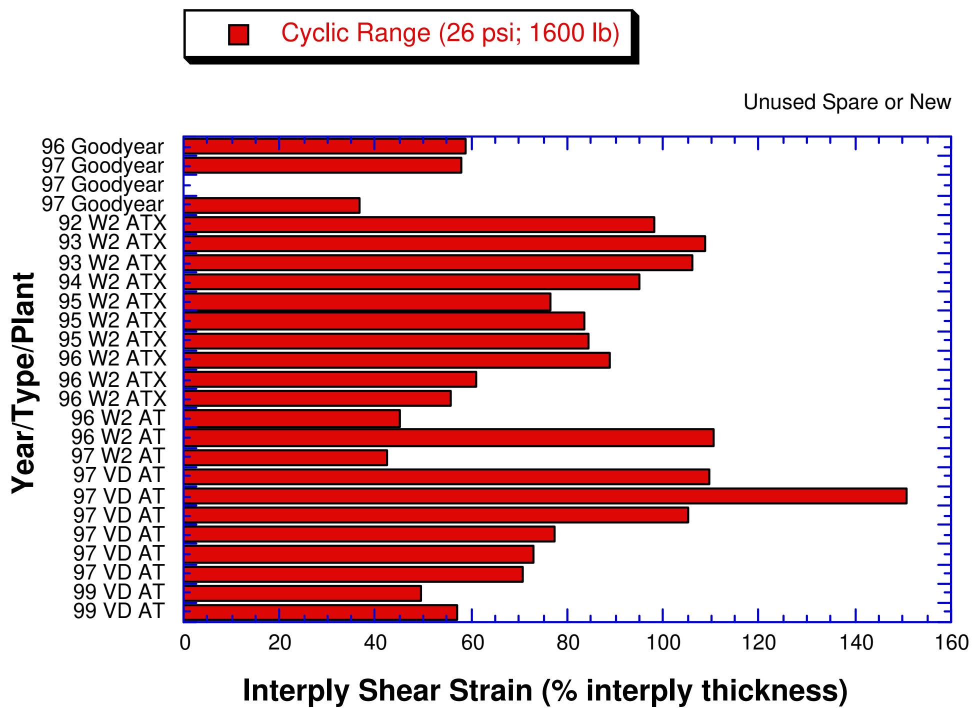

Figure 2.9 Interply shear strain range (% interply thickness) at inflation pressure 26psi and footprint load 1,600lb

In addition, cutting out a window in the tread to expose the belt edge of the crossply and the interply rubber between the belts is hard and specific measurement data of the angle of the line rotation scribed through the thickness of the belts are highly dependent on an inspector.

Chapter 3

QUASI-STATIC BEHAVIOR OF COUPON SPECIMEN

3.1 Experimental Techniques

3.1.1 Materials and Specimen Preparation

Table 2.1 lists the variations of angle-plied cord-rubber composite laminates that have been provided by the Pirelli Pneumatici, S.P.A[1]. for the current study. The following variations are incorporated for the composite systems received:

(a) ply lay-up (2-ply balanced vs. 4-ply balanced/symmetric configuration),

(b) the cord reinforcement construction (3+9+15X.22 vs. 3/6X.35) (Figure 3.1),

(c) the cord angle (+/-19, +/-25, +/-38°),

(d) the cord end count (45 vs. 48 epdm[2]), that is amount of cord ends within 100mm width a ply (Figure 3.2),

(e) the interply insert (none vs. rubber A), and

(f) matrix rubber composition (MAC2-SVI vs. MAC2 carbon black-filled rubber).

The compositions of rubber compounds, such as MAC2-SVI, MAC2, or rubber A, are of proprietary nature and are therefore not disclosed. All composite laminate panels were press-molded from calendered ply stocks with unknown conditions of curing.

---

[1] The anonym S.P.A stands for "Societá per Azioni" and indicates that the Pirelli tire corporation is governed by a body of share holders. From now on Pirelli Pneumatici, S.P.A will simply be referred to as Pirelli.

[2] epdm stands for "end count per deci-meter".

Cord construction	End count (epdm)	Compound	Nom. Thickness (mm)	Angle (deg)	2 or 4 plies	Sheet number
3+9+15x0.22 +0.15LC	45	MAC2-SVI	2.2	19	4	C3
3+9+15x0.22 +0.15LC	45	MAC2-SVI	2.2	19	2	C1
3+9+15x0.22 +0.15LC	45	MAC2-SVI	2.2	25	4	C4
3+9+15x0.22 +0.15LC	45	MAC2-SVI	2.2	38	4	C19
3+9+15x0.22 +0.15LC	45	MAC2	2.2	19	2	C15
3+9+15x0.22 +0.15LC	45	MAC2-SVI	2.2	19	1	C20
3+9+15x0.22 +0.15LC	45	MAC2-SVI	2.2 + rubber A[3]	19	2	C7
3+9+15x0.22 +0.15LC	45	MAC2	2.2	19	4	C17
3/6x0.35LC	48	MAC2-SVI	2.1	19	4	C5
3/6x0.35LC	48	MAC2-SVI	2.1	19	2	C2
3/6x0.35LC	48	MAC2-SVI	2.1	25	4	C6
3/6x0.35LC	45	MAC2	2	19	2	C16
3/6x0.35LC	45	MAC2	2	19	4	C18
3/6x0.35LC	48	MAC2-SVI	2.1 + rubber A	19	2	C8
3/6x0.35LC	45	MAC2-SVI	2.2	19	1	C21
Rubber only		rubber A	2.2			

Table 2.1 Angle-plied cord-rubber composite laminates from the Pirelli Pneumatici, S.P.A.

[3] Rubber A is a same compound with MAC2-SVI.

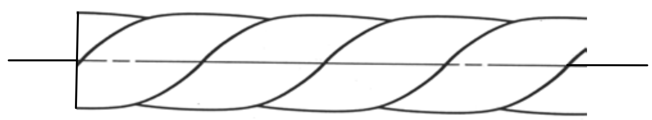

(a)

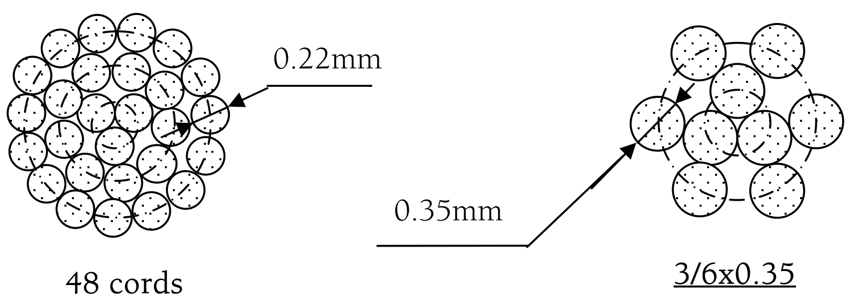

(b)

Figure 3.1 Schematic drawing of cord reinforcement; (a) twisted cord (b) section views of 3+9+15/x0.22 and 3/6x0.35

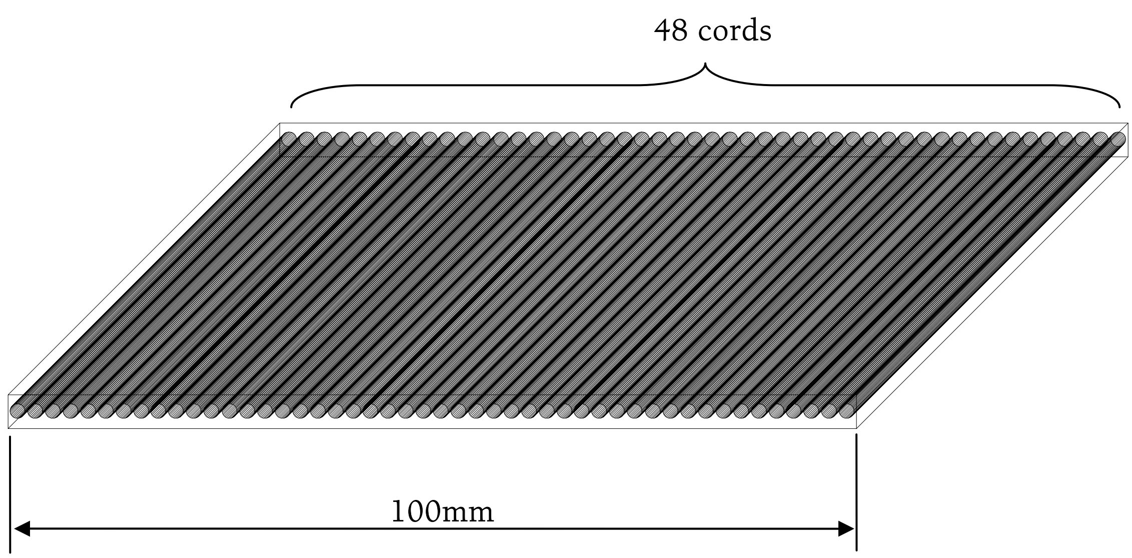

Figure 3.2 Definition of the cord end count; for example, 48 epdm

Coupon specimens of 25 mm width and 200 mm length which includes 50 mm long tabs at both ends were machined from each panel (Figure 3.3). The composite coupon specimen had free edges with the cut ends of reinforcing cords exposed.

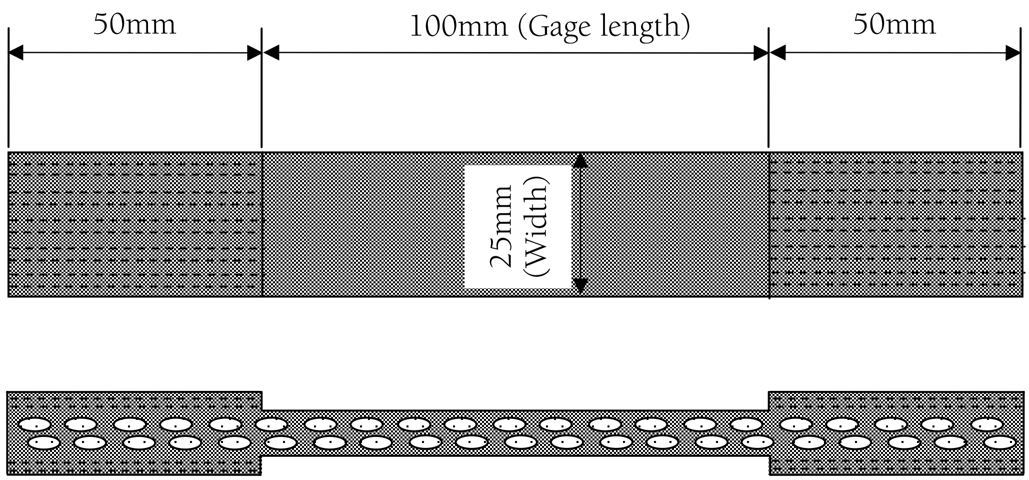

Figure 3.3 Schematic drawing of coupon specimen

3.1.2 Quasi-Static Testing

Unless noted otherwise, all static and fatigue tests were conducted at room temperature using a MTS servo-hydraulic system with controller TestStar IIs (MTS). An environmental chamber was added for both static and fatigue testing at elevated temperatures (Figure 3.4).

Composite specimens were subjected to uniaxial tension in either static mode or load-controlled “sinusoidal” cyclic mode. The gage length-to-width ratio employed in both static and cyclic testing was 4mm/mm unless noted otherwise (Figure 3.3). With regard to static stress-strain data, the deflection rate was 0.2 mm/sec.

3.1.3 Measurement of Interply Shear Strain

The interply shear strain of the angle-plied composite laminate specimens was measured by observing the distortion of a line drawn at the edge of the specimen as shown in Figure 3.5.

With reference to Figure 3.5, the magnitude of the interply shear strain is defined to be tan θ and was calculated from the measured angle (θ) of line rotation due to a relative displacement of two plies with opposite cord angles. Because of difficulties in measuring interply shear-strain under cyclic tension, the majority of the measurements were done under static tension to draw a correlation between axial strain and interply shear strain for each type of composite laminate.

Figure 3.4 MTS servo-hydraulic system with an environmental chamber

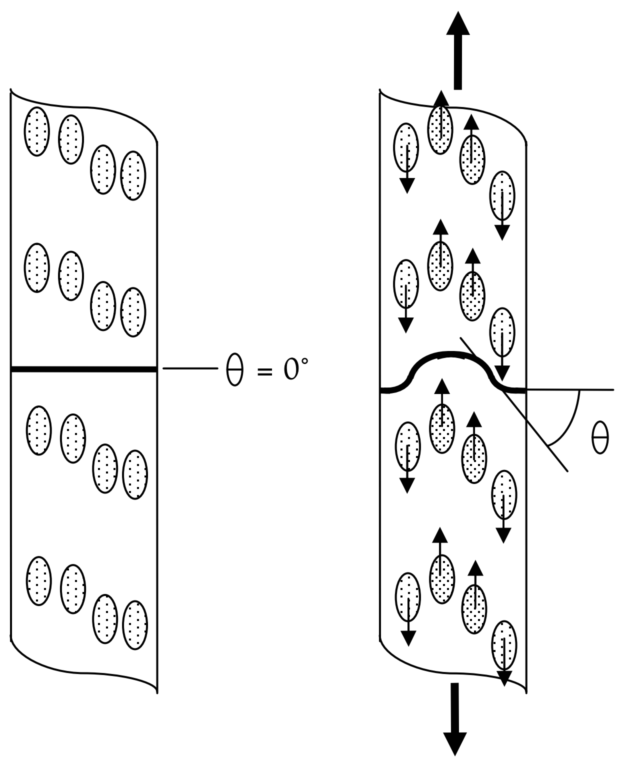

Figure 3.5 Schematic drawing for the measurement of interply shear strain

3.1.4 Acoustic Emission

The monitoring of AE was performed using a MIASTRA AE system manufactured by the Physical Acoustics Corporation (PAC). Considering that the test results are highly dependent on wave signal processing techniques, results from the study performed in the previous phase of this investigation (Lee et al., 1993b) were used to assess the influence of the following three factors on the AE behavior of cord-rubber composites:

(1) the type of piezoelectric transducer;

(2) a frequency range of bandpass filter for preamplifier; and

(3) a frequency range of bandpass filter for amplifier.

Relying on these results, the current test set-up utilized an R50 transducer connected to a model 1220A preamplifier with a 100-1200 kHz wide bandpass filter manufactured by PAC. The frequency range of the bandpass filter for the amplifier was fixed at 400-600 kHz. The transducer was mounted to the specimen using rubber bands. A thin layer of vacuum grease couplant was placed between the transducer and the specimen surface to aid the transmission of AE signals. For signal data processing, the following settings were used for the key variables:

(1) 20 dB gain;

(2) 45 dB amplitude threshold;

(3) 20 μs peak definition time (PDT);

(4) 150 μs acoustic event definition time (HDT); and

(5) 300 μs acoustic event lockout time (HLT).

The following three parameters were used to characterize the intensity of the AE activities:

(1) the number of AE events, that is, the number of stress wave generated;

(2) AE counts, that is, the number of crossings of stress waves over a threshold value; and

(3) AE energy, that is, the area under the stress waves.

3.2 Experimental Results and Discussion

3.2.1 Interply Shear Deformation

The angle-plied cord-rubber composite laminate specimens received from Pirelli exhibited various degrees of interply shear deformation depending on the level of tensile load applied in static or cyclic mode. As discussed in earlier studies by Lee et al. (1993, 1994, 1998, 2000), Liu and Lee (1996), and Ku et al. (1998), interply shear strain develops in any angle-plied composite laminate when the constituent plies exhibit in-plane shear deformation of opposite direction. In general, the magnitude of interply shear strain increases with the reinforcement angle load level being equal. Unusually high levels of interply shear strain in cord-rubber composite laminates result from the load-induced change of reinforcement angle allowed by the extreme compliance of the rubber matrix. Actually, the cord angle *decreases* under load due to the lateral contraction of the specimen width for increasing interply shear deformation.

In this study, the interply shear strain was measured for both laminate constructions of 2-ply balanced lay-up (e.g. +19/-19°) and 4-ply balanced/symmetric lay-up (e.g. [+19/-19°]2s which means +19/-19/-19/+19°). A symmetric lay-up of 4 plies was used in our experiments to avoid tension-bending coupling which led to “twisting” of the specimen of 2-ply laminate under axial tension applied. Preliminary results under static loading indicate that the relationship between interply shear strain and axial tensile strain is affected by the twisting action induced by the specimen’s anisotropy (Figure 3.6).

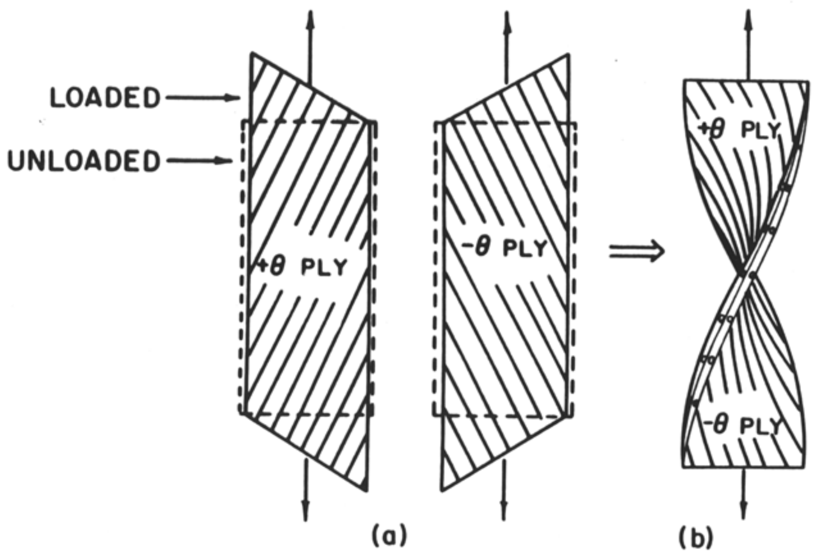

Figure 3.6 Twisting of two-ply ±**θ** laminate under uniaxial tensile loading

The values of the correlation factors defined as linear relationship between interply shear strain and axial tensile strain were found to be 17.678 and 12.186 for 2-ply and 4-ply laminates, respectively. At a given axial tensile strain, i.e., elongation of the specimen, the interply shear strain of 4-ply symmetric laminate is about 30% lower than that of 2-ply laminate which is subjected to twisting action.

It is interesting to note that the axial strain at gross failure of a 2-ply laminate is approximately 15%, which is somewhat lower than the failure strain of about 18% for 4-ply laminate (Figure 3.7). On the other hand, at a given axial strain, the interply shear strain of 2-ply laminate is higher than that of 4-ply laminate as discussed above. Because of these two opposing trends, the values of interply shear strain for 2-ply and 4-ply laminates tend to converge near the gross failure point. Although it is premature to draw a definitive conclusion without further in-depth study, the observed trends suggest that, while the twisting action of 2-ply laminate results in locally higher interply shear strain at a given elongation of the specimen, a critical level of interply shear strain which governs the gross failure of composite laminate is independent of different lay-up of 2-ply vs 4-ply.

Compared to a composite laminate (C3) with the cord angles of [+19/-19°]2s, the laminate (C4) with the cord angles of [+25/-25°]2s exhibited a *smaller* magnitude of interply shear deformation at a given axial strain because of its larger reinforcement angle (Figure 3.8). The values of the correlation factor between interply shear strain and axial tensile strain were found to be 10.861 and 12.186 for [+25/-25°]2s and [+19/-19°]2s laminates, respectively.

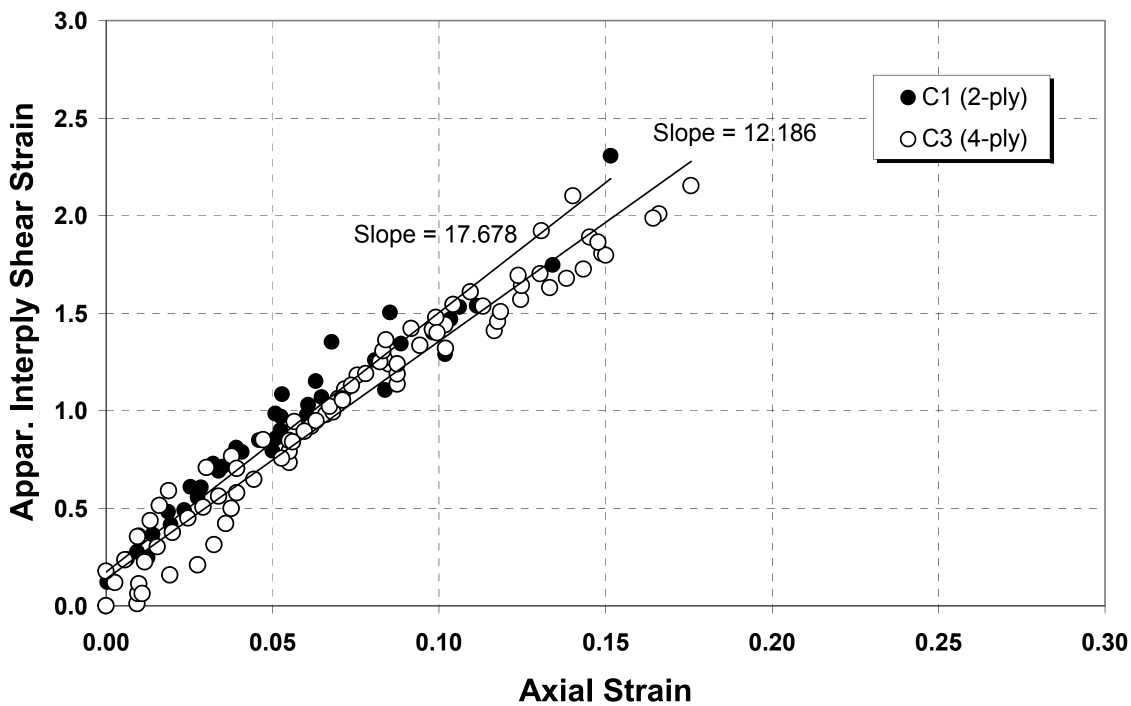

Figure 3.7 Interply shear strain vs. axial strain for different ply lay-up (2 and 4-Ply)

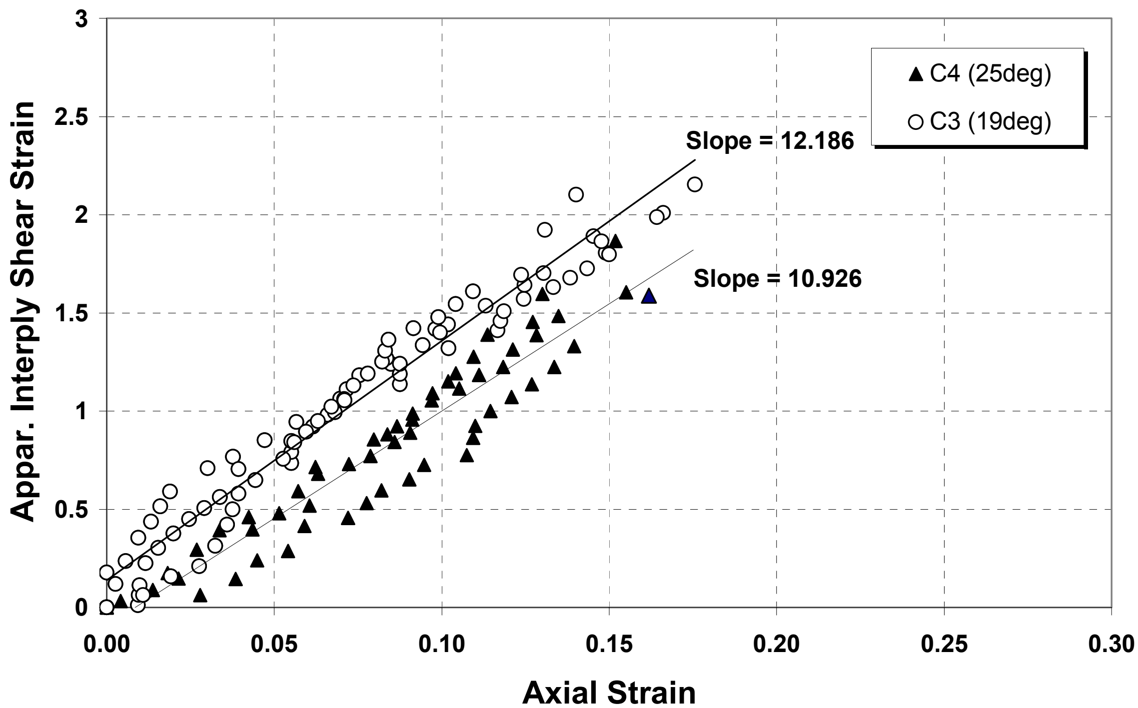

Figure 3.8 Interply shear strain vs. axial strain for two different cord angles

In addition, similar values of axial strain at gross failure were observed for both laminates, presumably due to too great data scatter to discern the increased compliance of composite laminates with larger cord angles. Because of predominance of lower interply shear strain at a given axial strain, the laminate (C4) with the cord angles of [+25/-25°]2s was associated with *smaller* values of interply shear strain at failure than the case of the laminate (C3) with the cord angles of [+19/-19°]2s.

Compared with the composite laminate (C3) with MAC2-SVI rubber matrix, the laminate (C17) with MAC2 rubber matrix exhibits a *smaller* magnitude of interply shear deformation at a given axial stress because of its higher stiffness (Figure 3.9).

3.2.2 Failure Modes

Earlier research work (Lee et al., 1993, 1994, 1998, 2000; Liu and Lee, 1996; Ku et al., 1998; Breidenbach and Lake, 1979, 1981) repeatedly demonstrated that high levels of interply shear strain at the edges of the specimen is a significant parameter which contributes to the failure of angle-plied cord-rubber composite laminate. Besides, it was observed that the axial strain for static failure is least affected by the strain distribution across the specimen width and instead governed by maximum interply shear strain attained at the edges where cord-matrix debonding starts (Ku et al., 1998). The current test results confirmed that, above a critical level of interply shear strain of around 1.0, localized damage is readily observed in the form of cord-matrix debonding around the cut ends of the cords at the edges of the specimen (Figure 1.7).

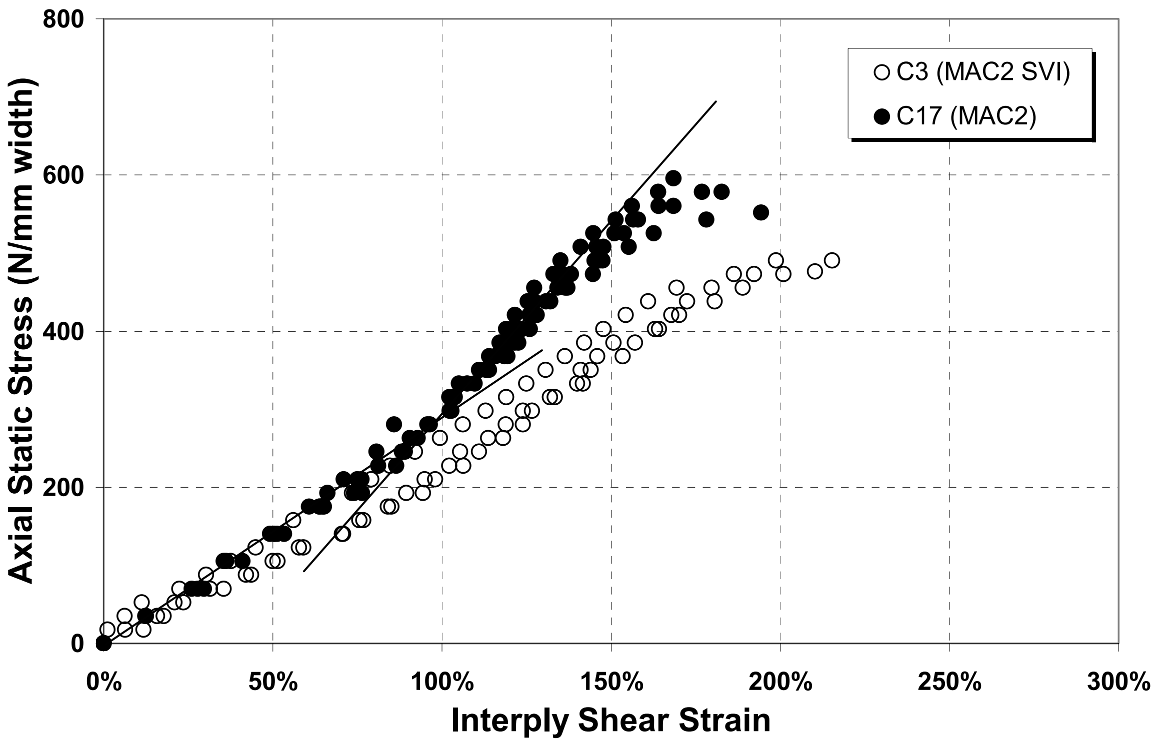

Figure 3.9 Axial static stress vs. interply shear strain for different rubber matrix

In agreement with previous observation, further increase of strain resulted in the propagation of cracks into the matrix, eventually developing into the delamination. Also the initiation of the cord-matrix debonding process tended to appear in the region just below a knee point of static stress-strain curve which results from the presence of a higher modulus region due to strain stiffening (Figure 3.9). The knee point typically occurred at the tensile strain level which was roughly half of gross failure strain and coincided with the tensile stress level roughly equivalent to 45 % of static strength.

3.2.3 Acoustic Emission Behavior under Static Tensile Loading

As discussed earlier, AE analysis has been evaluated in this program as a potential technique for monitoring damage accumulation. AE responses were monitored throughout the static tensile test up to the gross failure. Both type C16 (2-ply) and type C3 (4-ply) composites were utilized to achieve fundamental AE characteristics of cord-rubber composite, especially Felicity ratio.

Under static tension, AE occurs after the load exceeds a critical level of load defined as a boundary point, σ_0. As can be seen in Figure 3.10, AE energy was linearly proportional to applied load in log-linear scale. There were an analogous trend in AE responses; AE energy, counts, and events. The boundary point of this specimen was shown around 27.5MPa and was 34.4% of failure strength (80MPa). This value was about 10% lower than the knee point from the stress-strain relation. Therefore, AE technique could be used to monitor the initiation of cord-matrix debonding process. However, a great caution is urged in view of the data scatter.

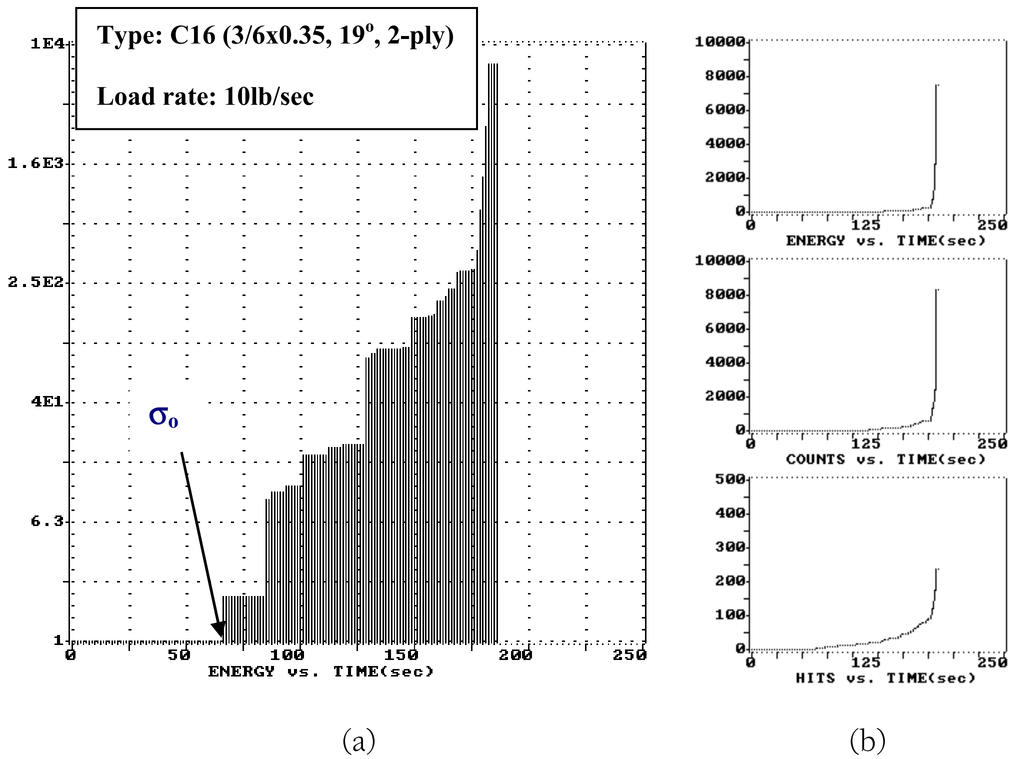

Figure 3.10 Acoustic emission behaviors under static tensile loading; (a) AE energy vs. time on log-linear plane (b) energy, counts, and events vs. time on linear scale

The Felicity ratios (FR) for type C3 composite were obtained at the maximum applied stress levels of 0.76, 0.67, 0.61, 0.55, 0.42, and 0.3. Load rate was 5lb/sec and unloading rate 50lb/sec was used throughout the tests. At zero stress, holding time was 10 seconds. This sequence is shown in Figure 3.11.

As shown in Figure 3.12, the FR under static loading was ≥ 1 for low load levels and the FR was ≤ 1 at higher load levels. For high load levels over 40MPa, it could be expressed that the effective reduction in cross-sectional area results on unload due to a redistribution of stress and consequently new AE on reloading. Therefore, Felicity ratio of cord-rubber composites is dependent of maximum applied stresses.

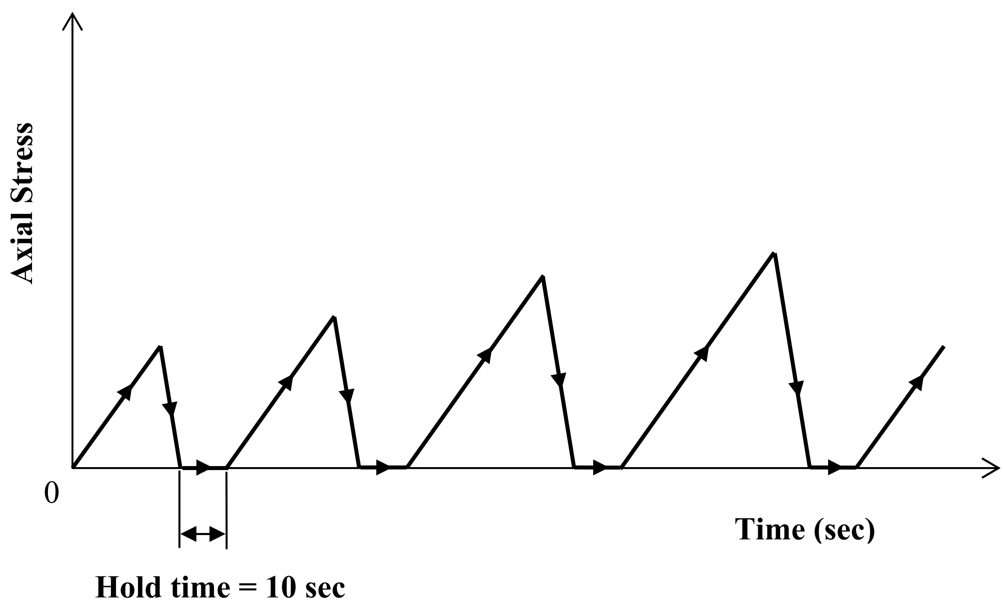

Figure 3.11 Loading sequence used for measuring Felicity ratio (FR)

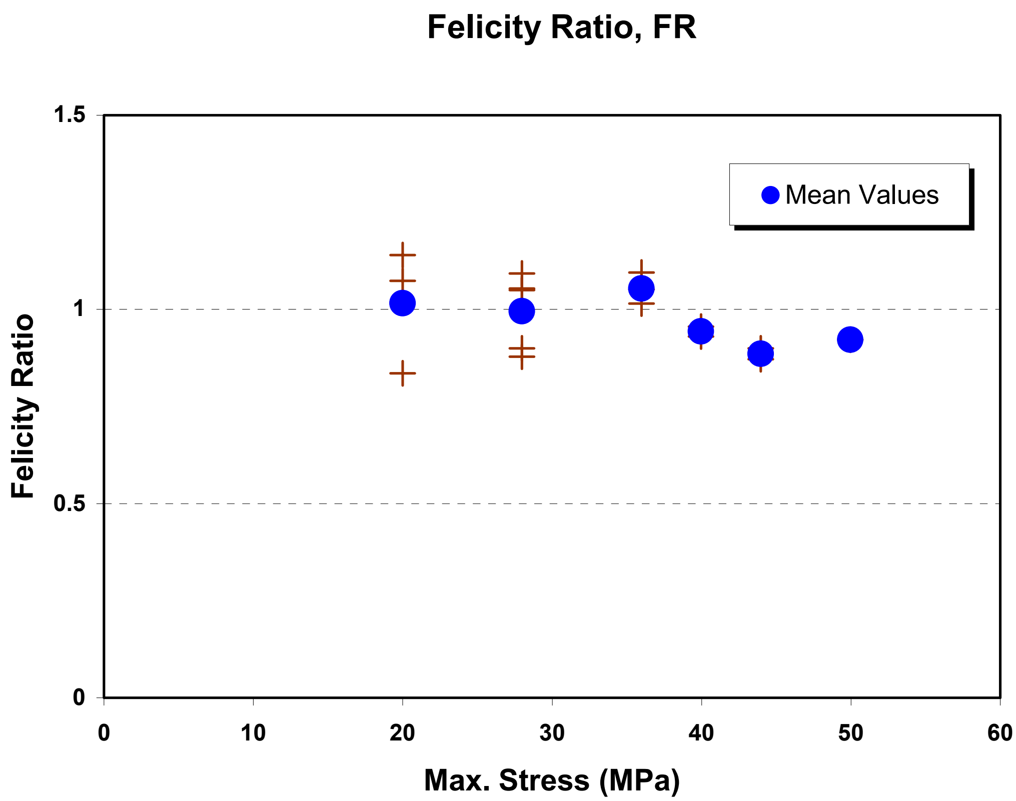

Figure 3.12 Felicity ratio (FR) of type C3 composite under static tensile loading

Chapter 4

FATIGUE BEHAVIOR OF COUPON SPECIMEN

4.1 Experimental Techniques

4.1.1 Fatigue Testing

All fatigue tests were conducted at room temperature using a MTS servo-hydraulic system with controller TestStar IIs (MTS) except for elevated temperature testing. An environmental chamber was added for fatigue testing at elevated temperatures for all static testing.

Composite specimens were subjected to uniaxial tension in load-controlled sinusoidal cyclic mode (Figure 4.1). The gage length-to-width ratio employed in cyclic testing was 4mm/mm, the same used in the static testing. The S-N (stress range vs. fatigue life) data and dynamic creep profiles were established by carrying out a series of cyclic tests under constant stress amplitude (1/2 stress range) at different nominal stress levels and with a continuous monitoring of resulting axial strain. The levels of minimum stress were kept at zero, although several experiments of tension/compression fatigue were performed with negative values of minimum stress. For all tests, a frequency of 1 Hz was used to minimize the hysteretic heating effect which is typical of rubber composites (Lee et al., 1993a). The cyclic loading mode was based on a sine wave function.

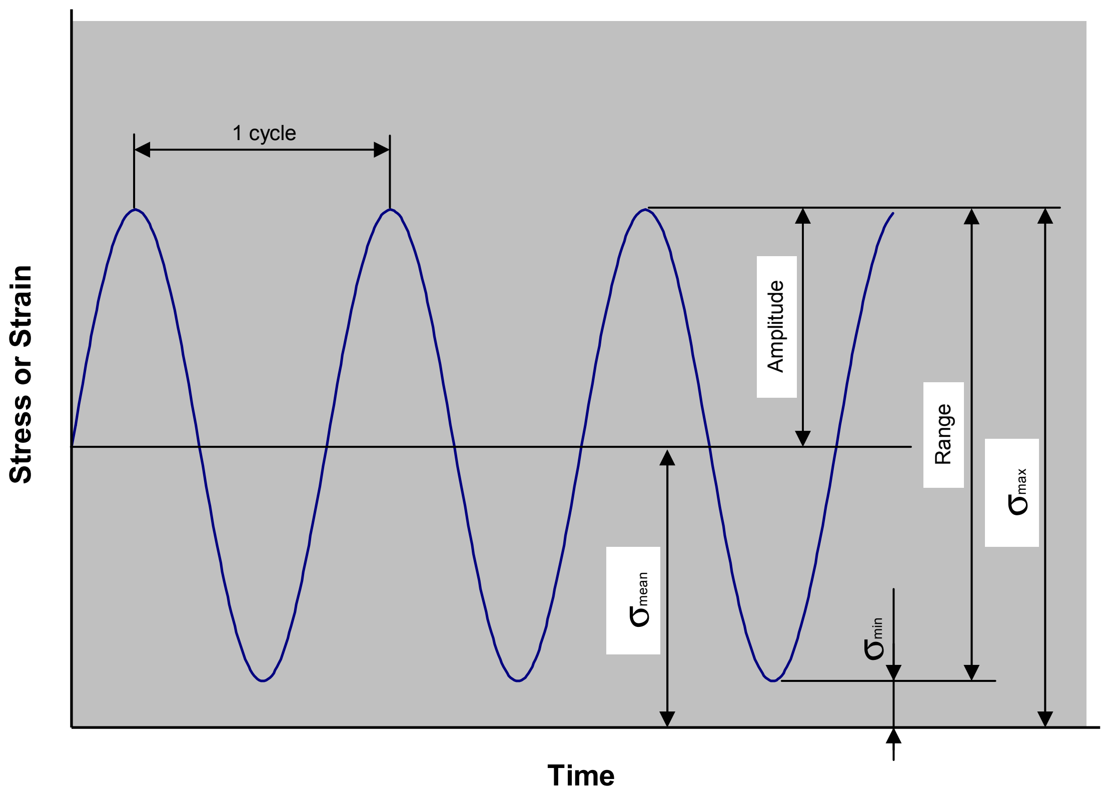

Figure 4.1 Sinusoidal loading for fatigue testing

4.1.2 Temperature Measurement

In the case of 4-ply balanced/symmetric laminate, the temperature of the specimens was monitored by thermocouples inserted between two center plies of the same cord angle. For example, in the laminate with the cord angles of [+19/-19°]2s i.e., +19/-19/-19/+19°, thermocouples were inserted in the slit formed by a razor-cut between two center plies with the cord angle of -19° (Figure 4.2). This technique allowed a continuous monitoring of temperature in a highly repeatable manner. In contrast, the temperature monitoring of 2-ply balanced laminates (e.g. +19/-19°) was less repeatable since thermocouples had to be attached to the specimen surface instead of the interply region subjected to shear strain.

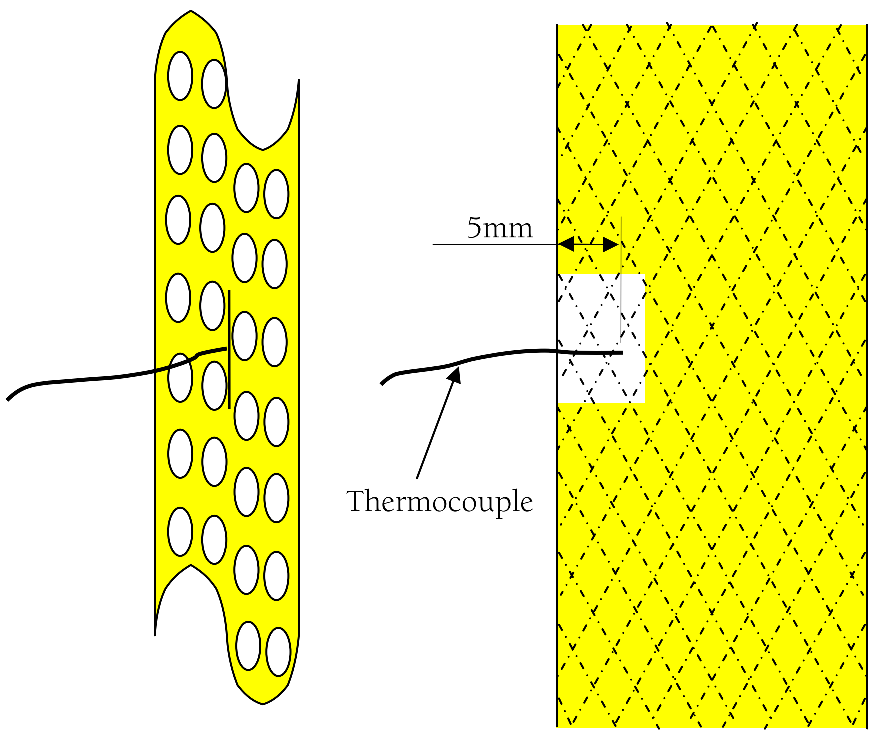

Figure 4.2 Illustration of the placement of a thermocouple via a razor slit for the continuous monitoring of interply temperature

4.1.3 Acoustic Emission

As is the case of the quasi-static tests, the monitoring of AE was performed using a MIASTRA AE system manufactured by Physical Acoustics Corporation (PAC) with the current test set-up utilized R50 transducer connected to a model 1220A preamplifier with a 100 to 1200 kHz wide bandpass filter manufactured by PAC. The frequency range of the bandpass filter for amplifier was fixed at 400-600 kHz. The transducer was mounted to the specimen using rubber bands. A thin layer of vacuum grease couplant was placed between the transducer and the specimen surface to aid in the transmission of AE signals. For signal data processing, the following settings were used for key variables: 20 dB gain; 45 dB amplitude threshold; 20 μs peak definition time (PDT); 150 μs acoustic event definition time (HDT); 300 μs acoustic event lockout time (HLT).

Again, the following three parameters were used to characterize the intensity of the AE activities: the number of AE events (the number of stress wave generated), AE counts (the number of crossings of stress waves over a threshold value), AE energy (the area under the stress waves).

4.2 Experimental Results and Discussion

4.2.1 Failure Modes

As with previous works, a similar sequence of failure processes was observed under cyclic tension with various levels of stress amplitude. The failure processes of composite laminates were visually examined at the edges of specimens. Although the debonding process was observed in the very early stage of fatigue life, the number of cord-matrix debonding sites counted by taking photographs was found to increase steadily under cyclic loading. In the meantime, some matrix cracks were formed around the debonded areas, apparently due to the stress concentration. Matrix cracks were widened and eventually developed into the delamination. The delamination length was also found to increase steadily as a function of cycles throughout the later stage of fatigue life. This process of fatigue damage accumulation was accompanied by the increase of resultant cyclic strain ("dynamic creep") and temperature changes. Figure 4.3 illustrates the dynamic creep for $[+25/-25^{o}]2s$ laminate at a stress range of 7.5 kg/mm width. Gross failure of the laminate occurred when the delamination extended across the full specimen width.

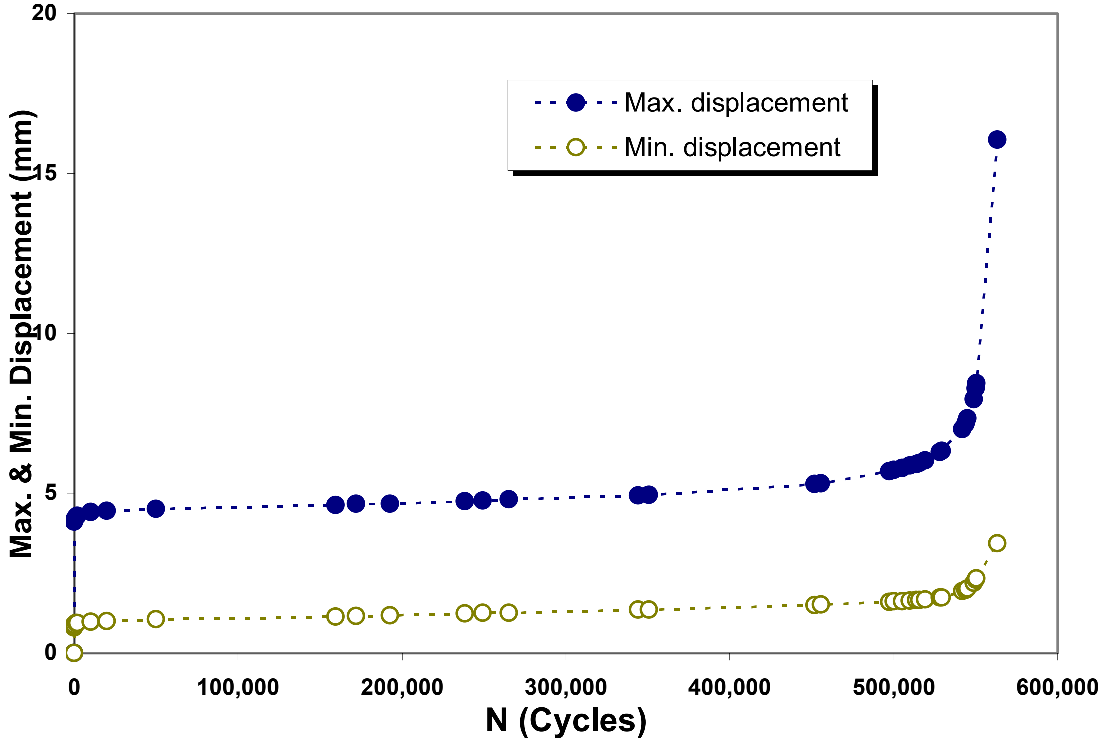

Figure 4.3 Typical dynamic creep curve

4.2.2 S-N Data

In the current study, a series of S-N (stress range vs. fatigue life) curves were generated for the tire belt composites from Pirelli, with zero minimum cyclic stress (Figure 4.4 – Figure 4.11). The effects of the following variations of materials and constructions could be examined:

(a) ply lay-up (2-ply balanced vs. 4-ply balanced/symmetric),

(b) the cord construction (3+9+15X.22 vs. 3/6X.35),

(c) the cord angle (+/-19 vs. +/-25^{o}),

(d) interply insert of rubber A, and

(e) matrix compound (MAC2-SVI vs. MAC2).

The frequency was kept at 1 Hz, which is very low level, in order to assess the role of strain parameters in the fatigue failure processes with minimal influence of material degradation due to hysteretic heating. This choice of frequency was also made in anticipation of the forthcoming study on the effect of elevated temperature of surroundings on the fatigue lifetime of composites at low frequency. However, a considerable amount of hysteretic heating still occurred under the frequency of 1 Hz.

4.2.2.1 Influence of Cord Construction

As shown in Figure 4.4, 4-ply symmetric [+19/-19^{o}]2s composite laminates of (C3) and (C5) with two different cord reinforcements, 3+9+15X.22 vs 3/6X.35, exhibit the same S-N relationship.

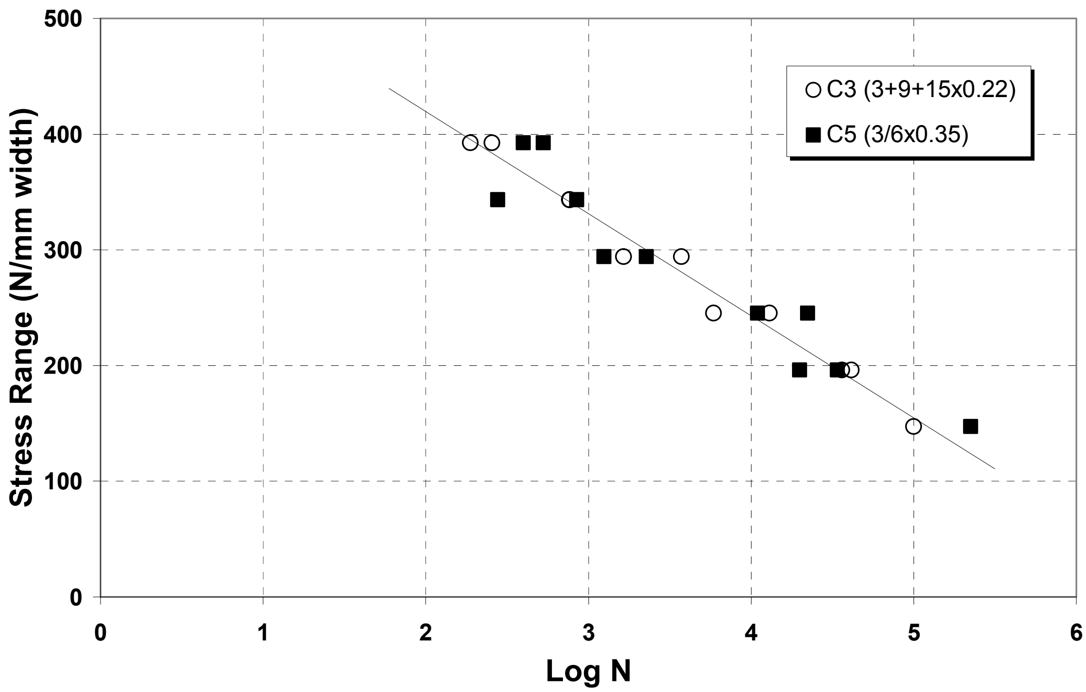

Figure 4.4 S-N data for two different cord constructions (3+9+15x0.22 vs. 3/6x0.35)

This indicates that the failure modes such as cord-matrix debonding, matrix cracking and delamination are matrix-dominated, which the cord construction appears to have no influence on the fatigue life of angle-plied composite laminates, since they are constructed with the same rubber matrix (MAC2-SVI), the same cord angle (+19/-19^{o}), similar cord volume (45 vs 48 epdm), and the same ply lay-up (4-ply). It should be noted that this conclusion has proven only in the case of tensile fatigue. The situation may be different in the case of bending fatigue.

4.2.2.2 Influence of Ply Lay-up

With the same cord reinforcement of 3+9+15X.22 at the end count of 45 epdm, the 2-ply +19/-19° composite laminates of type C1 were found to exhibit exponentially shorter fatigue lifetime, at a given stress range, than the case of 4-ply symmetric [+19/-19°]2s laminates of type C3 (Figure 4.5). As a specific example, the fatigue life of 2-ply laminate is approximately 500 cycles under the stress range of 20 Kg/mm width, while the fatigue life of 4-ply laminate is around 30,000 cycles. A similar trend was also observed for the cases of +19/-19° vs. [+19/-19°]2s laminates with the cord reinforcement of 3/6X.35 at the end count of 48 epdm (Figure 4.6). The observed trend of exponentially shorter fatigue lifetime of 2-ply laminates can be attributed to the fact that the static tensile strength of 2-ply laminates is roughly one-half of the strength of 4-ply laminates (Table 4.1), where by strength is meant the load per unit width to compare effects of constituent materials of cord-rubber composite laminates.

Interestingly, when plotted against the stress range divided by single-cycle strength, two normalized S-N curves (% single cycle strength vs. fatigue life) were merged into one trend (Figure 4.7). The value of single-cycle tensile strength was estimated by extrapolating each S-N curve to the case of failure in one cycle which means "one-shot" static tensile loading to failure (at a strain rate prescribed by the frequency and failure strain). Extrapolated value of single-cycle tensile strength is supposed to be the same as that of static tensile strength measured independently at the same strain rate.

Table 4.1 Values of static strength, axial failure strain and apparent interply shear strain for cord-rubber composite laminates

Sheet number	Static Strength (kg/mm width)	Static Strength (psi)	Static Strength (MPa)	Axial failure strain (%)	Apparent interply shear strain (%)	Note
C1-2	25.9	8,734.0	60.2	24.5	196.0	2-ply 3+9+15x. 22 19 deg
	25.9	8,734.0	60.2	21.4	230.8	
	27.3	9,216.4	63.5	22.5	180.1	
Average	26.4	8,894.8	61.3	22.8	202.3	
C2-2	26.8	8,931.3	61.6	22.8	192.5	2-ply 3/6x.35 19 deg
	26.5	8,828.0	60.9	20.5	154.9	
	24.1	8,024.8	55.3	21.3	153.7	
Average	25.8	8,594.7	59.3	21.5	167.0	
C3-2	50.0	8,284.2	57.1	17.6	215.3	4-ply 3+9+15x. 22 19 deg
	48.6	8,047.3	55.5	14.0	210.2	
	50.0	8,284.2	57.1	16.4	198.8	
Average	49.5	8,205.3	56.6	16.0	208.1	
C4-2	33.9	5,739.4	39.6	16.2	158.9	4-ply 3+9+15x. 22 25 deg
	38.4	6,495.5	44.8	15.2	186.6	
	37.5	6,343.3	43.7	15.5	160.5	
Average	36.6	6,192.7	42.7	15.6	168.7	
C5-2	44.7	7,440.8	51.3	20.0	168.5	4-ply 3/6x.35 19 deg
	48.2	8,035.7	55.4	21.1	172.4	
	49.1	8,184.0	56.4	19.1	175.5	
Average	47.3	7,886.8	54.4	20.1	172.1	
C7-1	30.4	8,500.8	58.6	19.2	194.0	2-ply C1-2 with Rubber A
	31.3	8,750.0	60.3	22.0	215.4	
Average	30.8	8,625.4	59.5	20.6	204.7	
C8-1	29.1	8,132.2	56.1	22.7	183.7	2-ply C2-2 with Rubber A
	29.1	8,157.4	56.2	17.3	171.6	
	29.2	8,163.0	56.3	18.2	179.9	
Average	29.1	8,150.9	56.2	19.4	178.4	

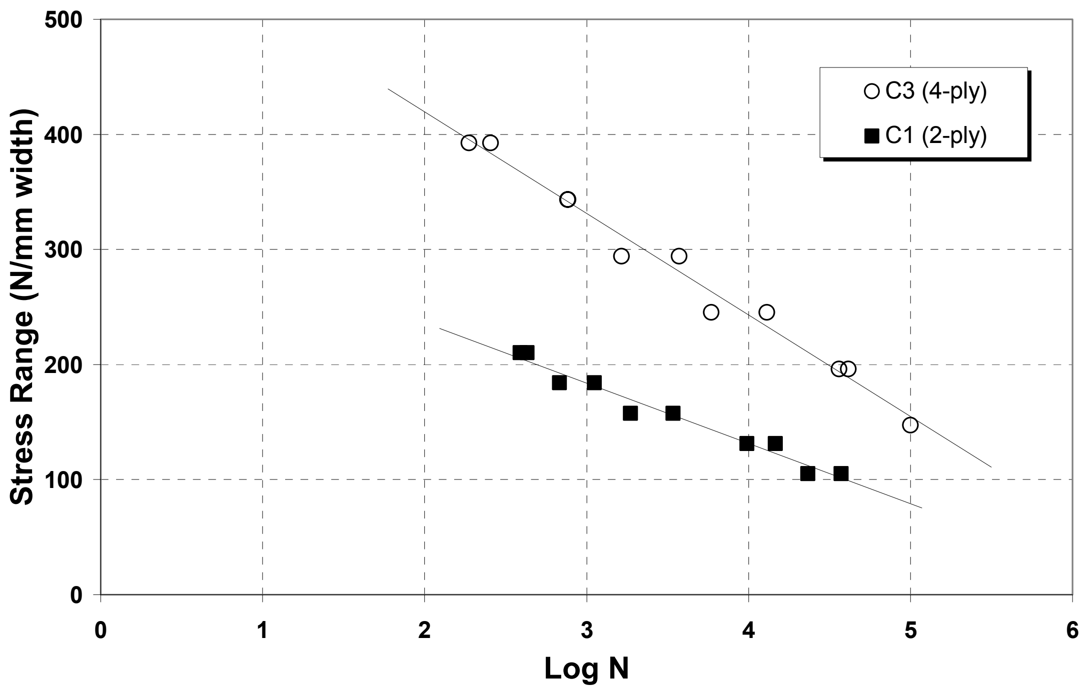

Figure 4.5 S-N data for two different ply lay-up (2-ply vs. 4-ply) with 3+9+15x0.22 cord construction

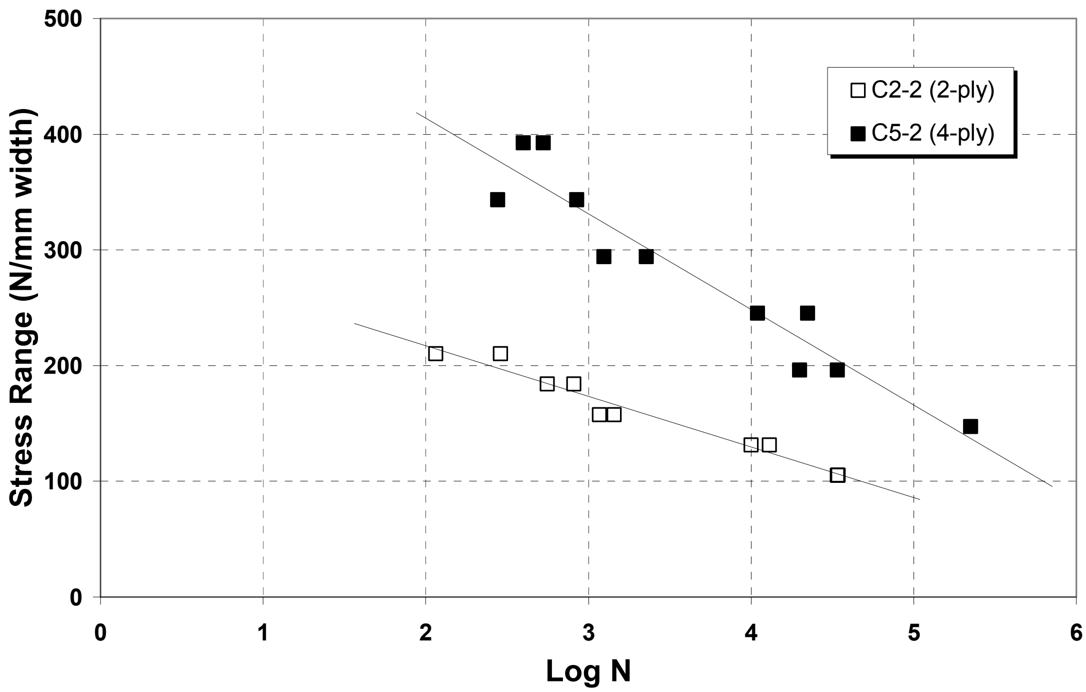

Figure 4.6 S-N data for two different ply lay-up (2 ply vs. 4-ply) with 3/6x0.35 cord construction

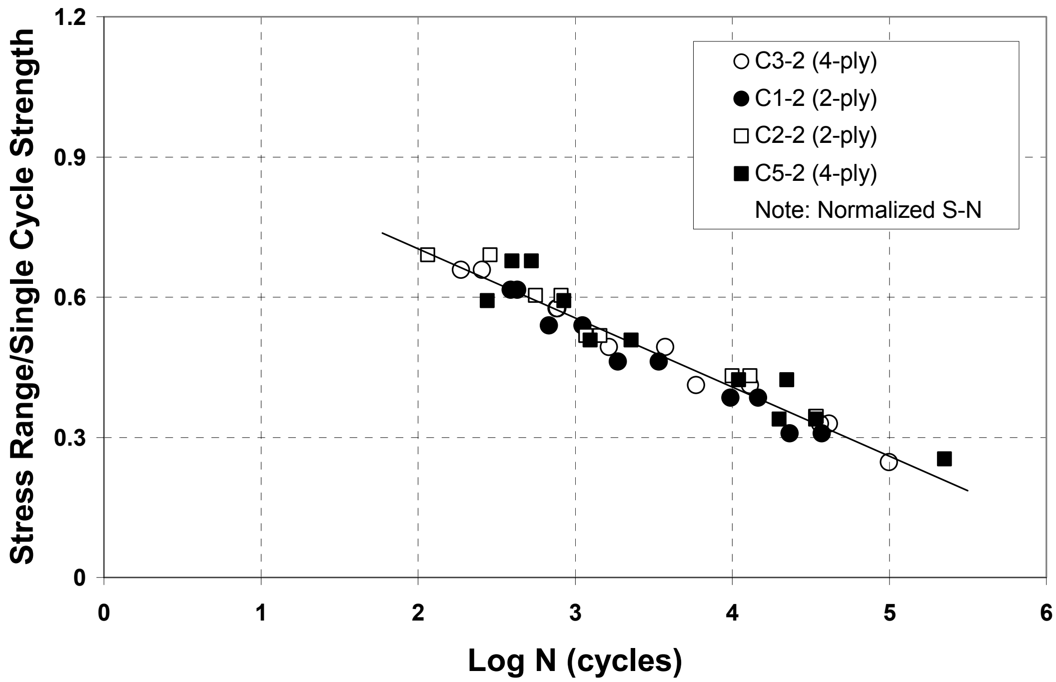

Figure 4.7 Normalized S-N data (% single cycle strength vs. fatigue life) for two different ply lay-up (2 ply vs. 4-ply)

The result confirms that as a result of *lower virgin strength*, the fatigue lifetime of 2-ply composite laminates became exponentially shorter than that of 4-ply laminates at a given stress range. Apparently the torque developed in the 2-ply laminates has *no* influence on the matrix-dominated failure mechanisms of composites due to the interply shear deformation.

4.2.2.3 Influence of Cord Angle

The observed relationship linking the *lower virgin strength* leading to the exponentially shorter fatigue life of cord-rubber composite laminates was also observed in the analysis of the cord angle effect. The increase of cord angle reduces the interply shear strain (Figure 1.10 and Figure 4.8), but lowers the strength of angle-plied cord-rubber composites at the same time. With the same cord reinforcement of 3+9+15X.22 at the end count of 45 epdm, the 4 ply symmetric [+25/-25^o]2s laminates of type C4 was found to have a lower static strength than the case of [+19/-19^o]2s laminates of type C3 (Table 4.1). As a consequence of the lower virgin strength, the fatigue lifetime of [+25/-25^o]2s laminates becames exponentially shorter than that of [+19/-19^o]2s laminate at a given stress range. Similarly, with cord reinforcement of 3+9+15X.22, 4-ply composite laminates of [+38/-38°]2s lay-up have lower single cycle strength than laminates of [+25/-25°]2s lay-up. As a result, the fatigue life time of [+38/-38°]2s laminate is exponentially shorter than that of [+25/-25°]2s laminate that is shorter than [+19/-19^o]2s at a given stress amplitude (Figure 4.8). However, three normalized S-N relationships (% single cycle strength vs. fatigue life) tend to merge into a single trend (Figure 4.9).

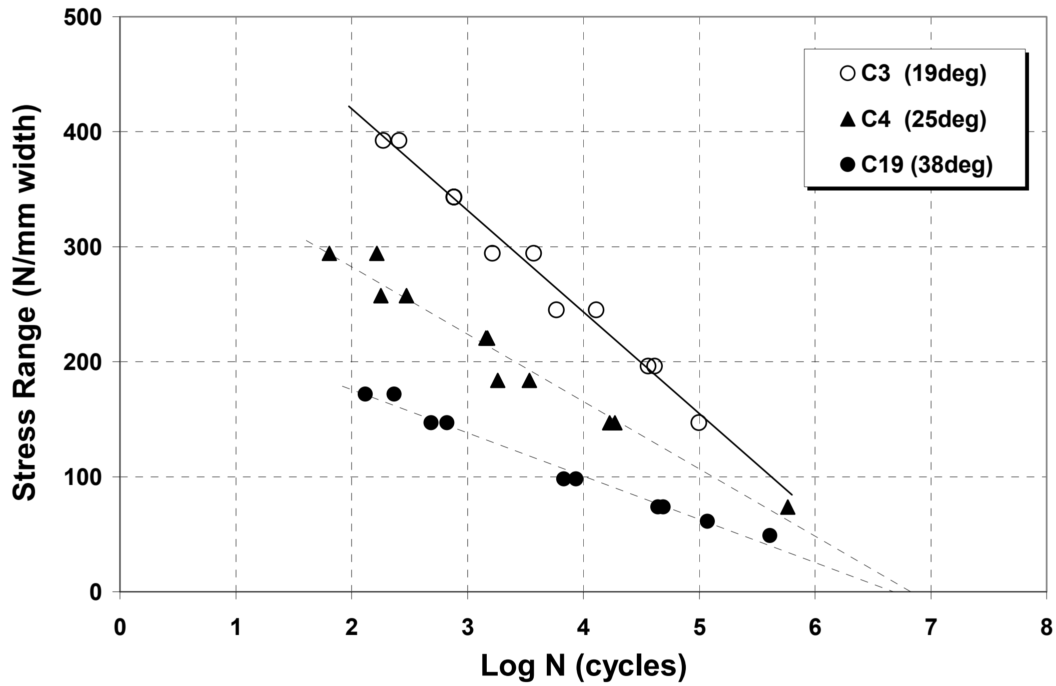

Figure 4.8 S-N data for three different cord angles (19°, 25°, and 35°)

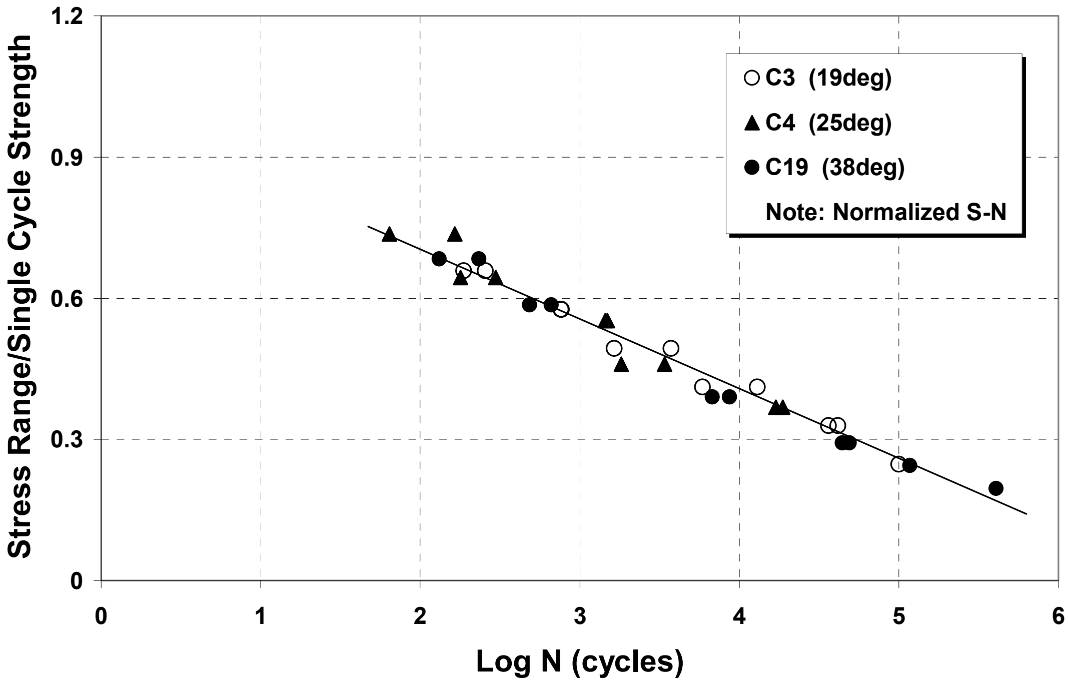

Figure 4.9 Normalized S-N data (% single cycle strength vs. fatigue life) for three different cord angles (19°, 25°, and 35°)

4.2.2.4 Effect of Matrix Compound

At static tension tests performed using 4-ply symmetric laminate specimens with different rubber matrix (MAC2), it was observed that MAC2 matrix laminates are stiffer and have lower interply shear strain than corresponding MAC2-SVI matrix laminates (Figure 3.6). As a result, the fatigue life time of MAC2 matrix laminates is exponentially longer than that of MAC2-SVI matrix laminates at a given stress amplitude, shifting S-N curve of MAC2 matrix laminates to the right (Figure 4.10). However, when plotted against the stress range divided by single-cycle strength, two normalized S-N relationships (% single cycle strength vs. fatigue life) tend to merge into a single trend (Figure 4.11). The results confirm that there is no change of failure mode.

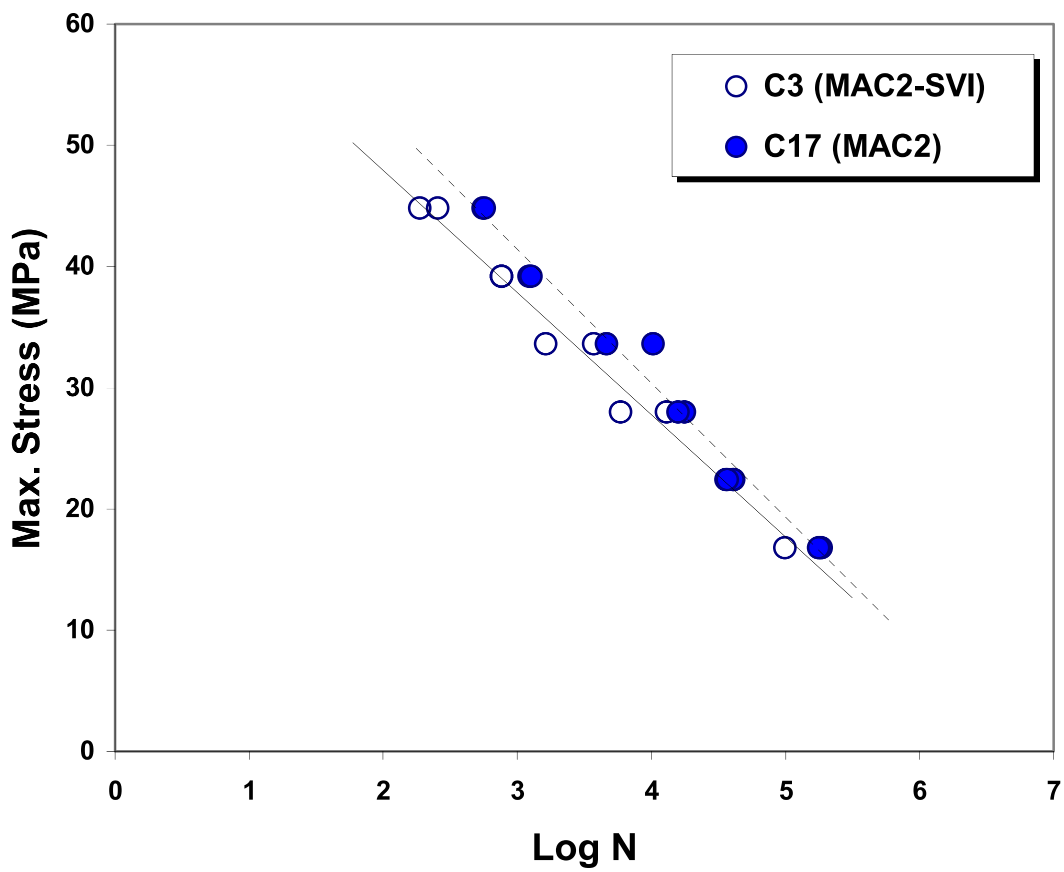

Figure 4.10 S-N data for two different rubber matrixes (MAC2-SVI vs. MAC2)

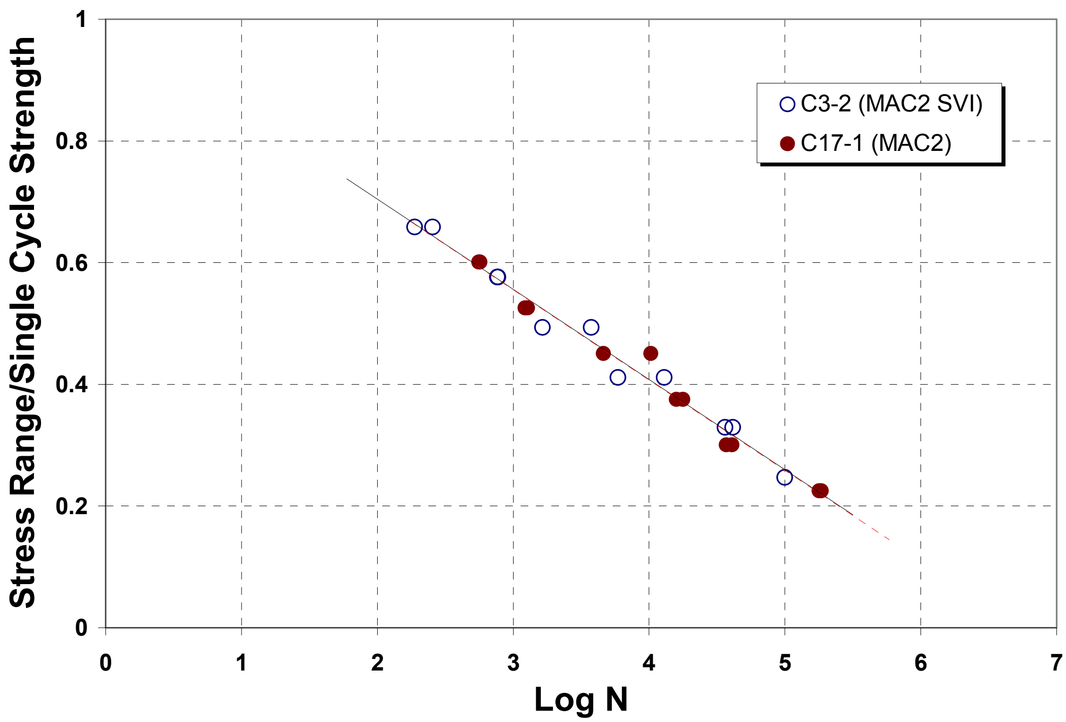

Figure 4.11 Normalized S-N data (% single cycle strength vs. fatigue life) for two different rubber matrixes (MAC2-SVI vs. MAC2)

4.2.2.5 Effect of Compressive Minimum Stress

Prior to the study of tension-compression fatigue behavior of tire belt composites, static compression tests were performed using 4-ply symmetric laminate specimens type C3 with cord reinforcement angles of +19/-19/-19/+19 degree. It was observed that *buckling* of tire belt specimens occurs under static compressive stresses ranging from -5.4 to -7.1 kg/mm width. Tension-compression fatigue tests were performed with various levels of minimum cyclic stress not exceeding –5.4 kg/mm width. Even under the minimum cyclic stress in compressive regime, the belt composites exhibited *tensile* minimum strain from an early phase of fatigue life and a steady increase of resultant strain (i.e. dynamic creep) with the progression of damage (Figure 4.12). The S-N data showed that, at a given stress range, tire belt composites exhibit longer fatigue life with the minimum cyclic stress in compressive regime than the case of zero minimum stress (i.e. tensile cyclic stress only) (Figure 4.13). However, when plotted in terms of maximum cyclic stress instead of stress range, the fatigue life data for tension-tension cycle vs. tension-compression cycle tended to appear the same for the two types of tests (Figure 4.14). This trend indicates that, even with small compressive cyclic stresses, the fatigue life of belt composites is predominantly influenced by the magnitude of maximum stress in tension. The initiation and propagation of belt edge cracks due to the interply shear deformation are believed to occur only under tensile axial stresses.

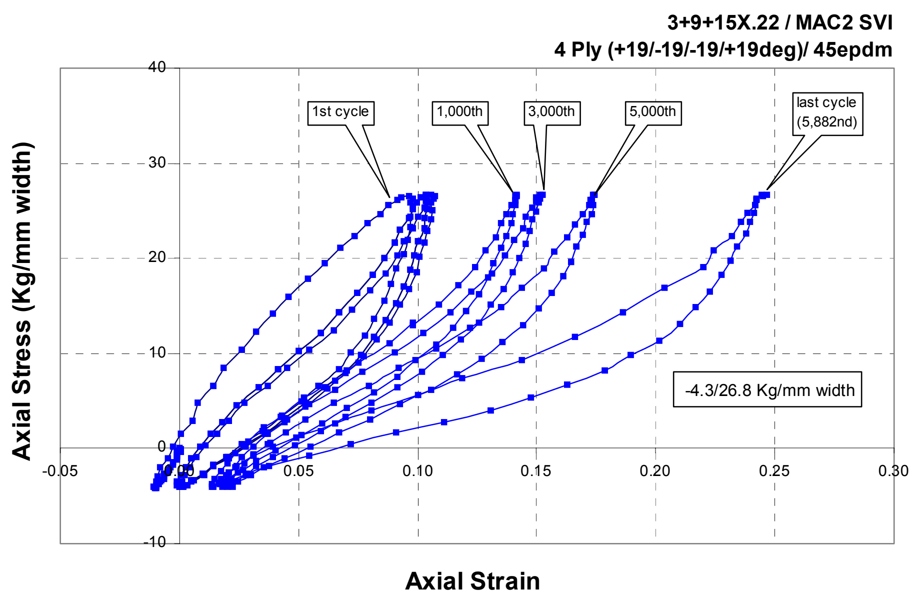

Figure 4.12 Hysteresis effect showing tensile minimum strain for compressive minimum stress

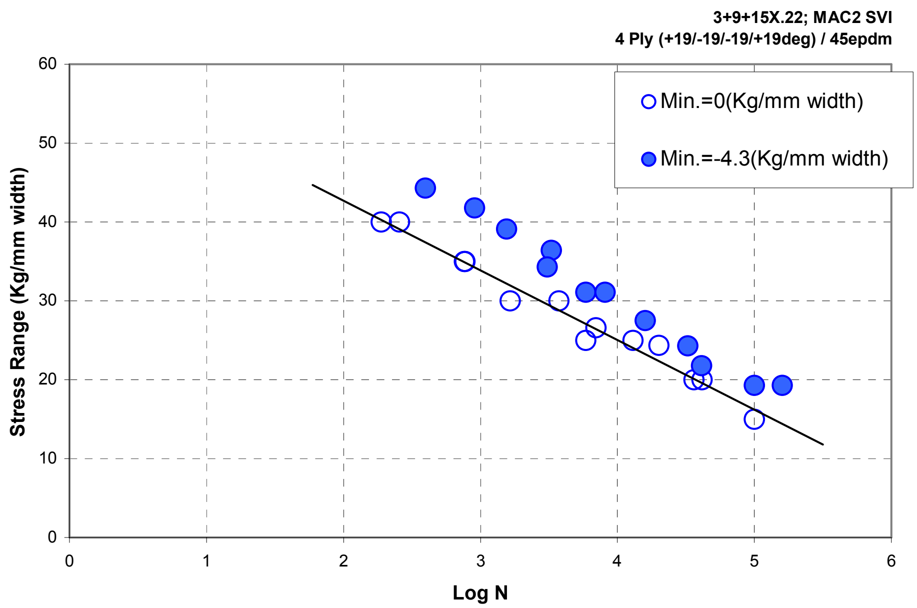

Figure 4.13 Stress range vs. fatigue life for two different minimum stresses

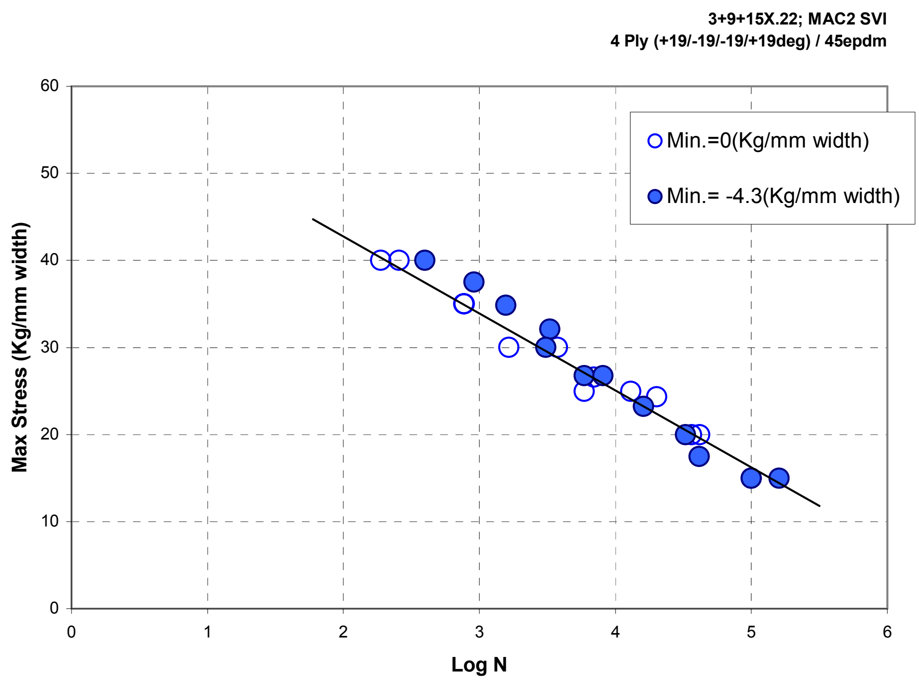

Figure 4.14 Maximum stress vs. fatigue life for two different minimum stresses

4.2.2.6 Temperature and Aging Effect

The study of fatigue behavior of tire belt composites under higher ambient temperatures (60°C, 100°C, and 140°C) was pursued to evaluate the thermo-mechanical response. Prior to the study of fatigue behavior of tire belt composites, static tension tests were performed using 4-ply symmetric laminates type C3 at elevated temperatures (60 and 100°C). It was observed that the static strength of specimens at the 60°C is 53.8MPa and that at 100°C is 44.8MPa. As a result, the fatigue lifetime at room temperature (25°C) is exponentially longer than that under high elevated temperature (100°C) at a given stress amplitude (Figure 4.15). However, when plotted against the stress range divided by static strength, the three normalized S-N relationships (% static strength vs. fatigue life) tend to merge into a single trend (Figure 4.16). The S-N data at 60°C indicated that this temperature level especially under short term testing with high stress, did not significantly influence the fatigue life of belt composites.

As observed above, the fatigue life time of MAC2 matrix composites is exponentially longer than that of MAC2-SVI matrix composites at a given stress amplitude (Figure 4.10) and two normalized S-N relationships (% single cycle strength vs. fatigue life) confirmed that there is no change of failure mode (Figure 4.11).

As can be seen in Figures 4.15 and 4.17, MAC2-SVI matrix composites have essentially the same single cycle stress at different temperatures (25°C, 60°C, and 100°C) (Figure 4.15) and MAC2 matrix composites have essentially the same single cycle stress at high elevated temperatures (100°C and 140°C), but not at 25°C (Figure 4.17).

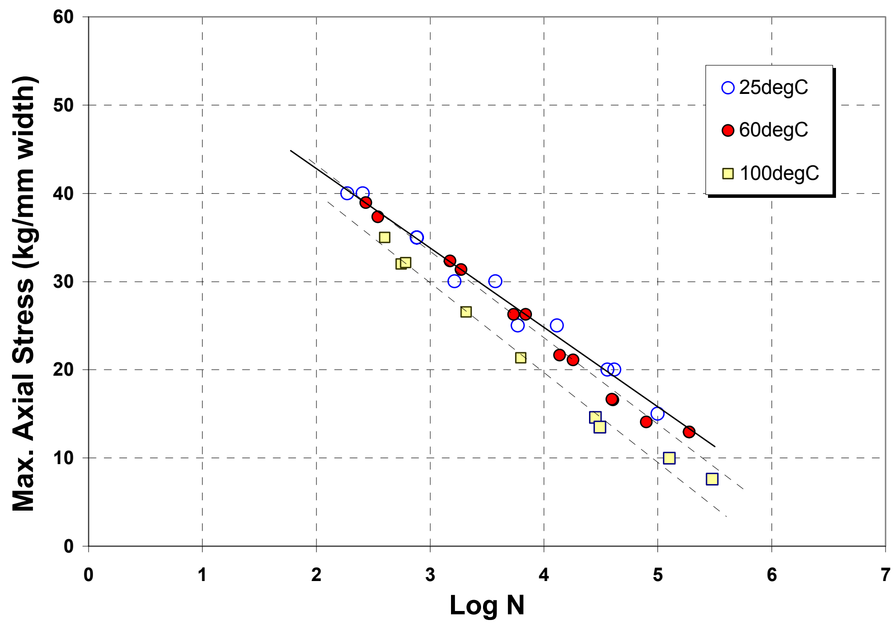

Figure 4.15 S-N data with MAC2-SVI under three different ambient temperatures

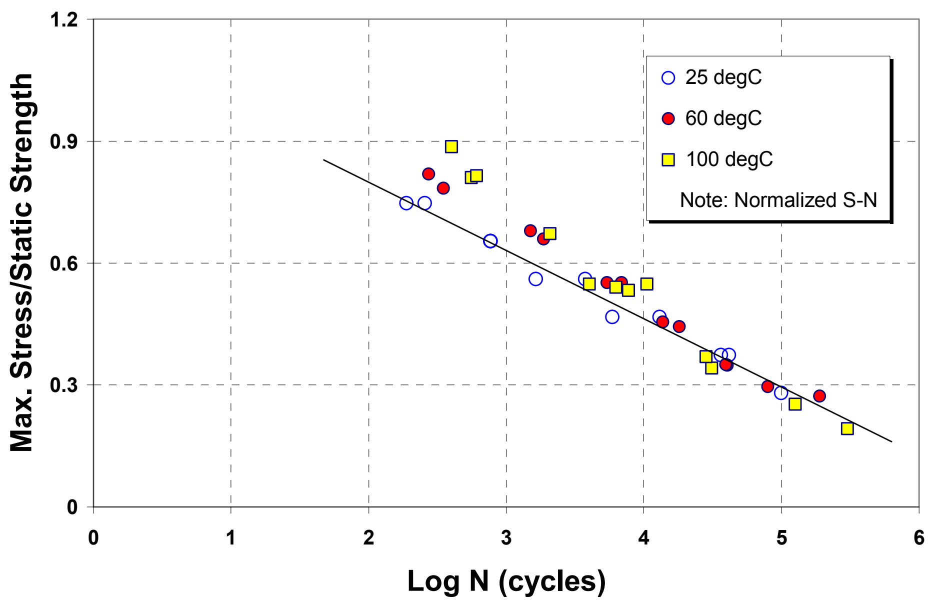

Figure 4.16 Normalized S-N data with MAC2-SVI under three different ambient temperatures

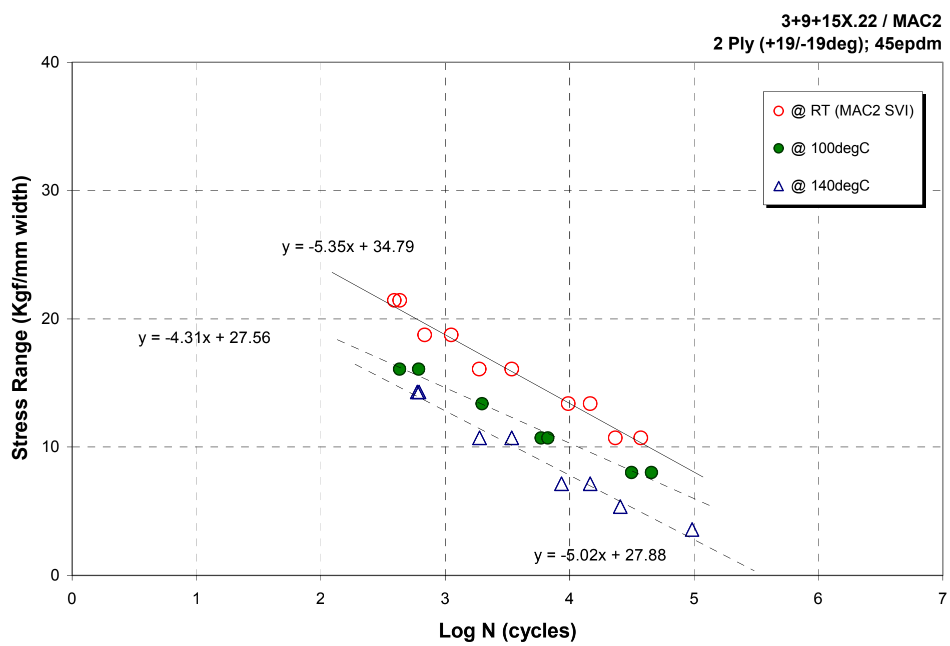

Figure 4.17 S-N data with MAC2 under two different ambient temperatures

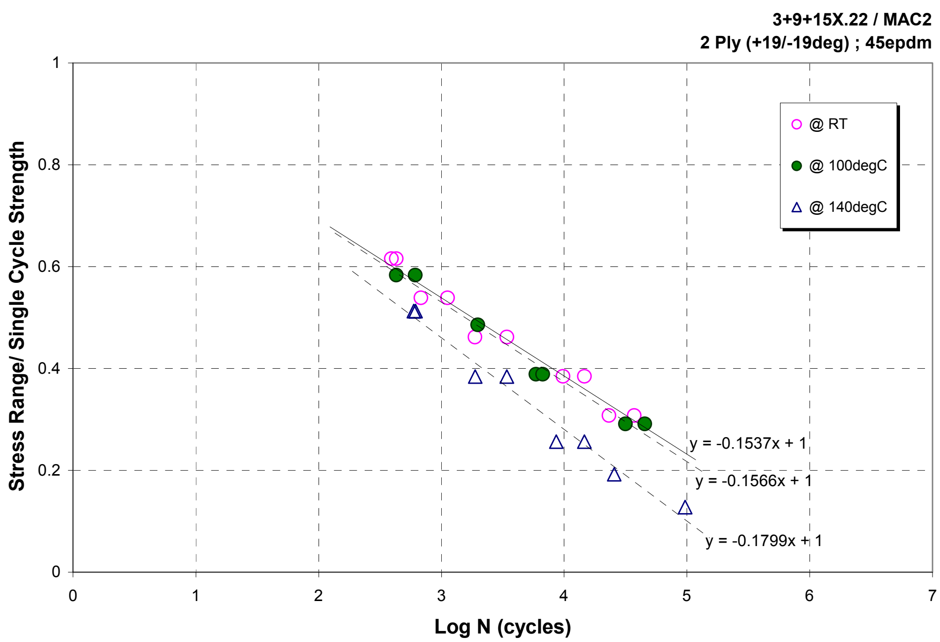

Figure 4.18 Normalized S-N data with MAC2 under two different ambient temperatures

As a result, MAC2-SVI matrix composites have slight changes of failure mode at 60°C and 100°C (Figure 4.16), however, MAC2 matrix composites have no change of failure mode up to 100°C although there seems to be a change of failure modes at 140°C (Figure 4.18).

For the study of heat aging effects in the fatigue behavior of tire belt composites, MAC2-SVI matrix composites were aged for 70 hours at 100°C. The single cycle strength of the aged specimens was essentially the same as that of the pre-aged specimens as shown in Figure 4.19. However, there is a change of failure mode due to matrix degradation (Figure 4.20). As a result of the hardening of the rubber matrix due to heating, the values of maximum cyclic strain at failure for pre-aged laminates were lower than those for before aging (Figure 4.21). In addition, as can be seen in Figures 4.22 and 4.23, the S-N data and failure modes of MAC2-SVI matrix composites under an elevated temperature of 100°C and after aging tend to merge into one trend. Therefore, this indicates that the effect of an elevated temperature of 100°C and the aging effect for 70 hours at 100°C are essentially the same.

4.2.2.7 Effect of Interply Rubber Insert

To assess the effect of interply rubber thickness, the panels with the insert of rubber A, which is same with MAC2 SVI, between the plies of 2-ply +19/-19° composite laminates reinforced with two different cords, 3+9+15X.22 and 3/6X.35, were tested. The insert of rubber A increased the laminate thickness by 20%.

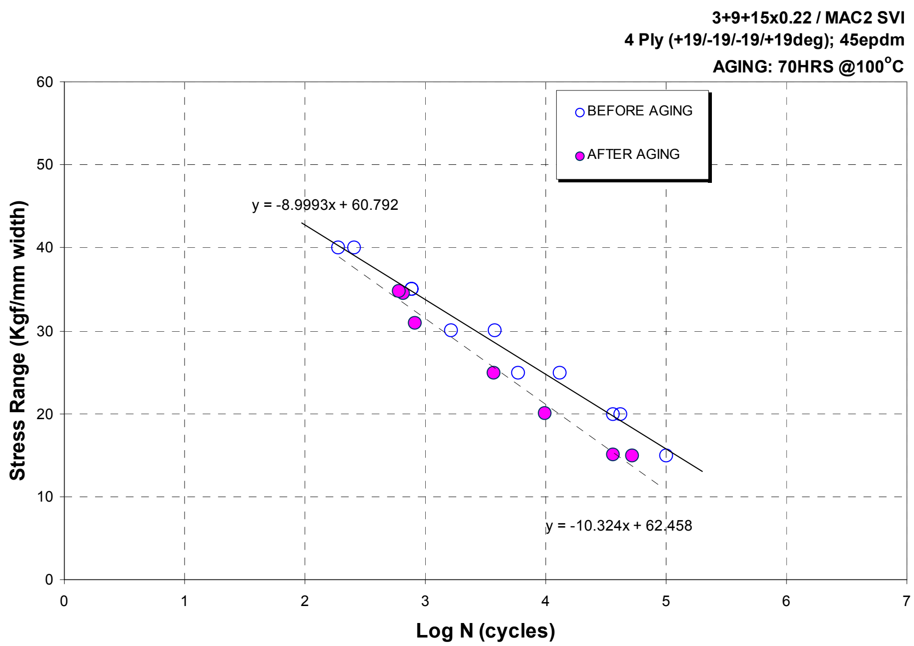

Figure 4.19 S-N data for aging effect for type C3

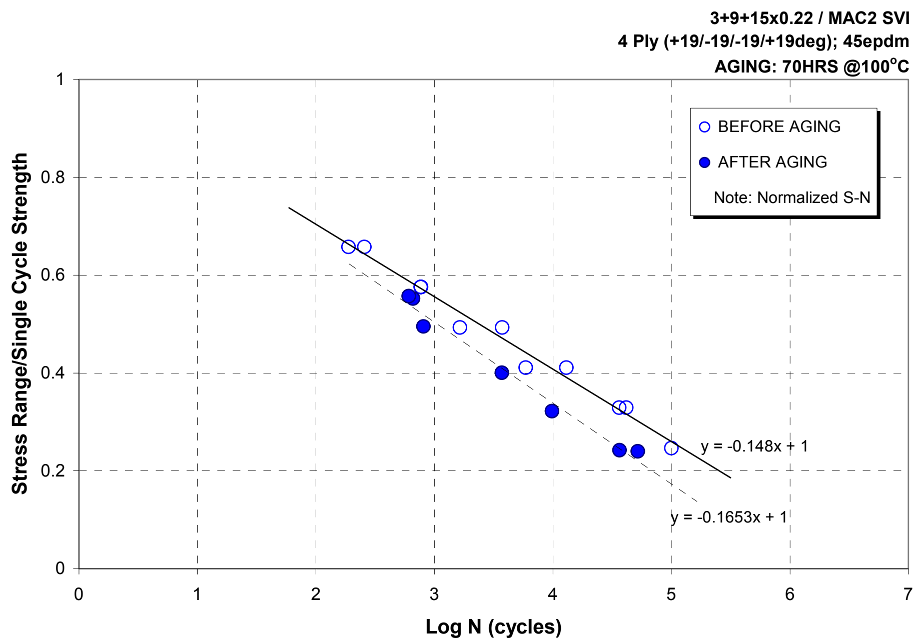

Figure 4.20 Normalized S-N data for aging effect for type C3

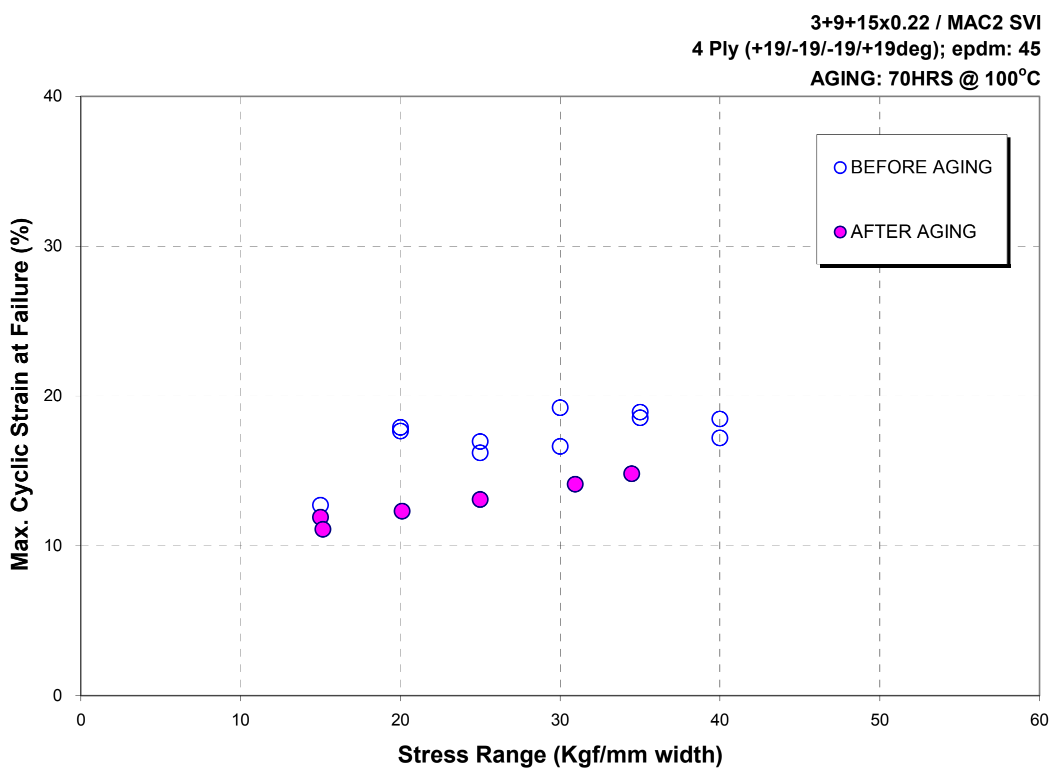

Figure 4.21 Cumulative strain at failure before and after aging for type C3

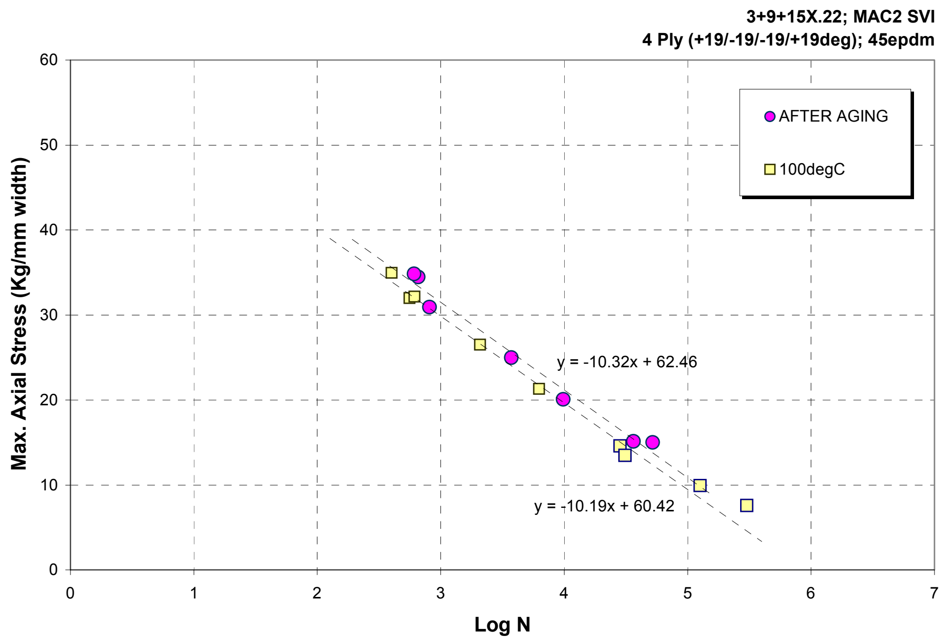

Figure 4.22 Comparison between temperature and aging effect for type C3

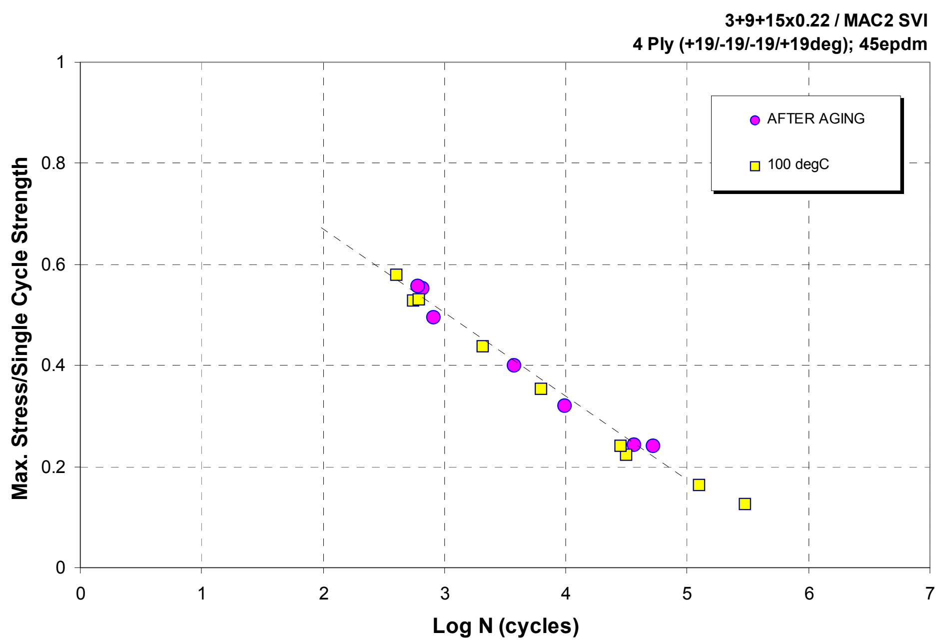

Figure 4.23 Normalized S-N data for temperature and aging effect for type C3

This increase of interply rubber thickness led to *higher* values of static tensile strength for both composite laminates (Table 4.1). In accordance with the relationship between static strength and the S-N data, the increase of interply rubber thickness tended to *raise* the fatigue lifetime of the composite laminate at an intermediate level of stress amplitude (Figures 4.24 and 4.25). However, the increase in the fatigue lifetime of the composite laminate became less noticeable at very low stress amplitudes. The data scatter associated with the fatigue life at very high stress amplitude in Figure 4.24 is regarded as an anomaly. These preliminary results suggest that the increase of interply rubber thickness raises a critical level of interply shear strain or stress for cord-matrix debonding but may not be able to lower the rate of edge crack propagation under cyclic loading.

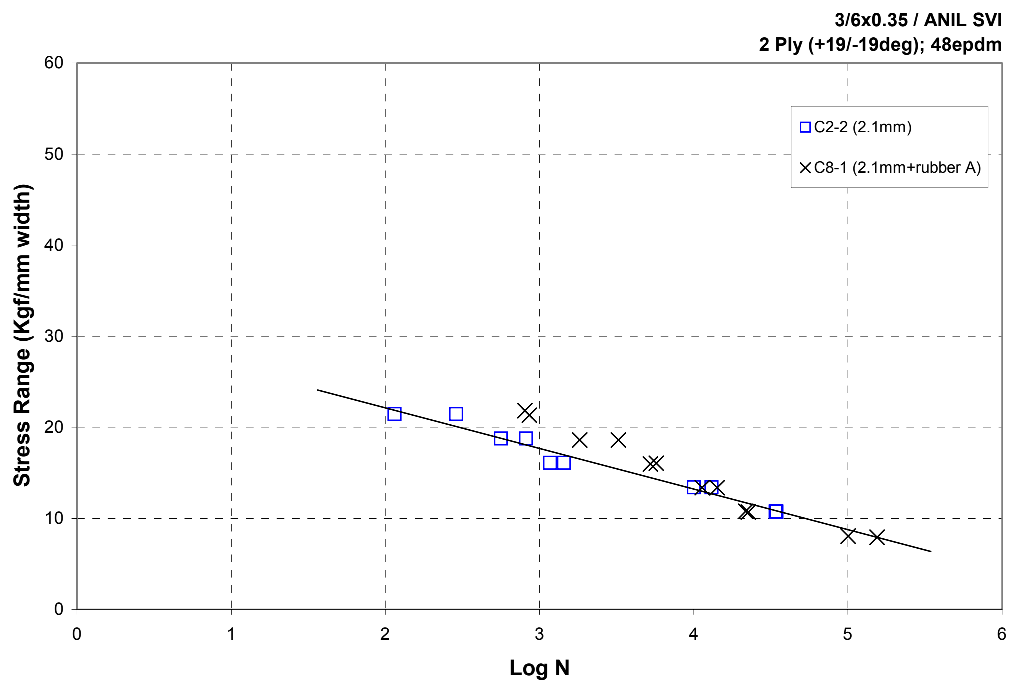

Figure 4.24 S-N data for rubber insert effect for type C2 with 3/6x0.35 cord

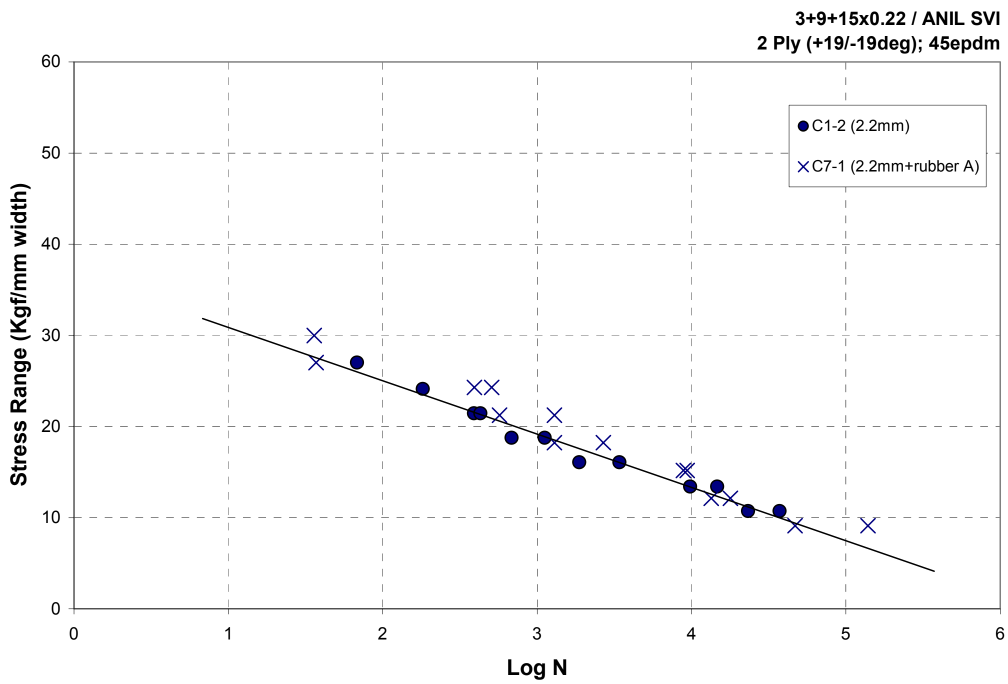

Figure 4.25 S-N data for rubber insert effect for type C1 with 3+9+15x0.22 cord

4.2.3 Dynamic Creep

For all composite laminates discussed in relation to the S-N data, the values of effective cyclic strain were continuously monitored to define a *dynamic creep rate* and a *maximum cyclic strain value at failure*. Maintaining the constant cord angle, the composites' maximum cyclic strain at failure, which measures the total strain accumulation or cumulative creep strain for gross failure, was found to be nearly independent of stress amplitude and close to the level of static failure strain (Figure 4.26). Therefore, as in the case of static failure strain (Figure 3.4), the values of maximum cyclic strain at failure for 2-ply laminate of type C1 were lower than those for 4-ply laminate of type C3. On the other hand, the values of maximum cyclic strain at failure were slightly higher for the [+25/-25^{o}]2s laminates with respect to the case of the [+19/-19^{o}]2s laminates due to the increased compliance of composites with larger cord angle (Figure 4.26). This behavior is different from that observed in the case of the static failure strain (Figure 3.5). As discussed earlier, similar values of static strain at gross failure were observed for both laminates, presumably due to excessive data scatter that made it difficult to discern the increased compliance of composite laminates with larger cord angles.

In contrast to the case of maximum cyclic strain at failure, the values of dynamic creep rate, the rate of resultant strain increase, which is taken to reflect the rate of irreversible damage accumulation, were exponentially higher with increasing stress amplitude.

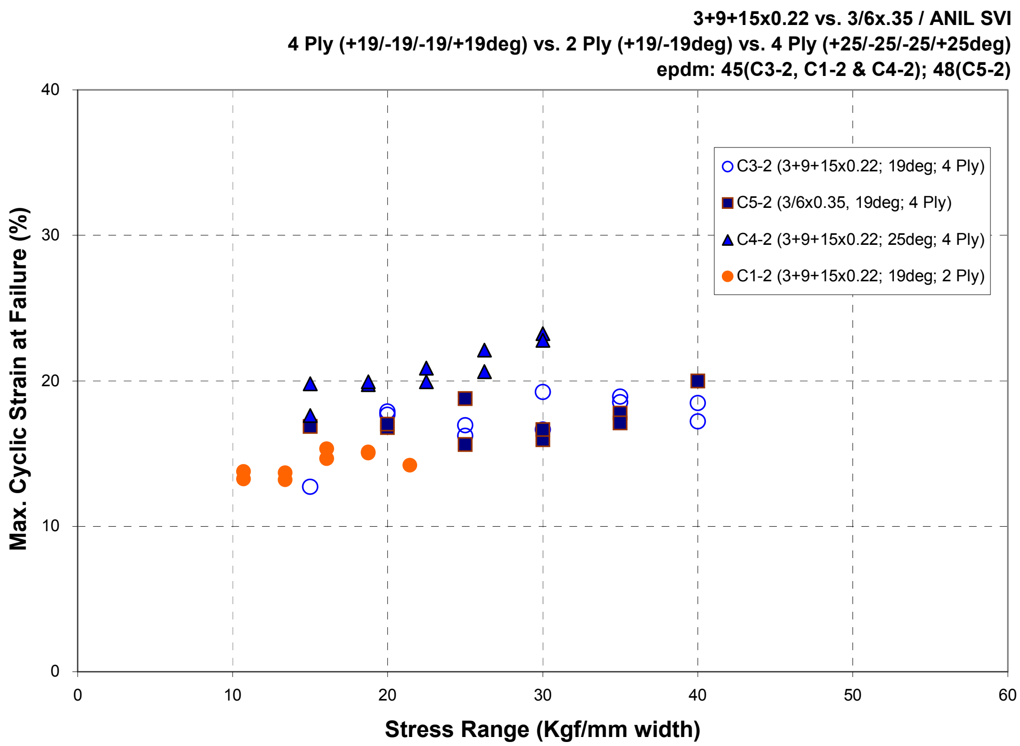

Figure 4.26 Master curve for max cyclic strain at failure vs. stress range

Confirming the same trend observed in earlier studies, fatigue lifetimes of all composite laminates in the current study were linearly proportional to the *inverse* of the dynamic creep rate, i.e., the time required to increase cyclic strain by a unit amount (Figure 4.27). Since the maximum cyclic strain for failure is nearly constant (Figure 4.26), the results indicate that the use of higher stress amplitude leads to the decrease of fatigue life by simply shortening the time to reach the critical level of strain for gross failure. As observed earlier, the damage initiation and eventual structural failure of angle-plied cord-rubber composite laminates seems to be an exclusively "strain-controlled" process.

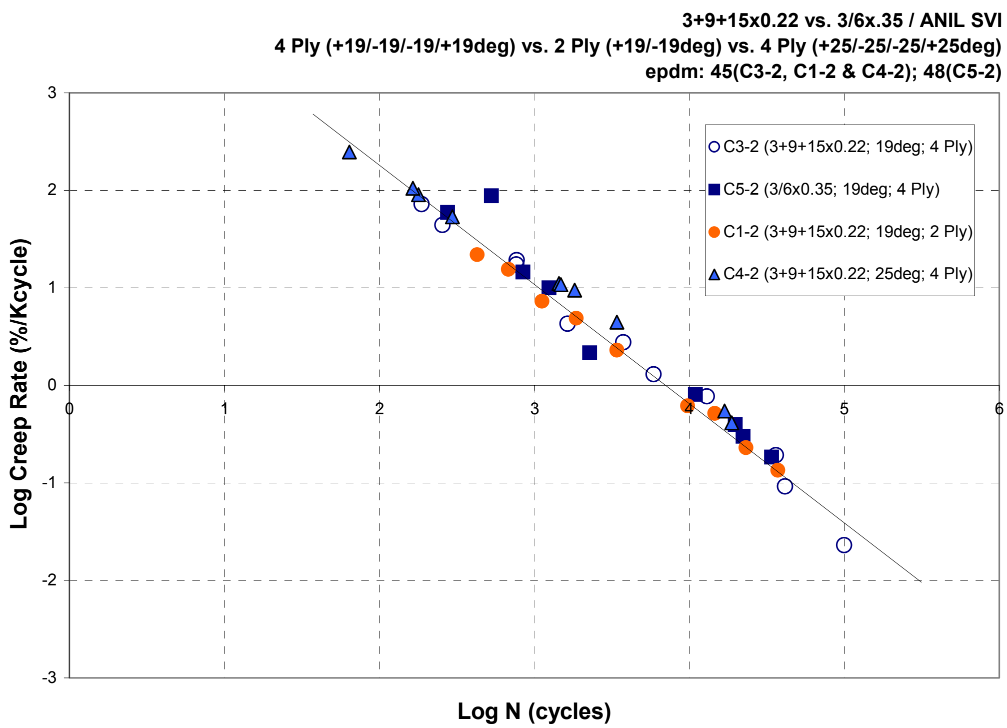

Figure 4.27 Master curve for dynamic creep rate vs. fatigue life

4.2.4 Heat Dissipation

The heat dissipation of belt composites, based on temperature measurements obtained by inserting a thermocouple between two center plies of the same cord angle, was found to occur in a cyclic fashion, essentially "in-phase" with the stress cycles (Figures 4.28 and 4.29). Cyclic changes of temperature could be monitored only when the stresses were relatively high (Figures 4.28 and 4.30). The temperature measurement was affected by the time lag due to heat transfer from the interlaminar region to the thermocouple. As a result, low cyclic loading condition of Figure 4.30 eventually led to the temperature rise over a larger period of time (Figure 4.31).

Along with the values of resultant cyclic strain, heat dissipation characteristics were monitored for all 4-ply symmetric laminates. A considerable amount of heat dissipation due to hysteretic loss in the rubber matrix was observed even at the relatively low frequency of 1 Hz. The shorter fatigue lifetimes of composites at higher stress amplitude were accompanied by greater rates of heat dissipation (Figure 4.32). The *temperature rise rate* of composite laminates becomes exponentially higher with increasing stress amplitude, similarly to what is observed in the case of the dynamic creep rate. However, for shorter fatigue lifetimes, that is at higher stress amplitudes, higher *temperatures* were not always observed (Figure 4.33). One important finding is that a linear correlation can be drawn between the dynamic creep rate and temperature rise rate for all composite laminates for tests with frequency of 1 Hz (Figure 4.34).

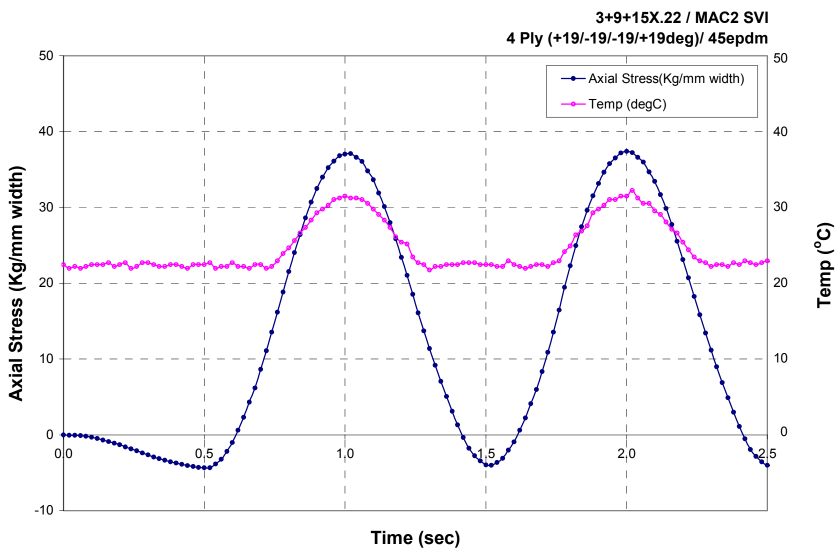

Figure 4.28 Temperature and axial stress profile for type C3

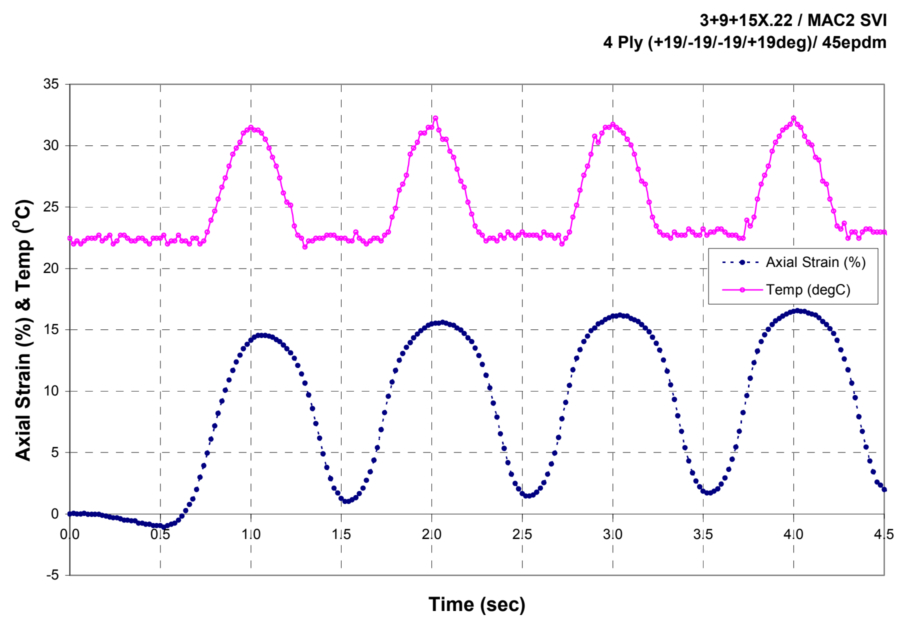

Figure 4.29 Temperature and axial strain for type C3

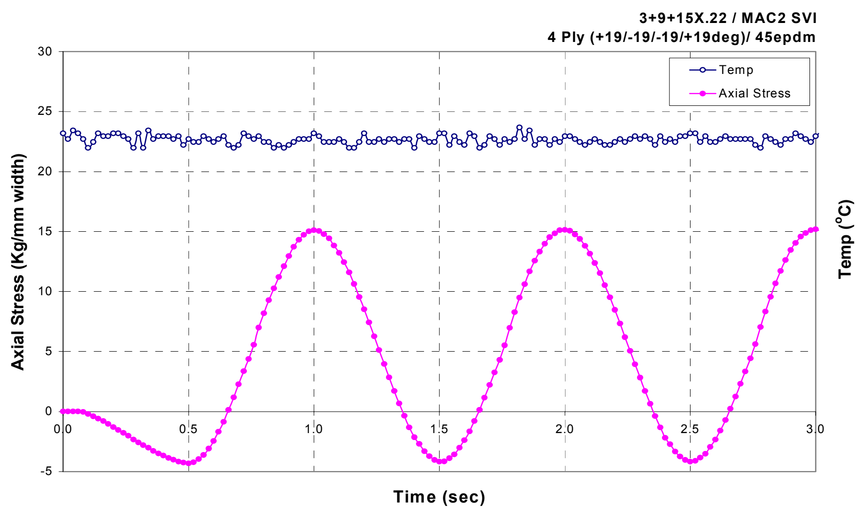

Figure 4.30 Initial temperature profile under low cyclic loading for type C3

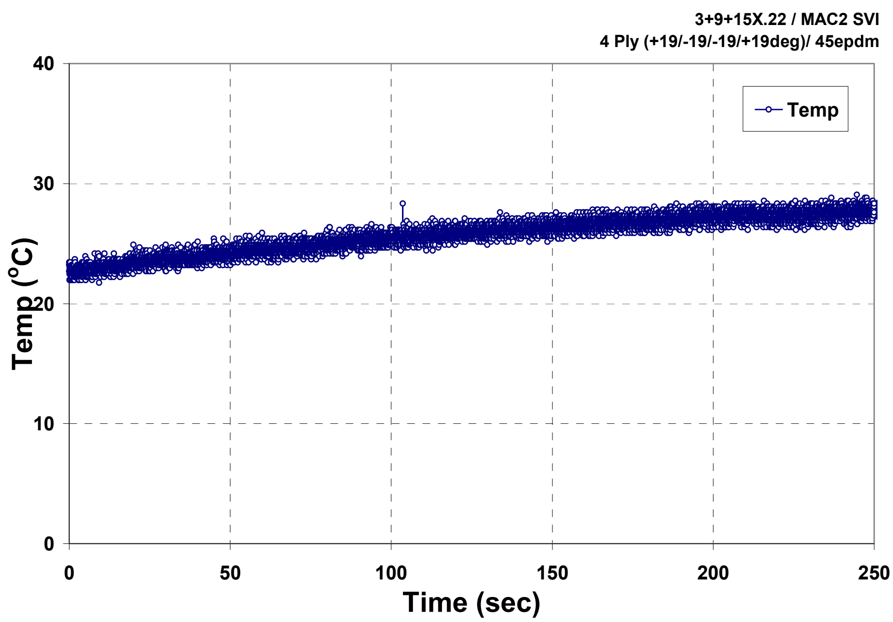

Figure 4.31 Temperature profile after moderate time under low cyclic loading for type C3

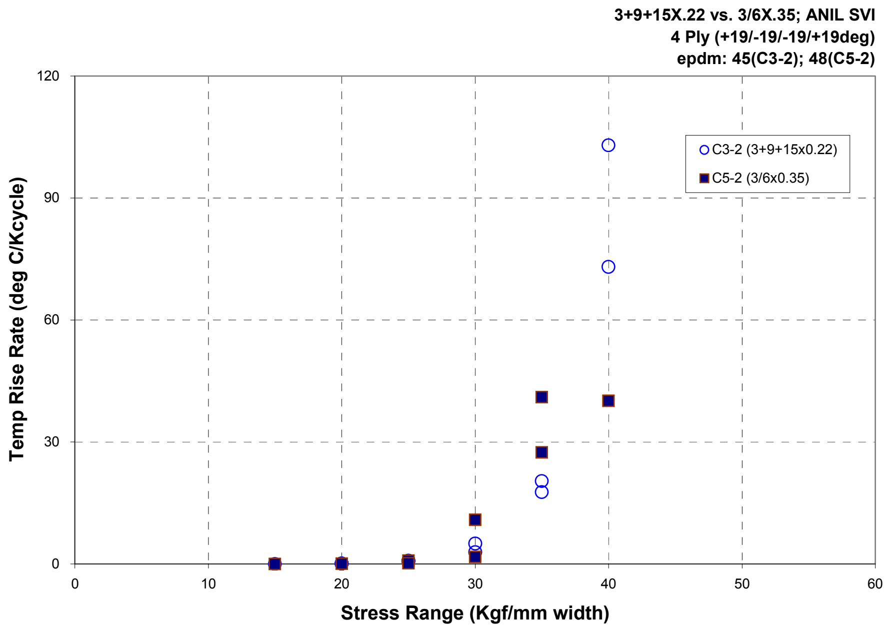

Figure 4.32 Temperature rise rate vs. stress range for different cord construction

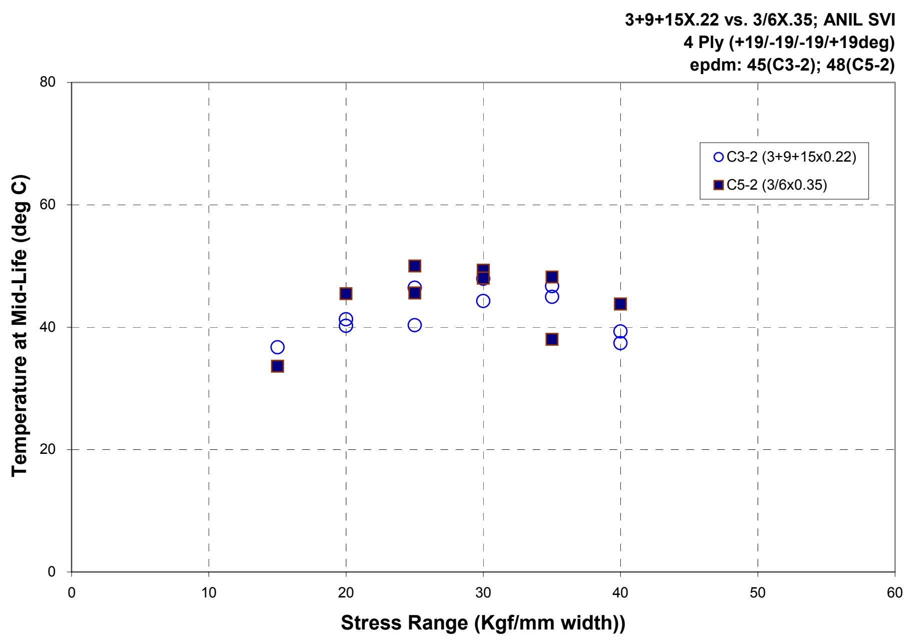

Figure 4.33 Temperature at mid-life vs. stress range for different cord construction

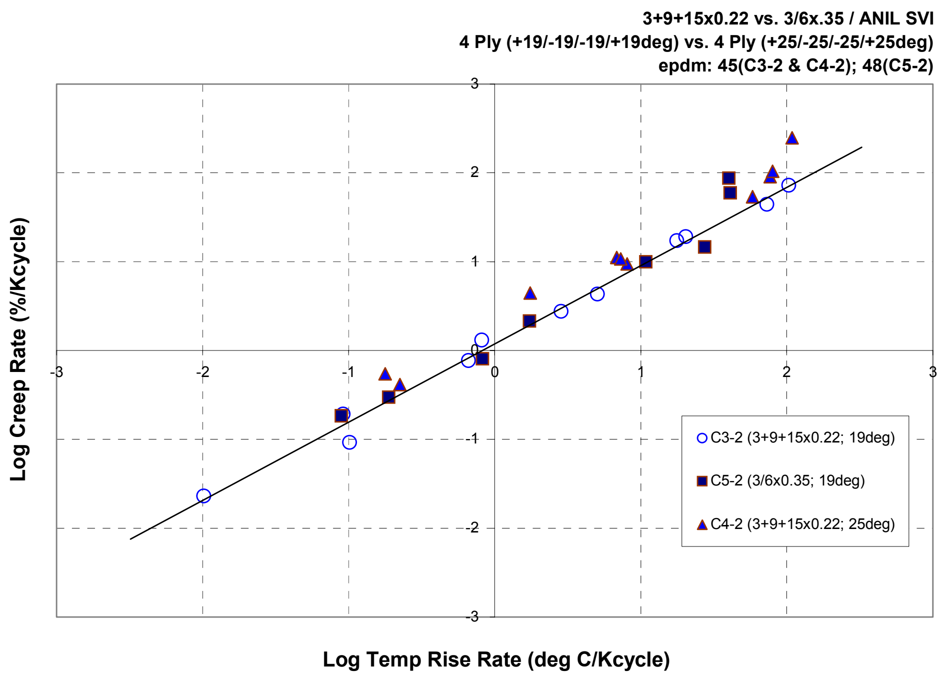

Figure 4.34 Master curve for temp rise rate vs. dynamic creep rate

4.2.5 Acoustic Emission Behavior during Fatigue Loading

As a potential technique for monitoring of damage accumulation, the acoustic emission (AE) analysis has been evaluated in this program. Before AE response was monitored, specimens were pre-loaded for the duration of 300 cycles at 40.0MPa maximum applied stress level in order to minimize data scattering problems. After pre-loading, AE analysis was conducted under several different maximum stress levels to get a relationship between fatigue lifetime and AE response (Figure 4.35). There was a sudden increase of AE energy which was caused by the friction of the specimen against the grips, background noises, or unexpectedly large damage due to material discontinuity. However, when there was no increase of AE response for a while after a sudden increase of AE, this phenomenon could not be interpreted as noise interference.

Under cyclic tension, AE occurs as soon as the loading starts. With progressive build-up of damage in composites, cumulative values of AE counts, events, or energy tended to increase steadily. These cumulative values of AE were compared each other (Figure 4.36). Since AE events showed the best linear relation between AE accumulation and number of cycles to failure, AE events accumulation data will be evaluated to predict fatigue lifetime of cord-rubber composite in next chapter.

The rate of increase in cumulative AE activities was found to be closely related with the fatigue life of cord-rubber composite specimen. As shown in Fatigue 4.37, the rates of AE events accumulation were linearly proportional to the maximum applied stress of C3 composite.

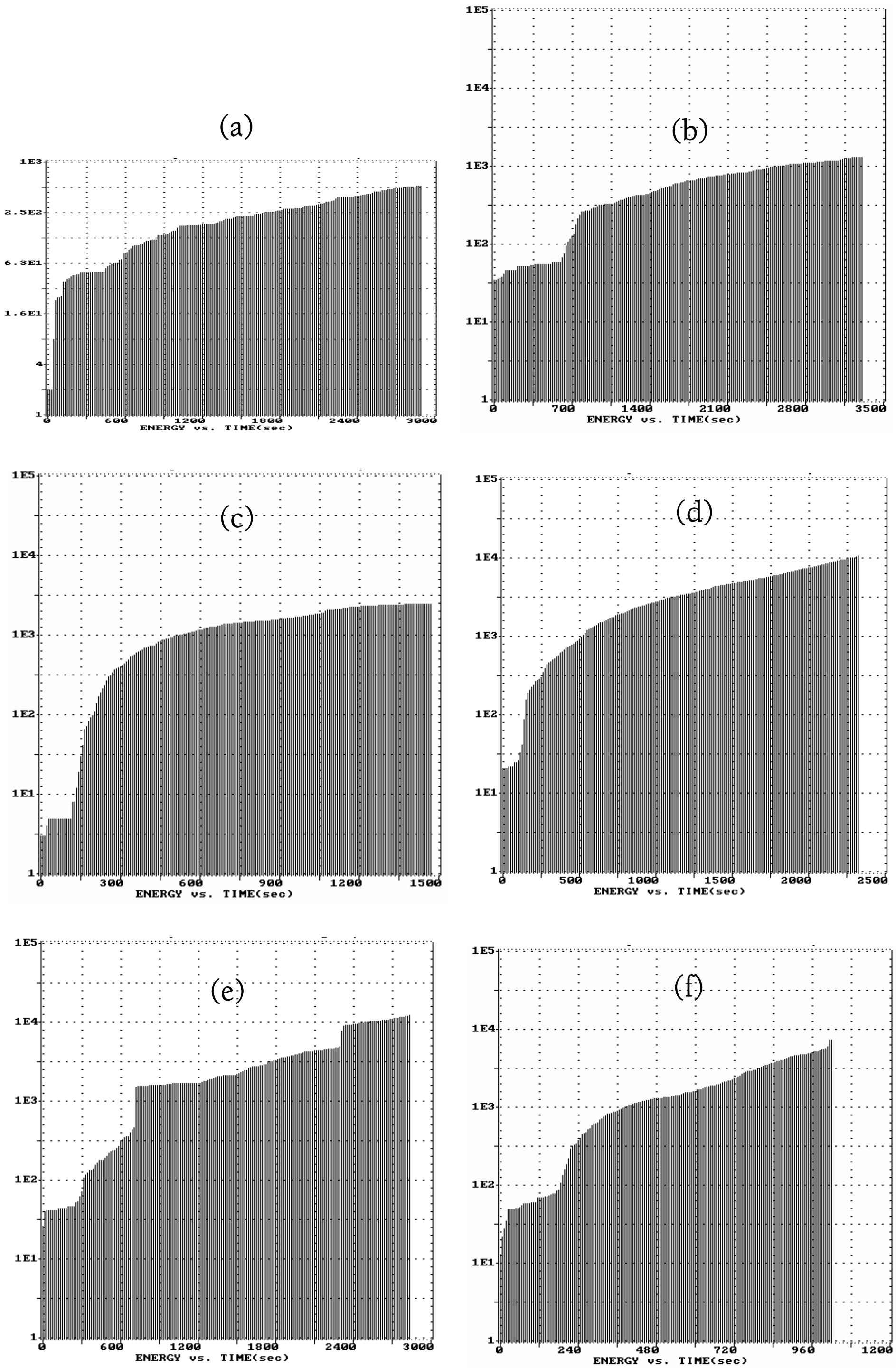

Figure 4.35 AE energy vs. time for type C3 composite under 1Hz at varied maximum stresses; (a) 16.8MPa, (b) 22.4MPa, (c) 28MPa, (d) 33.6MPa, (e) 36MPa, and (f) 39.2MPa

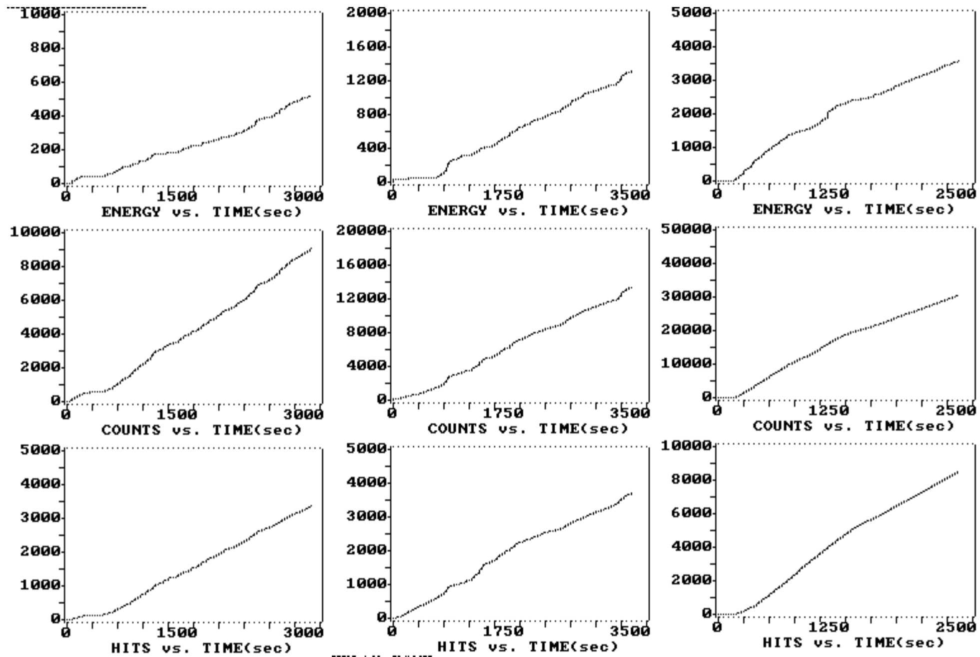

(a) 16.8MPa (b) 22.4MPa (c) 28MPa

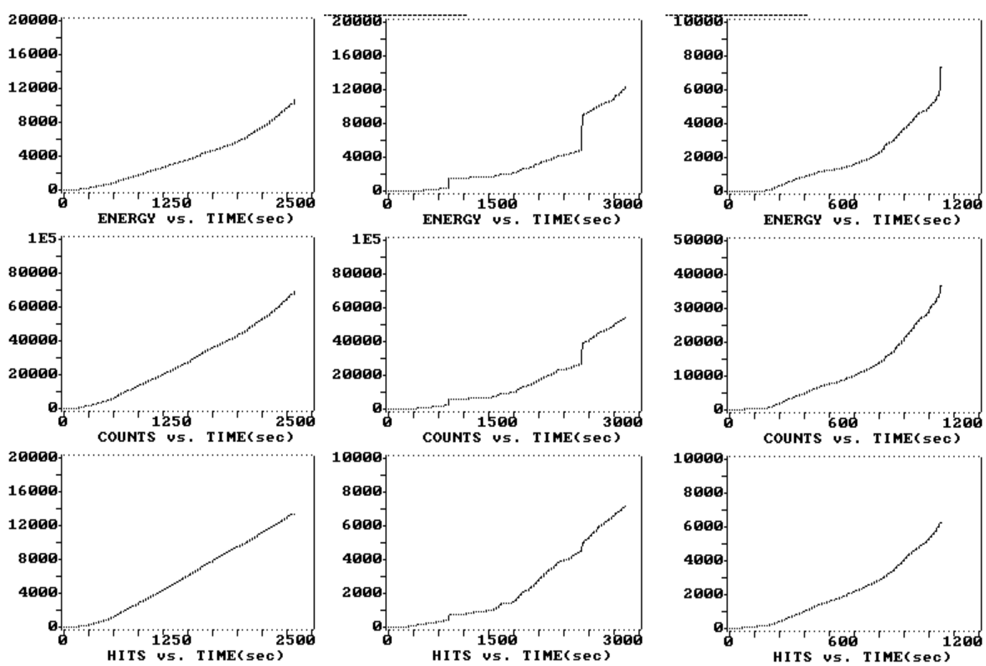

(d) 33.6MPa (e) 36MPa (f) 39.2MPa

Figure 4.36 AE signal accumulation trends at different maximum applied stresses

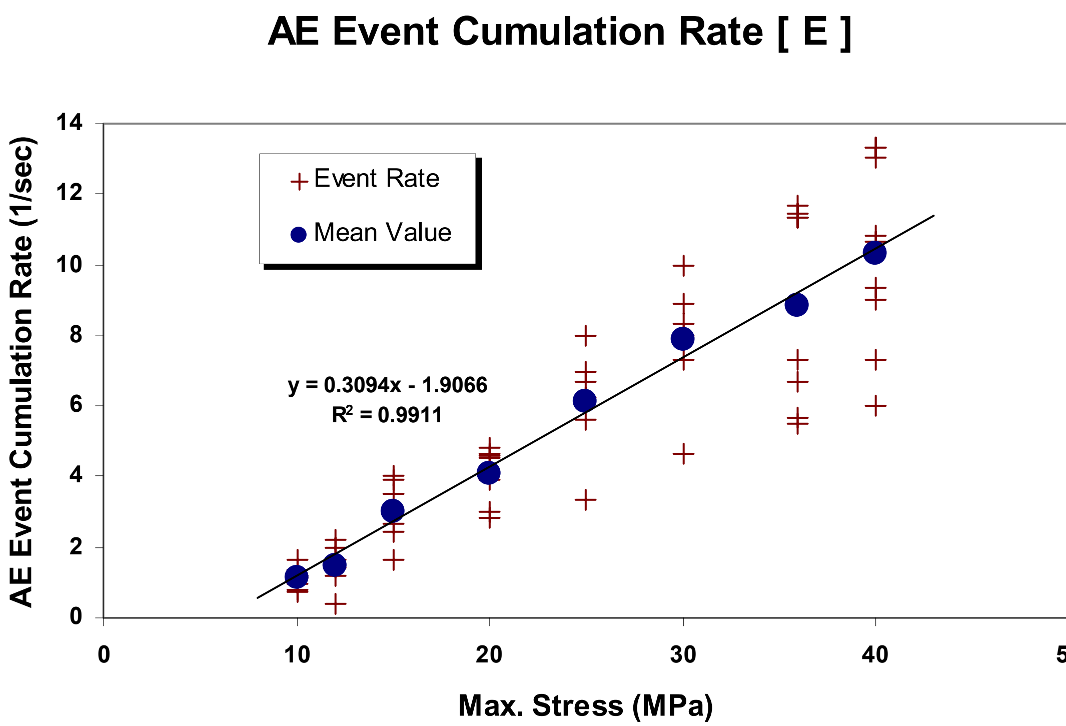

Figure 4.37 The accumulation rate of AE event vs. maximum applied stress for type C3 after 300 cycles under maximum stress 40MPa

As discussed earlier, the maximum applied stress level is logarithmically proportional to the fatigue life of cord-rubber composite except at very high cycles fatigue. Therefore, it is clear that the rate of AE signal accumulation is logarithmically proportional to the fatigue life of the materials tested. Nevertheless, an improvement of the test or analysis method is certainly needed to reduce the data scatter for more accurate investigation.

Chapter 5

FATIGUE LIFE PREDICTION

In conventional structural materials, cumulative damage and resulting fatigue life generally depend on the load history. Although there are several empirical relations which predict fatigue life of composite materials, the most popular method of characterizing the fatigue behavior is still the generation of S-N curves. For the composites with rigid matrix materials, in which cyclic strain increases with a progressive build-up of damage under stress-controlled fatigue loading, Hwang and Han derived a theoretical criterion for fatigue failure using a concept called "fatigue modulus." The prediction from their strain-based model agreed well with experimental data in the case of glass fiber-reinforced epoxy composite.

For the case of angle-plied cord-rubber composites, their cumulative damage and resulting fatigue life showed a strong dependence on the strain level under stress-controlled fatigue loading, and damage growth was found to be closely associated with the increase of maximum cyclic strain (referred as dynamic creep). In turn, the fatigue life of composite laminate was linearly proportional to the inverse of dynamic creep rate. The fact that observed cumulative creep strain for gross failure of composites under cyclic loading equals a static tensile strain at gross failure confirms one of the assumptions made in a strain-based fatigue failure criterion proposed by Hwang and Han for rigid matrix composites.

In addition, the acoustic emission analysis conducted in this study showed that the rate of increase in cumulative AE activities was closely related to the fatigue life of a cord-rubber composite specimen. There is a clear trend showing the fatigue life to be linearly proportional to the time required to increase AE by a unit amount.

With the observations mentioned above as a background, an attempt was made in this study to formulate a new empirical model which can accurately predict the fatigue life of angle-plied cord-rubber composite laminate. The result of this new model was compared with experimental results and other models. The discussion will start with the case of straight-line approximation of S-N curve.

5.1 Straight-Line Approximation of S-N Curve

When S-N data generated for type C3 were put together, a straight line could be drawn through a broad data band according to the following relation (Figure 5.1):

$$\sigma_{\max} = -a \ln N + b \tag{5.1}$$

where $\sigma_{\max}$ is the applied maximum stress, a is the slope of S-N curve, N the number of cycles to failure, and b the single cycle stress. Two constants of the above relation were found to be: a = 4.2787; b = 67.658. Using the above equation, the failure life of materials can be predicted as follows:

$$N = \exp\left(\frac{b - \sigma_{\max}}{a}\right) \tag{5.2}$$

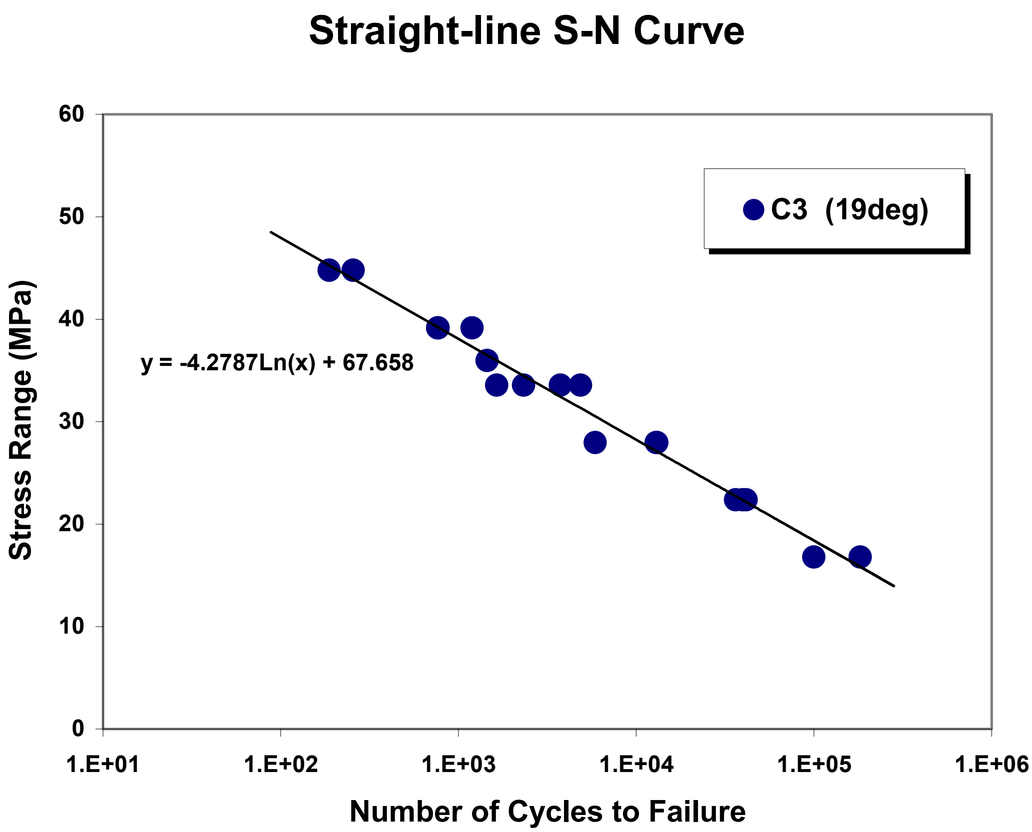

Figure 5.1 S-N curve for type C3 cord-rubber composite

5.2 Hwang and Han's model based on "Fatigue Modulus"

When the angle-plied cord-rubber composite laminate under study is subjected to cyclic loading with constant amplitude of stress, maximum cyclic strain increases steadily as the loading proceeds due to the increase of damage. Noting that the model of fatigue failure proposed by Hwang and Han is based on the increase of strain, fatigue data under study were reduced according to their criterion. As discussed earlier, Hwang and Han defined fatigue modulus $F(n)$ by assuming that applied stress has a linear relationship with resultant strain at an arbitrary fatigue loading cycle; i.e. $F(n) = \sigma_a / \varepsilon(n)$ where $\sigma_{\max}$ is applied maximum stress level and $\varepsilon(n)$ resultant strain at nth loading cycle. Since the fatigue modulus is only dependent on loading cycle in their analysis, the rate of fatigue modulus degradation, dF / dn, was assumed to be a power function of fatigue cycle, n, in the form of $dF / dn = -Acn^{c-1}$ where A and c are material constants.

The results for fitting of the fatigue modulus data into a power-law relationship, $F(0) - F(n) = An^c$, and the calculation of constants A and c are shown for four different maximum stresses in Table 5.1 and Figure 5.2. Unfortunately, the constants A and c were found to depend on a maximum stress. This result contradicts the assumption used in the model that fatigue modulus is not a function of applied stress, but a function of loading cycle only. For the case of cord-rubber composite laminate, different stress level can cause different resultant strains due to their highly nonlinear relationship. Therefore, fatigue modulus of cord-rubber composite should be a function of applied stress level as well as loading cycle for an accurate analysis.

Max. Stress (MPa)	Constant A	Constant c	$F(0)$
22.4	36.933	0.1205	289.18
30.0	35.341	0.1674	305.90
33.6	22.035	0.2311	251.61
42.0	24.646	0.2513	291.65
Average	29.739	0.1926	284.59

Table 5.1 Constants A and c for type C3 defined according to Hwang and Han's model

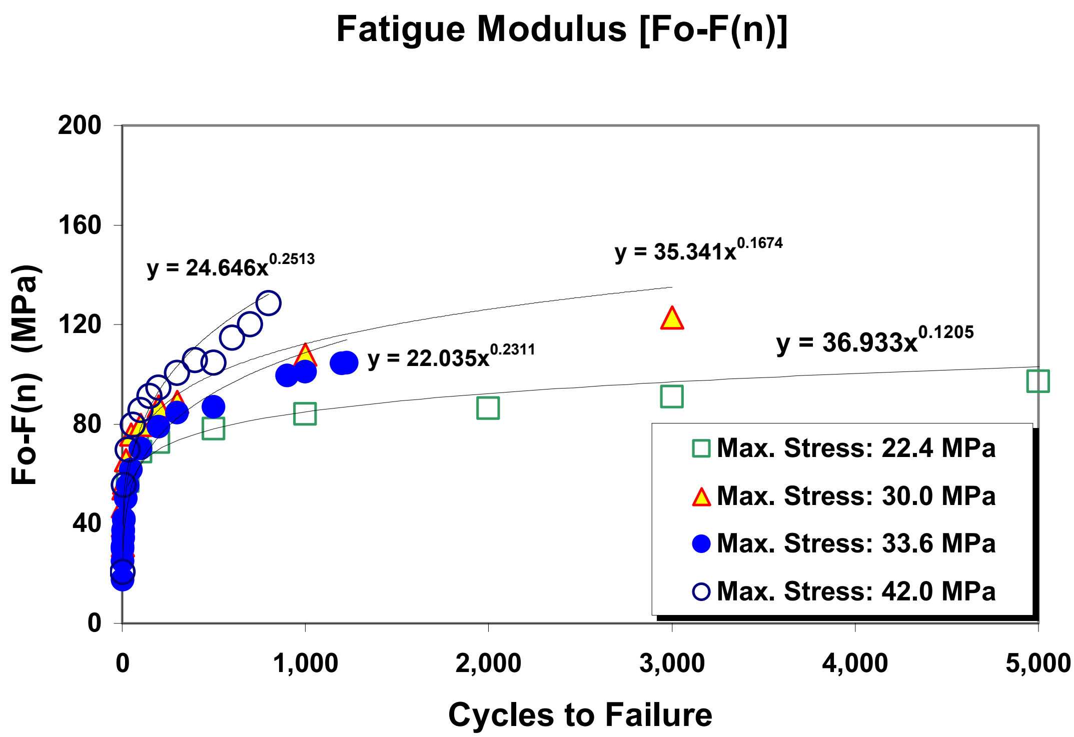

Figure 5.2 Fatigue modulus vs. the number of cycles to failure under four different maximum stresses for type C3 composite

This discrepancy between the actual data for cord-rubber composite and the predicted values from Hwang and Han's model becomes more apparent in the case of fatigue life (Figure 5.3). Fatigue life of materials, N, is predicted from the relation $N = [B(1-r)]^{1/c}$ where $B = F(0)/A$ and $r = \sigma_{max}/\sigma_u$.

When Hwang and Han compared the calculated fatigue life with experimental data, specimens used were made of glass epoxy (G-10CR Grade) composite material. Those results show an improved agreement of the proposed relationship with experimental data than the straight-line S-N curve and Basquin's relation. In the case of these specimens, the experimental fatigue life data showed a convex shape on semi-logarithmic scale, i.e. stress level vs. log scale of number of cycles to failure. As can be seen in Figure 5.3, the results predicted by Hwang and Han's model show similar convex curves for our cord-rubber composites having a straight-line trend. Therefore, a realistic trend of fatigue life profile could not be predicted from Hwang and Han's equation. Particularly, fatigue lives predicted at lower stress level are underestimated. This discrepancy stems from the assumption that the rate of fatigue modulus degradation has a power-law relationship with loading cycle. As shown in Figure 5.2, the actual data do not fit well into a power function. In addition, non-linear properties of cord-rubber composite and material constants, *A* and *c*, which are actually irregular, contribute to this disagreement. Fortunately, attempts can be made to modify Hwang and Han's theory using the logarithmic function for the fatigue modulus degradation and mean values of material constants at several maximum stress levels. These modifications will be discussed in the following section.

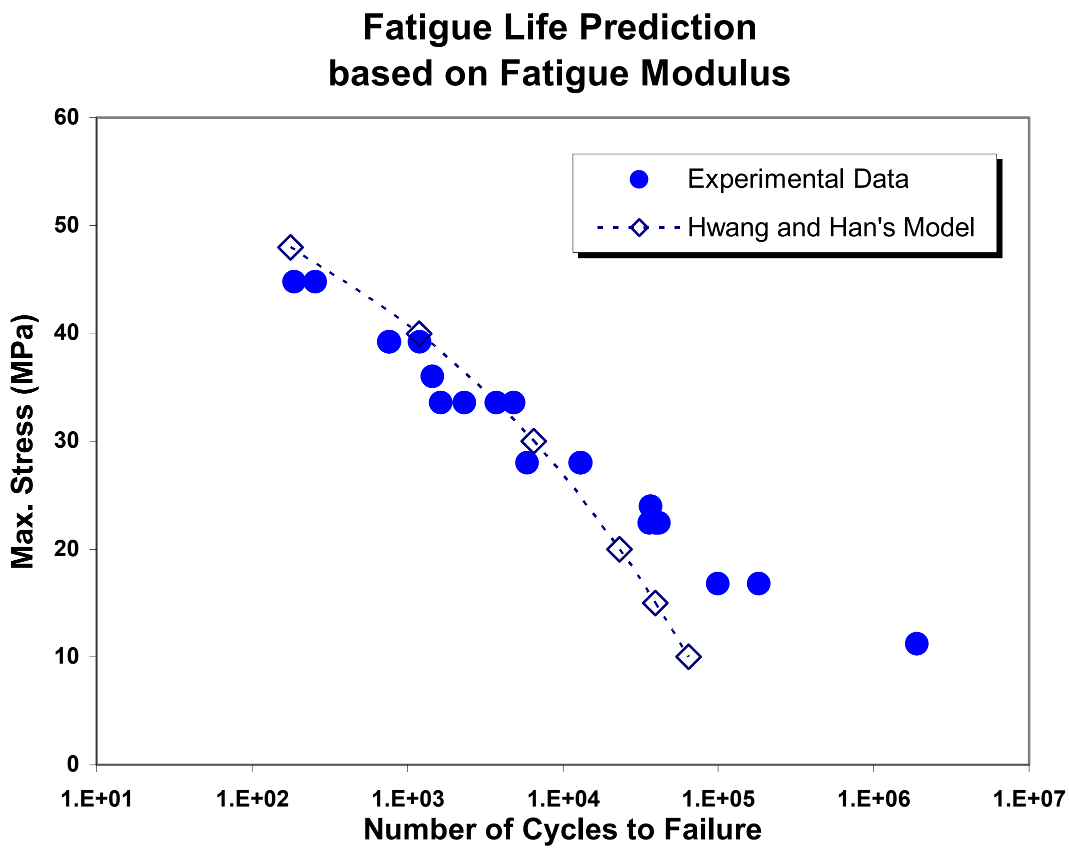

Figure 5.3 A comparison between the actual S-N curve and fatigue lifetime predicted by Hwang and Han's fatigue modulus model for type C3 composite

5.3 Our Modified Models

5.3.1 Modified Models based on Fatigue Modulus Concept

As shown in Figure 5.4, the fatigue modulus can be assumed to be followed by a logarithmic function of fatigue cycle, n, i.e.,

$$F(n) = D\ln n + k\ , \qquad n=1,\ \ldots,\ \mathrm{N} \tag{5.3}$$

where, D and k are material constants.

At failure, where $n=N$, the above equation becomes,

$$F(N) = D\ln N + k \tag{5.4}$$

Therefore, the number of cycle to failure is expressed as follows;

$$N = \exp[(F(N) - k)/D] \tag{5.5}$$

where $F(N) = \sigma_{\max} / \varepsilon_u$.

Using the above equation, the fatigue life of materials can be predicted under a strain failure criterion such that final failure of a material occurs when the fatigue resultant strain reaches the static ultimate strain, ε_u.

To verify the proposed theory, an attempt was made to compare the calculated fatigue life with experimental data and Hwang and Han's model. The results are compared in Figure 5.5. As can be expected, there is a straight-line relationship between applied maximum stress level and log-scale of number of cycles to failure. However, there is an underestimation at higher stress level above 35MPa and overestimation at lower stress below 20MPa. This trend is just opposite to Hwang and Han's model. As a result, the experimental data are shown between Hwang and Han's model and this proposed model.

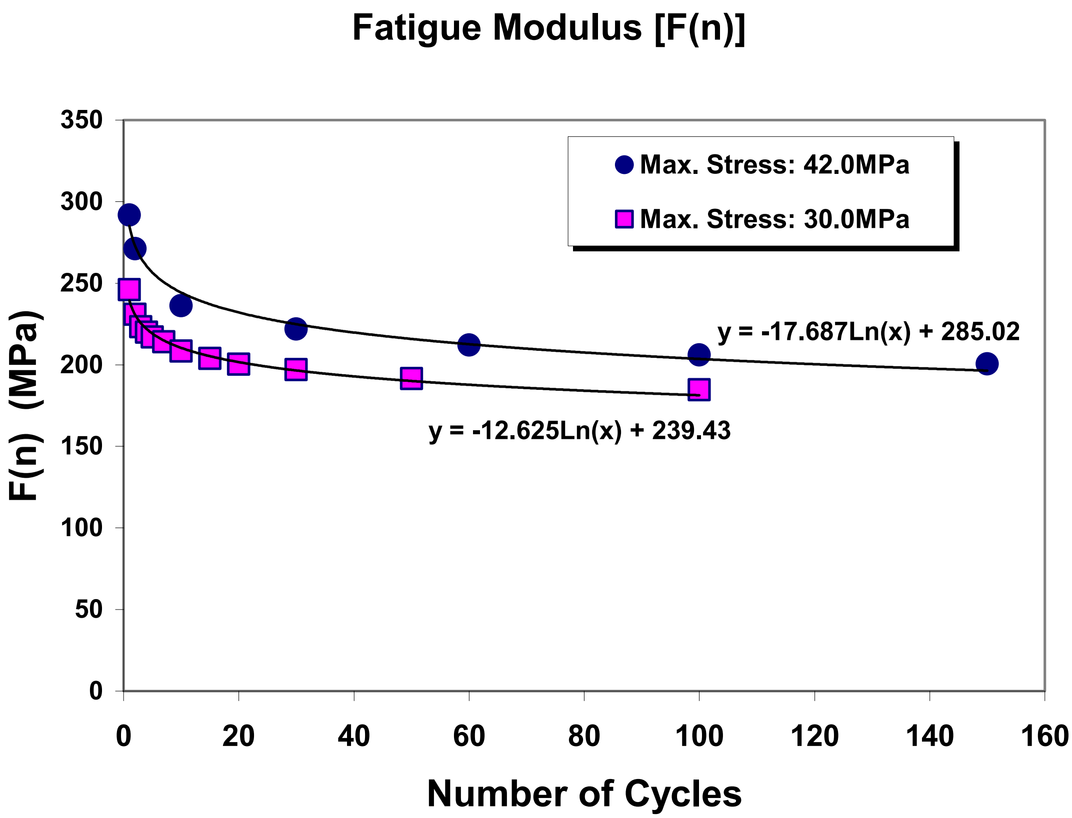

Figure 5.4 Fatigue modulus vs. number of cycles under different maximum stresses for type C3 composite

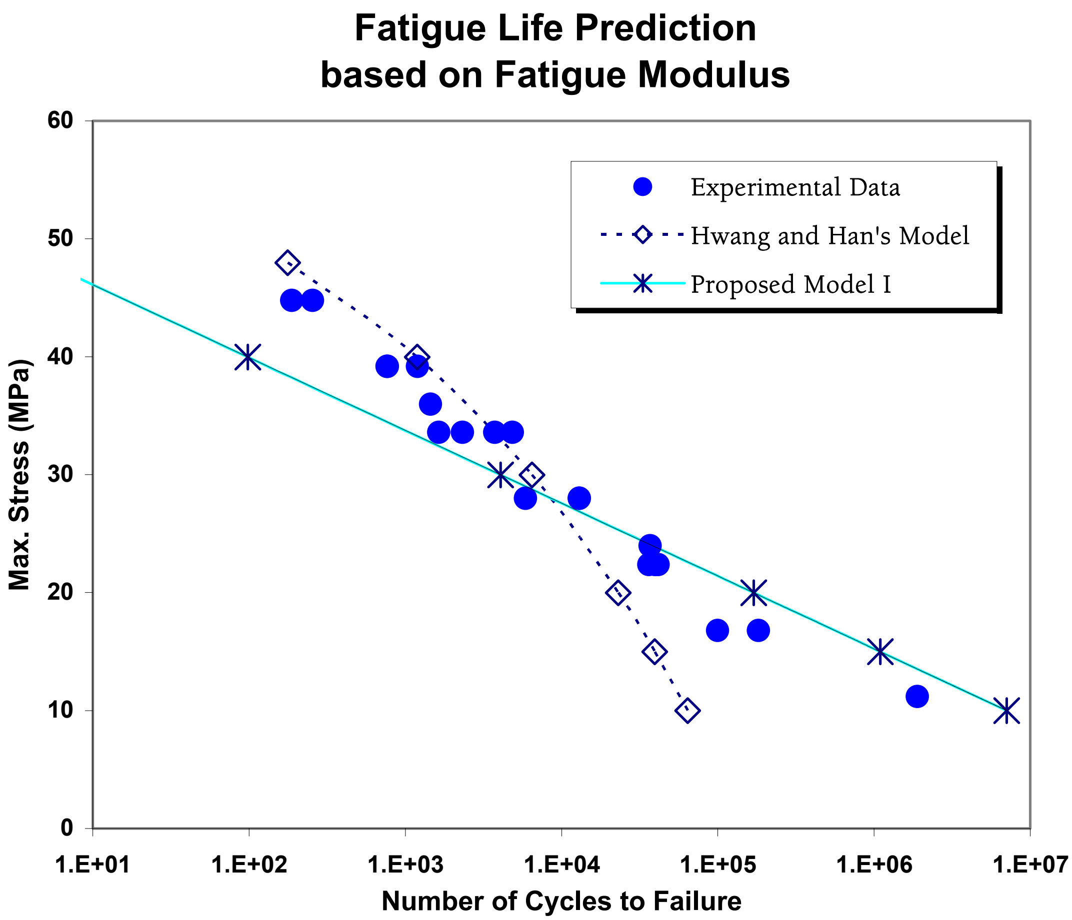

Figure 5.5 A comparison between the actual S-N curve and fatigue lifetime predicted by our modified fatigue modulus model I for type C3 composite

Therefore, more accurate fatigue life prediction can be made by combining these two models. The easiest method is to adopt mean values of two predicted fatigue lives. Therefore, the number of cycles to failure can be obtained as follows;

$$N = \frac{1}{2}\left[\left\{ B\left(1 - \frac{\sigma_{\max}}{\sigma_u}\right) \right\}^{1/c} + \exp\left\{ \frac{1}{D}\left(\frac{\sigma_{\max}}{\varepsilon_u} - k \right) \right\} \right] \tag{5.6}$$

where,

σ_u : ultimate strength

$\sigma_{\max}$: applied maximum stress

ε_u : ultimate strain (0.2 for our cord-rubber composites)

B, *c*, *D*, and *k*: material constants.

The fatigue lifetime profile of C3 cord-rubber composite laminate calculated by using the above equation is compared with experimental data in Table 5.2 and Figure 5.6. As shown by both, good agreement was found between the two cases.

5.3.2 Our Model based on AE

Before the AE response was monitored, specimens were pre-loaded for the duration of 300 cycles at a 40.0MPa applied maximum stress level in order to minimize data scattering problem. After pre-loading, an AE analysis was conducted under several different maximum stress levels to get a relationship between fatigue lifetime and AE response. Under cyclic tension, AE occurs as soon as the loading starts. With progressive build-up of damage in composites, cumulative values of AE counts, events, or energy tended to increase steadily.

Max. Stress (MPa)	Experimental Data	Hwang and Han's Model (1)	Proposed Model I (2)	Proposed Model II [Average of (1) & (2)]
44.8	2.2E+02	4.1E+02	1.6E+01	2.2E+02
39.2	9.1E+02	1.4E+03	1.3E+02	7.7E+02
33.6	2.6E+03	3.7E+03	1.1E+03	2.4E+03
28.0	1.1E+04	8.6E+03	8.6E+03	8.6E+03
22.4	3.9E+04	1.7E+04	6.9E+04	4.3E+04
16.8	1.4E+05	3.3E+04	5.6E+05	3.0E+05
11.2	1.9E+06	5.7E+04	4.5E+06	2.3E+06

Table 5.2 Fatigue life comparison with experimental data

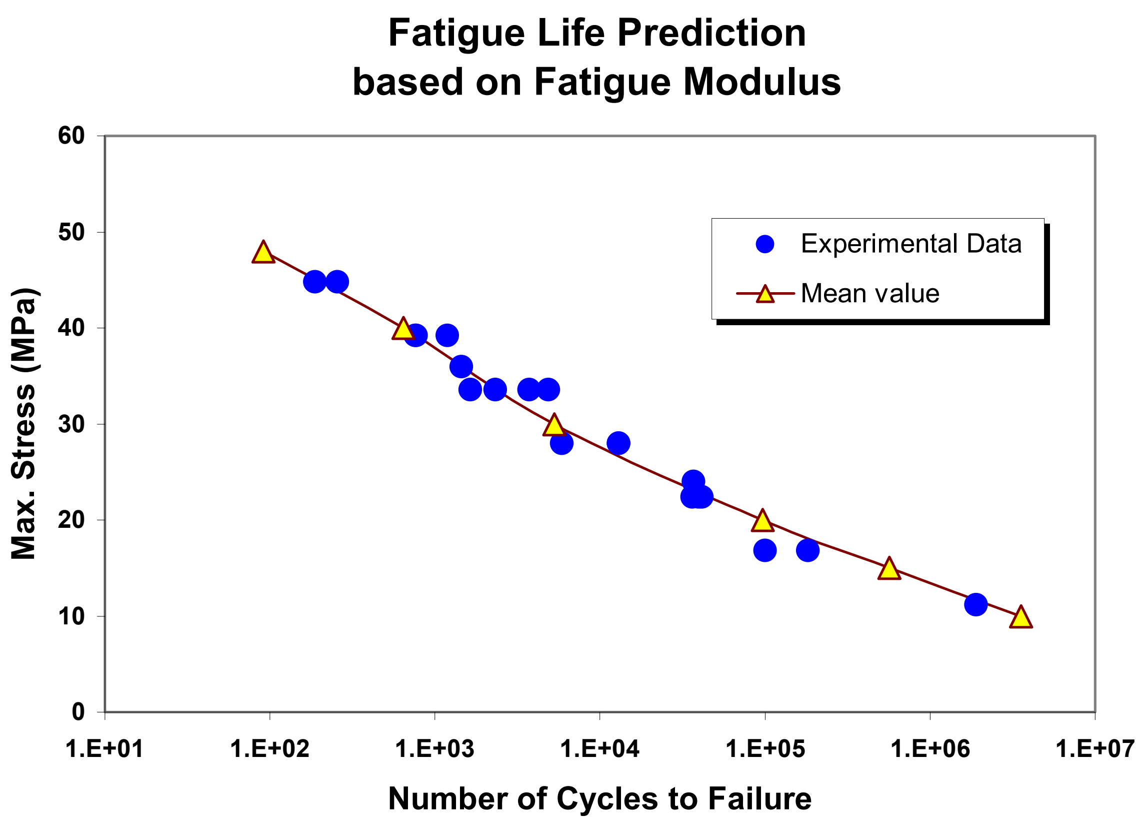

Figure 5.6 A comparison between the actual S-N curve and fatigue lifetime predicted by our modified fatigue modulus model II for type C3 composite

However, this tendency was often complicated by a sudden increase of AE which was probably caused by unexpected matrix cracking or debonding. Because there was no increase of AE response for a short time interval after a sudden increase of AE, this phenomenon could not be interpreted as noise interference.

The rate of increase in cumulative AE activities was found to be closely related with the fatigue life of cord-rubber composite specimen. As shown in Fatigue 4.37, the rates of AE signal accumulation were linearly proportional to the applied maximum stress of C3 composite. As discussed earlier, the applied maximum stress level is logarithmically proportional to the fatigue life of cord-rubber composite. Therefore, it is clear that the rate of AE signal accumulation is logarithmically proportional to the fatigue life of our materials (Figure 5.7). Nevertheless, an improvement of the test or analysis method is certainly needed to reduce the data scatter for more accurate investigation.

Despite the problem of data scatter, the rate of increase in cumulative AE event, $E(\sigma_{\max})$, is expressed as follows;

$$E(\sigma_{\max}) = r\sigma_{\max} + q \tag{5.7}$$

where r and q are material constants. Two constants of above equation were found to be: r=0.3094; q=-1.9066 (Figure 4.37).

Substitution of Equation (5.1) into the above equation follows;

$$E(\sigma_{\max}) = r(-a\ln N + b) + q \tag{5.8}$$

Therefore the rate of increase in cumulative AE event is expressed as follows;

$$E(\sigma_{\max}) = m\ln N + p \tag{5.9}$$

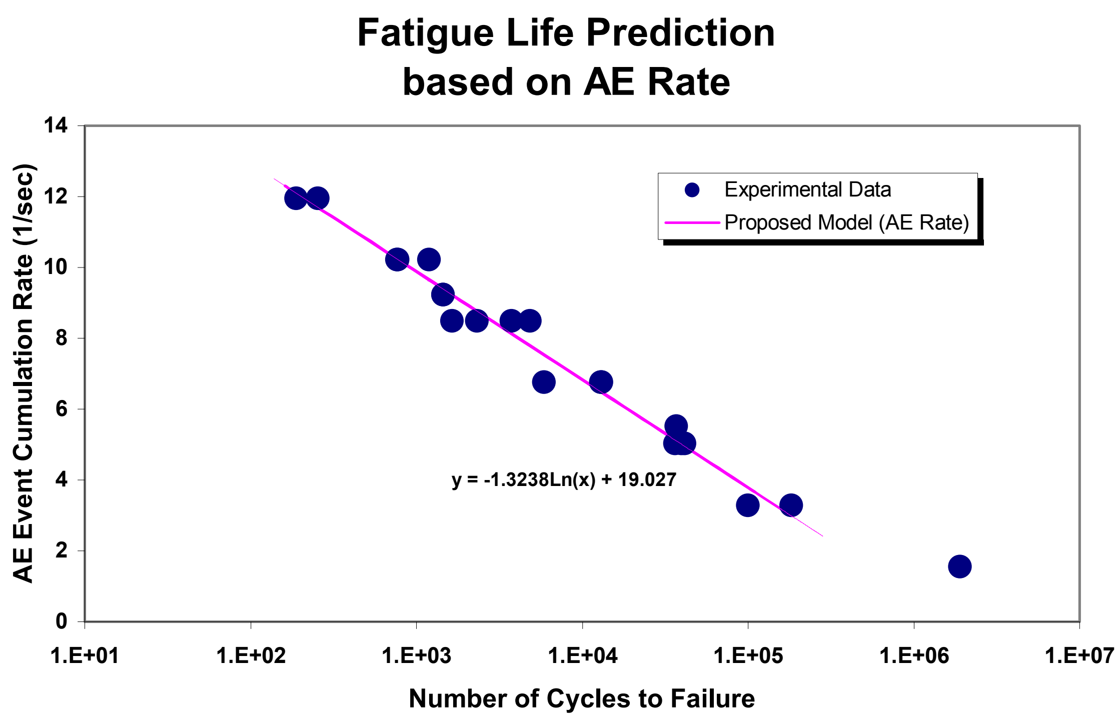

Figure 5.7 The mean value of the accumulation rate of AE event vs. the fatigue life for type C3

where

$m = -r^*a$

$p = r^*b + q$

Two material constants *m* and *p* were found to be -1.3238 and 19.027 respectively. As shown in Figure 5.7, the prediction using the above relation shows a remarkable agreement with experimental data. However, this relation can be used only when S-N curve and the rate of increase in cumulative AE event are known.

As discussed in Equation (5.7), our cord-rubber composite shows a linearly proportional relationship between applied maximum stress and the rate of increase in cumulative AE event. This linear relation could be explained through a simple assumption that the cumulative AE events increase linearly with the AE area, *S*, in cyclic loading condition which can produce AE activities. Figure 5.8 shows this area under sinusoidal loading condition. Under this scenario, cyclic loading condition could be derived as follows:

$$\sigma = \frac{\sigma_{\max}}{2}\left\{\sin(2\pi t - \frac{\pi}{2}) + 1\right\} \tag{5.10}$$

Then, the AE initiation stress, σ_0, which is the starting point to emit AE signal is expressed as follows:

$$\sigma_0 = \frac{\sigma_{\max}}{2}\left\{\sin(2\pi t_0 - \frac{\pi}{2}) + 1\right\} \tag{5.11}$$

where t_0 is the time at the AE initiation stress, σ_0.

Integration of Equation (5.10) from $t_1 = t_0$ to $t_2 = 0.5$ provides:

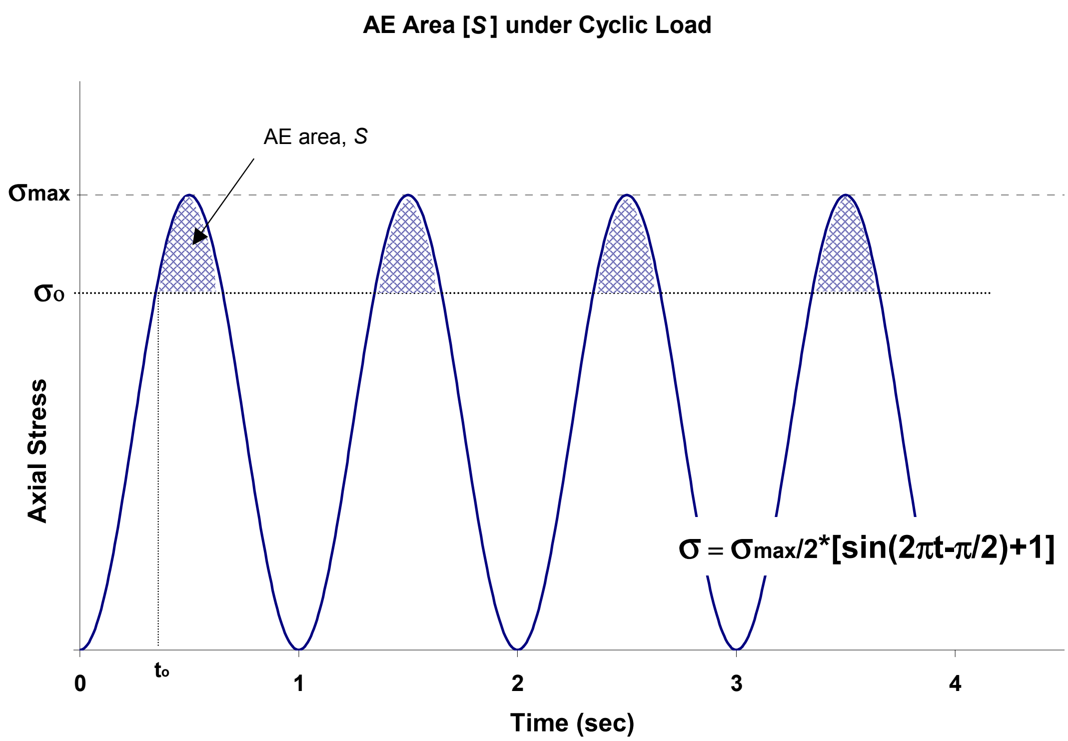

Figure 5.8 The area emitting AE under the applied maximum stress $\sigma_{\max}$ and 1Hz.

$$\int_{t_0}^{0.5} \frac{\sigma_{\max}}{2}\left\{\sin(2\pi t-\frac{\pi}{2})+1\right\}dt=\frac{\sigma_{\max}}{2}\left\{\frac{1}{2}+\frac{1}{2\pi}\cos(2\pi t_0-\frac{\pi}{2})-t_0\right\} \tag{5.12}$$

Using Equation (5.11) and the above equation, the area, *S*, is expressed as follows,

$$S=2\int_{t_0}^{0.5}\left[\frac{\sigma_{\max}}{2}\left\{\sin(2\pi t-\frac{\pi}{2})+1\right\}-\sigma_0\right]dt$$

$$=\sigma_{\max}\left\{\frac{1}{2}+\frac{1}{2\pi}\cos(2\pi t_0-\frac{\pi}{2})-t_0\right\}-(1-2t_0)\sigma_0$$

$$=\sigma_{\max}\left[\frac{1}{\pi}\sqrt{\frac{\sigma_0}{\sigma_{\max}}\left(1-\frac{\sigma_0}{\sigma_{\max}}\right)}\right]+(\sigma_{\max}-2\sigma_0)\left[\frac{1}{2}-\frac{1}{\pi}\sin^{-1}\left(\frac{2\sigma_0}{\sigma_{\max}}-1\right)\right] \tag{5.13}$$

As can be seen in Figure 5.9, the area for AE could be expressed to be linearly proportional to the applied maximum stress with an assumption that σ_0 is always constant during cyclic loadings. This assumption means the Felicity ratio, $\sigma_0/\sigma_{\max}$, is constant and independent of number of cycles under fixed applied maximum stress, $\sigma_{\max}$. This relationship can be approximated as follows:

$$S=u\sigma_{\max}+v \tag{5.14}$$

Two material constants *u* and *v* for type C3 were found to be 0.3893 and -7.4738 respectively. These constants for the different AE initiation stress, σ_0, can be determined by using Equation (5.13) and curve-fitting without any difficulty. Using the above equation and Equation (5.1), the fatigue lifetime of the material could be calculated as follows:

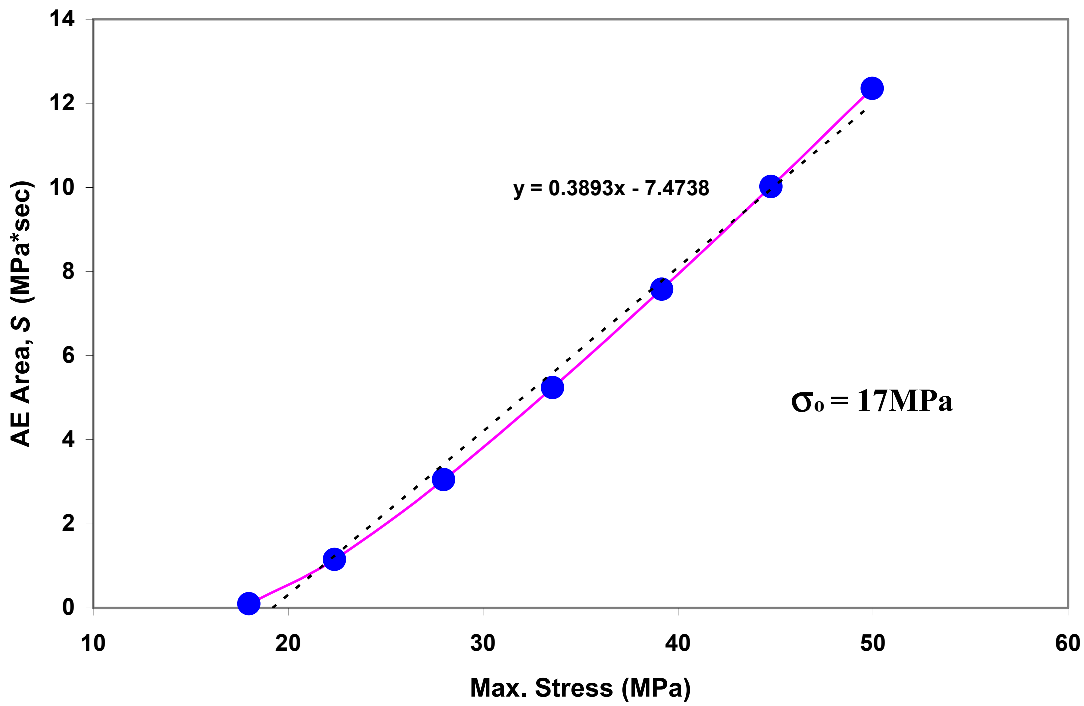

Figure 5.9 Applied maximum stress vs. the AE area for type C3 composite

$$N = \exp\left[\frac{\left\{b - \left(\frac{S - v}{u}\right)\right\}}{a}\right] \tag{5.15}$$

However, the above relation could not be used when σ_0 is higher than σ_{max}. Moreover, the Felicity ratio, σ_0/σ_{max}, is not constant for cord-rubber composite because the ratio is dependent of maximum applied stress as discussed previous chapter and damage occurs due to load cycling to the same load level. Therefore, cord-rubber composites required another relation such as the Felicity ratio under lower stress levels for a fatigue lifetime prediction.

One important finding from S-N curve was that high cycle fatigue (HCF) behavior under lower stress levels was different from low cycle fatigue (LCF) behavior, and the boundary point between lower and higher stress levels was similar to the AE event starting stress, σ_0. Therefore, fatigue life estimation for higher stress levels above σ_0 can be obtained from straight-line S-N curve (Equation 5.1) and that for lower stresses than σ_0 from power-law relation.

For deriving this power relation, two assumptions were used. Firstly, straight-line curve and power-law relation have a same value and a same slope at σ_0. The other assumption is that there is a fatigue limit, σ_{fl}, having longer fatigue lifetime than 10^7 cyclic cycles.

Using these assumptions, the power-law function could be expressed as follows:

$$\sigma = \sigma_f N^{-\alpha} + \sigma_{fl} \tag{5.16}$$

where σ_f and α are material constants. Differentiation of Equations (5.16) and (5.1) gives;

$$\frac{d\sigma}{dN} = -\alpha\sigma_f N^{-\alpha-1} \tag{5.17}$$

$$\frac{d\sigma}{dN} = -\frac{a}{N} \tag{5.18}$$

At the boundary point, where $\sigma = \sigma_0$, Equations (5.1) and (5.16) and Equations (5.17) and (5.18) have the same values, respectively. Using these boundary conditions, several expressions for material constants are given as follows;

$$\begin{aligned} \alpha &= \frac{a}{\sigma_0 - \sigma_{fl}} \\ \sigma_f &= \frac{a}{\alpha} N_0^{\alpha} \\ N &= \left(\frac{\sigma_f}{\sigma - \sigma_{fl}} \right)^{\frac{1}{\alpha}} \end{aligned} \tag{5.19}$$

As can be seen in the above equations, when the fatigue limit for cord-rubber composite is known, the fatigue lifetime for the material can be calculated very straightforwardly. Unfortunately, the fatigue limit for cord-rubber composite specimen is unknown and needs to be predicted experimentally or hypothetically.

In order to estimate the fatigue limit, it is reasonable to assume that the applied maximum stress at 10^7 cycles, σ_{10^7}, is a little higher than fatigue limit, σ_{fl}. At this point, where $\sigma = \sigma_{10^7}$ Equation (5.16) becomes,

$$\sigma_{10^7} = \sigma_f \left(10^7\right)^{-\alpha} + \sigma_{fl} \tag{5.20}$$

Then the above equation can be expressed as follows;

$$\Delta\sigma = \sigma_{10^7} - \sigma_{fl} = \sigma_f \left(10^7\right)^{-\alpha} \tag{5.21}$$

Further simplification can be made by assuming that the stress difference, $\Delta\sigma$, is very smaller than fatigue limit, σ_{fl}. In this study, fatigue life was calculated at five stress difference levels which were 0.1%, 1.0%, 5.0%, 10%, and 20% of the fatigue limit. The results are compared in Figure 5.10. The results show the better agreement in case of 10% of fatigue limit with experimental data than straight-line relation and the other predictions.

To verify the proposed theory using the boundary point between straight-line relation and power-law function, two attempts were made to compare the calculated fatigue life with experimental data. First one is compared in Figure 5.11 and specimens used were cord rubber composites made of natural rubber matrix with ±18° 2-ply laminate (South, 2002). The other is for type C3 at elevated temperature 100°C (Figure 5.12). The results show a good agreement with experimental data. In addition, fatigue limits for two cases can be estimated from these figures. As can be seen in Figure 5.13, the estimation of fatigue limit using this proposed model was just 14% lower than the experimental value, 414MPa. However, this prediction method of fatigue limit can be improved by obtaining an accurate boundary point.

Concluding the discussion, two empirical models proposed in this study for the prediction of the fatigue life of cord-rubber composite laminate compare well with the experimental data.

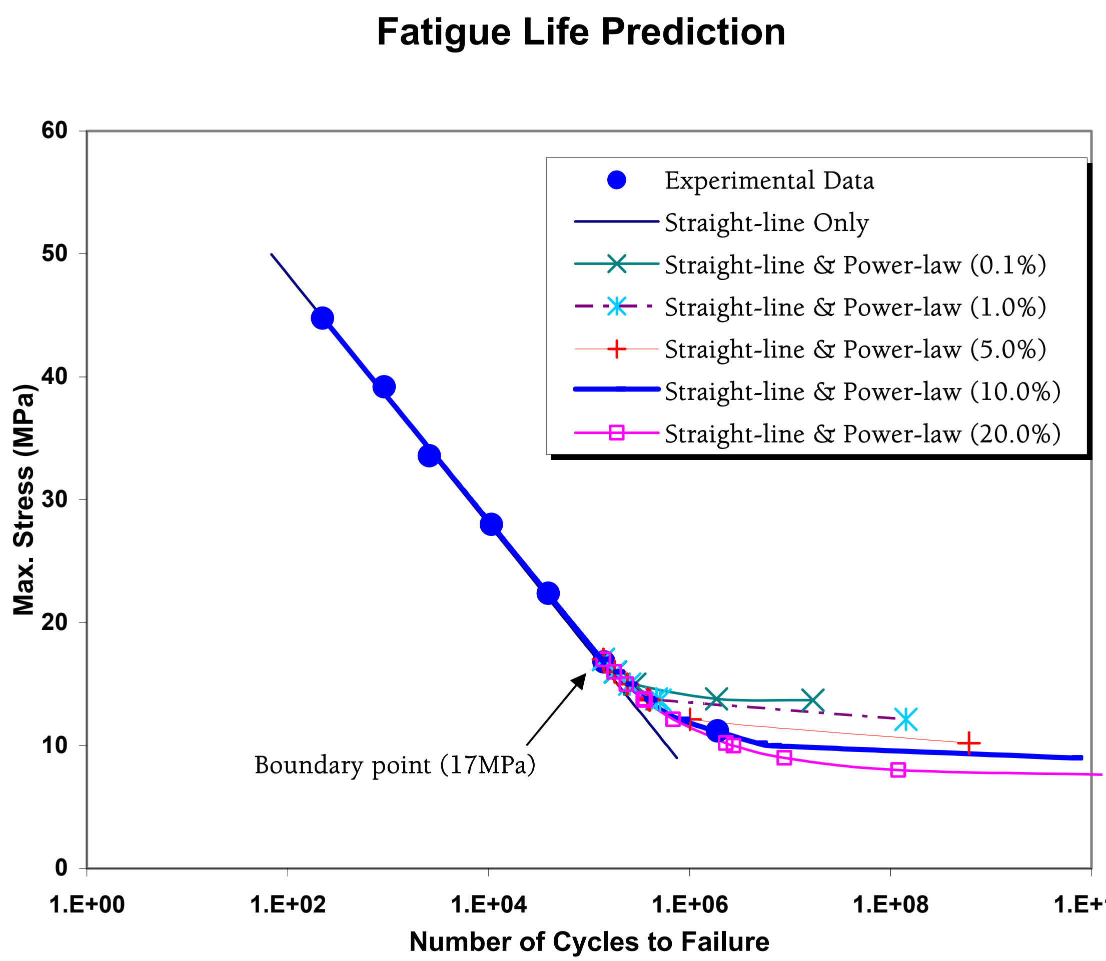

Figure 5.10 A comparison between the actual S-N curve and fatigue lifetime predicted by straight-line and power-law functions

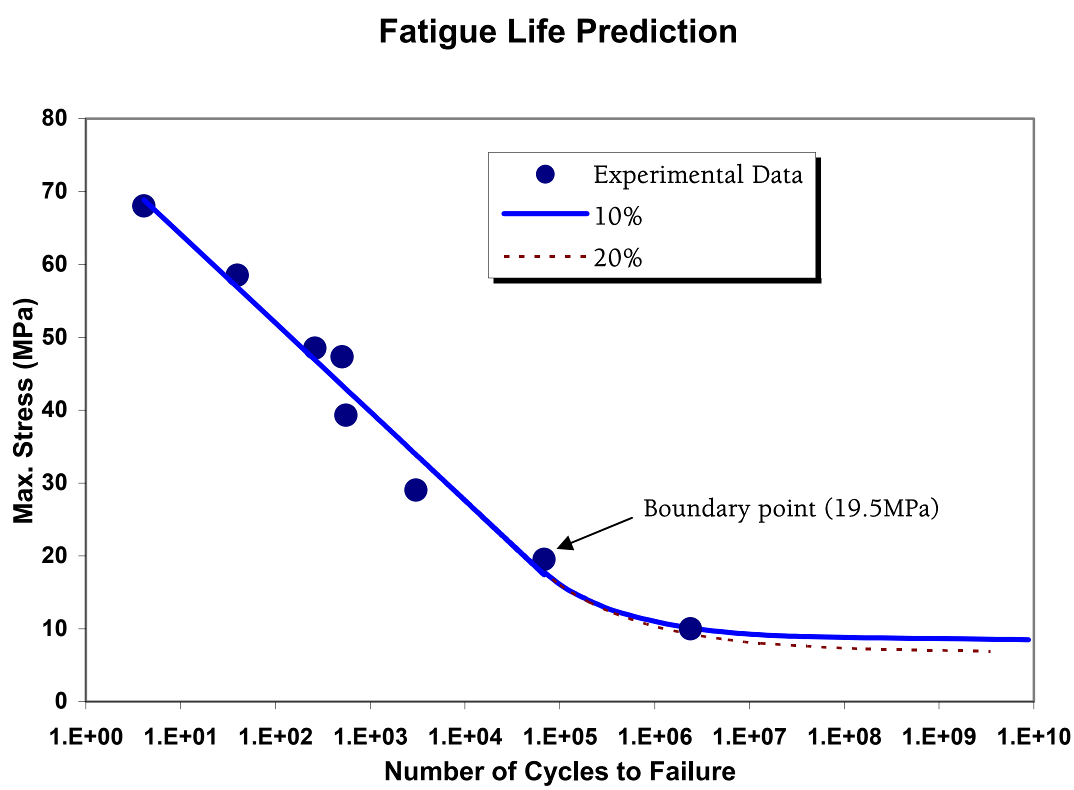

Figure 5.11 A comparison between fatigue lifetime predicted by straight-line and power-law function for natural rubber composites and the experimental data (South, 2001).

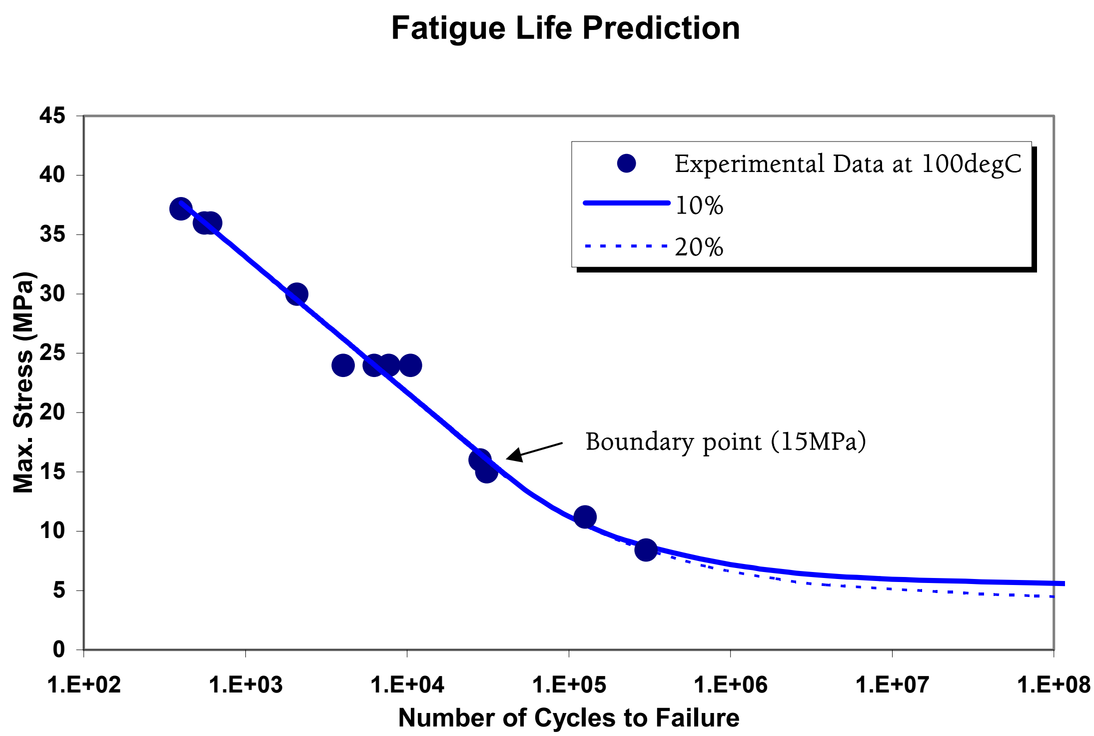

Figure 5.12 A comparison between the experimental data for type C3 under 100°C and fatigue lifetime predicted by straight-line and power-law function

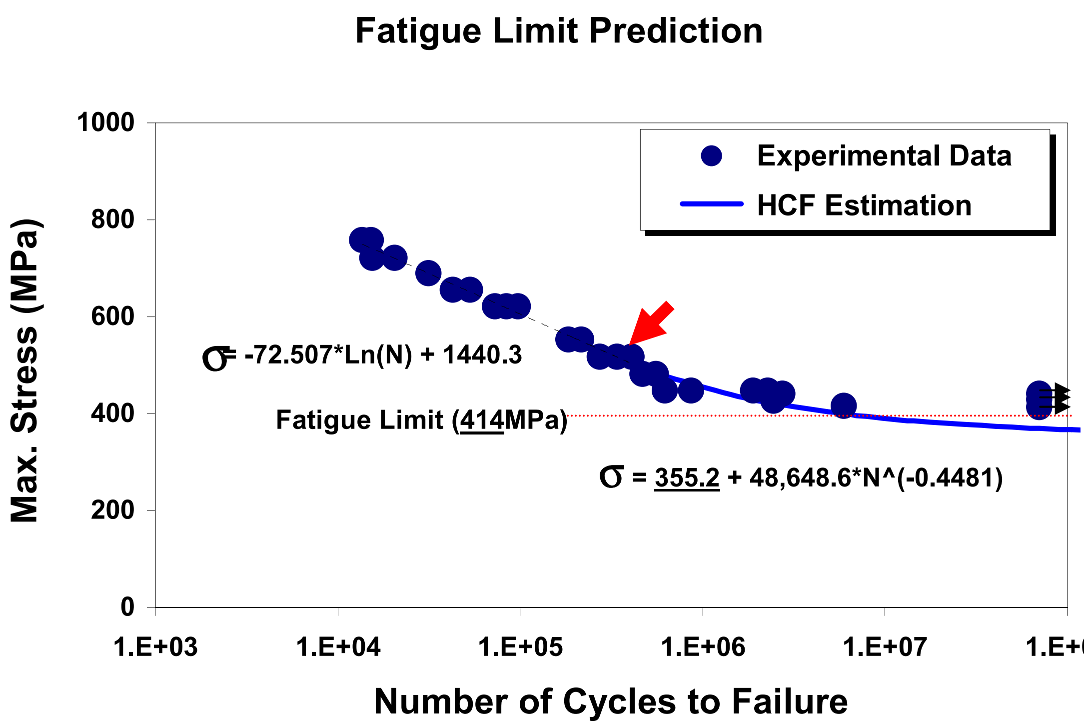

Figure 5.13 A comparison between fatigue limit predicted by HCF estimation model and the experimental data (Dowling, 1999)

Chapter 6

CONCLUSIONS

6.1 Conclusions

The focus of this research was to investigate the fatigue behavior of angle-plied cord-rubber composite laminates which represent the belt edge regions of passenger tires. The research into the mechanical properties was divided into two aspects quasi-static and dynamic. The quasi-static properties investigated were the ultimate stress, ultimate strain, interply shear strain, and acoustic emission behavior. The dynamic properties investigated were the fatigue life, acoustic emission behavior, and temperature profile.

In performing this research there have been tow significant contributions to the literature. The first is the use of a coupon laboratory specimen to investigate the fatigue behavior of an actual tire. The second is the prediction of S-N curves at high cycle fatigue of materials by using the boundary point obtained from acoustic emission test.

Based on proceeding discussions, the following conclusions could be drawn:

(1) Higher levels of interply shear strain of actual tires reduce the fatigue lifetime and interply shear strain is one of the crucial parameters for damage assessment. However, this interply shear strain measurement for actual tires has some limitations such as manufacturing actual tires needed and accuracy as well as repeatability of tests issued.

(2) The interply shear strain of 2-ply 'tire belt' composite laminate under circumferential tension is affected by twisting of specimen due to tension-bending coupling. At a given axial tensile strain, i.e., elongation of the specimen, the interply shear strain of 4-ply symmetric laminate is about 30% lower than that of 2-ply laminate which is subjected to twisting action.

(3) However, a critical level of interply shear strain, which governs the gross failure of composite laminate due to the delamination, appeared to be independent of different lay-up of 2-ply vs. 4-ply symmetric configurations. Although the axial strain at gross failure of 2-ply laminate is substantially lower than that of 4-ply laminate, the values of interply shear strain for both laminates tend to converge near the gross failure point.

(4) The composite laminate with larger angle-of-cord reinforcement exhibits a smaller magnitude of interply shear deformation at a given axial tensile strain. As a result of their similar axial strains at gross failure, the laminate with the cord angles of [+25/-25°]2s is associated with *smaller* values of interply shear strain at failure than the case of [+19/-19°]2s laminate.

(5) Above a critical level of interply shear strain of approximately 1.0 (100%), localized damage occurs in the form of cord-matrix debonding around the cut ends of the cords at the edges of the laminate specimen. Under both static and cyclic tension, further increase of strain results in the propagation of cracks into the matrix, eventually developing into the delamination.

(6) The initiation of the cord-matrix debonding process starts in the region just below a knee point of static stress-interply shear strain curve. The knee point typically

occurs at the tensile axial strain level which is roughly one-half of gross failure strain and coincided with the tensile stress level roughly equivalent to 45% of static strength.

(7) Reflecting the matrix-dominated failure modes of composites, tire belt laminates with different cord reinforcements (3+9+15X.22 vs. 3/6X.35) exhibit the same tensile S-N relationship as long as they are constructed with the same rubber matrix, the same cord angle, similar cord volume, and the same ply lay-up.

(8) Because of much *lower* values of *virgin strength* (in terms of load per unit width), the 2-ply composite laminates and [+25/-25°]2s laminate exhibit exponentially shorter fatigue lifetime, at a given stress range, than the case of 4-ply symmetric laminates and [+19/-19°]2s laminate, respectively. When plotted against the stress range divided by single-cycle strength, four normalized S-N curves (% single cycle strength vs. fatigue life) are merged into one trend. The increase of cord angle reduces the interply shear strain but lowers the strength of composite laminates.

(9) The increase of interply rubber thickness raises static strength of composite laminate and thereby lengthens their fatigue lifetime at an intermediate level of stress amplitude. However, the increase in the fatigue lifetime of the composite laminate becomes less noticeable at very low stress amplitude, suggesting that the increase of interply rubber thickness may not be able to lower the rate of edge crack propagation under cyclic loading.

(10) With the same cord angle maintained, maximum cyclic strain of composite laminates at failure, which measures the total strain accumulation (or cumulative

creep strain) for gross failure, is independent of stress amplitude and close to the level of static failure strain. As observed in the past, the damage initiation and eventual structural failure of tire belt laminates seems to be an exclusively "strain-controlled" process.

(11) Fatigue lifetimes of all tire belt laminate in the current study are linearly proportional to the *inverse* of the dynamic creep rate. Since the maximum cyclic strain for failure is nearly constant, the results indicate that the use of higher stress amplitude leads to the decrease of fatigue life by simply shortening the time to reach the critical level of strain for gross failure.

(12) For shorter fatigue lifetimes, which are at higher stress amplitudes, higher *temperatures* were not always observed. However, a linear correlation can be drawn between the dynamic creep rate and temperature rise rate for all composite laminates for tests with frequency of 1 Hz.

(13) Even with small compressive cyclic stresses, the fatigue life of belt composites is predominantly influenced by the magnitude of maximum stress. The initiation and propagation of belt edge cracks due to the interply shear deformation are believed to occur only under tensile axial stresses.

(14) The heat dissipation of belt composites, based on temperature measurements obtained by inserting a thermocouple between two center plies of the same cord angle, was found to occur in a cyclic fashion, essentially "in-phase" with the stress cycles. Cyclic changes of temperature could be monitored only when the stresses were relatively high. The temperature measurement was affected by the time lag due to heat transfer from the interlaminar region to the thermocouple. As a result,

low amplitude cyclic loading condition eventually led to the temperature rise over a larger period of time.

(15) Under static tension, AE energy is linearly proportional to applied load on log-linear scale and is initiated about 10% lower than the knee point from the stress-strain relation, suggesting AE as a potential technique to monitor the initiation of cord-matrix debonding process. Using the AE initiation stress value, better predictions of fatigue life is possible for the fiber-reinforced composites exhibiting distinct fatigue limits. The proposed prediction of high cycle fatigue (HCF) behavior using the boundary point concept shows a good agreement with the experimental data. In addition, this concept can be used for prediction of fatigue limit of materials.

(16) Despite data scatter, the accumulation rate of AE events during cyclic loading shows a linearly proportional trend to the maximum applied stress of composite laminates, and the Felicity ratio (FR) of cord-rubber composite is not constant, but dependent on stress level, which is ≥ 1 for low load levels and is ≤ 1 at higher load levels.

(17) Modified fatigue modulus model based on combination of power-law and logarithmic relation is formulated to predict the fatigue lifetime profile of cord-rubber composite laminates. A good agreement was found between the actual S-N curve and the predicted trend.

6.2 Recommendations

A great deal of work still remains to be done in these areas. The following recommendations can be made for the future work:

(1) Assess the contribution of viscoelastic properties of constituent materials to the dynamic creep of cord-rubber composites by performing static creep experiments at elevated temperatures.

(2) Develop test methodologies for the laboratory simulation of other type of fatigue processes of vehicle tires such as carcass ply ending failure in the bead and lower sidewall regions.

(3) Broaden data base to improve the concept of the boundary point, σ_0, which is turning point between linear relation and power-law function of S-N curve. Perform high cycle fatigue test to evaluate the fatigue limits of the cord-rubber composite laminates and compare with the estimations by our proposed linear and power-law model.

(4) Perform further AE testing during static and fatigue loading of the thermally aged composites and unaged specimens at elevated temperatures to refine the thermo-mechanical fatigue behavior of cord-rubber composites.

(5) Evaluate the Felicity ratio function dependent on the maximum applied stress and number of cycles for the better prediction of fatigue life of cord-rubber composites using the acoustic emission (AE) technique.

(6) Examine the effects of footprint load, inflation pressure and speed on the mileage to failure, deflection and temperature history of actual tires and asses their failure modes. Correlate these results with the fatigue data of cord-rubber composite laminates.

BIBLIOGRAPHY

"Company News; Ford is Ending Replacement of Firestone Tires," New York Times 29 March 2002: C4.

"Engineering Analysis Report and Initial Decision Regarding EA00-023: Firestone Wilderness AT Tires," National Highway Traffic Safety Administration, Department of Transportation, October (2001)

S. M. Arnold, B. A. Bednarcyk, T. E. Wilt, and D. Trowbridge, Micromechanics Analysis Code with Generalized Method of Cells (MAC/GMC) User Guide: Version 3.0, NASA TM-209070, NASA, Cleveland, OH (1999)

J. Awerbuch and H. T. Hahn, "Fatigue and Proof-Testing of Unidirectional Graphite/Epoxy Composite", in ASTM STP 636 "Fatigue of Filamentary Composite Materials," American Soc. for Testing and Materials, Philadelphia, PA, p. 248 (1977)

S. N. Bobo, "Fatigue Life of Aircraft Tires", Tire Science and Technology, Vol. 16, No. 4, p. 208 (1988)

R. F. Breidenbach and G. J. Lake, "Mechanics of Fracture in Two-Ply Laminates", Rubber Chemistry and Technology, Vol. 52, p. 96 (1979)

R. F. Breidenbach and G. J. Lake, "Application of Fracture Mechanics to Rubber Articles Including Tyres", Philosophical Trans. Royal Soc. London, Vol. A299, p.189 (1981)

L. J. Broutman and S. Sahu, " A New Theory to Predict Cumulative Fatigue Damage in Fiberglass Reinforced Plastics," Composite Materials: Testing and Design, ASTM STP 497, p.170, ASTM (1972)

K. Buckley, D. West, G. Venkatesan, and M. Kaveh, "*Detection and characterization of cracks for failure monitoring and diagnostics*", ICASSP 96, Vol. 5, p. 2738-2741, Atlanta, GA, May 7-10, (1996)

A. R. Bunsell, "Acoustic Emission for Proof Testing of Carbon Fiber-Reinforced Plastics," NDT International, NDITD, 10(1), p. 21-25 (1977)

L. Carsson and B. Norrbom, "Acoustic Emission from Graphite/Epoxy Composite Laminates with Special Reference to Delamination", Journal of Material Science, Vol. 18, p. 2503 (1983)

R. J. Cembrola and T. J. Dudek, "Cord/Rubber Material Properties", Rubber Chemistry and Technology, Vol. 58, p. 830 (1985)

F. H. Chang, D. E. Gordon, B. T. Rodini and R. H. McDaniel, "Real-Time Characterization of Damage Growth in Graphite/Epoxy Laminates", Journal of Composite Materials, Vol. 10, p.182 (1976)

P. C. Chou and R. Croman, "Residual Strength in Fatigue Based on the Strength- Life Equal Rank Assumption", Journal of Composite Materials, Vol. 12, p.177 (1978)

S. K. Clark, "Loss of Adhesion of Cord-Rubber Composites in Aircraft Tires", Tire Science and Technology, Vol.14, No. 1, p.33 (1986)

J. Deeskinazi and R. J. Cembrola, "A Parametric Study on Interlaminar Shear Strains in Cord-Rubber Composites", Rubber Chemistry and Technology, Vol. 57, p. 168 (1984)

Norman E. Dowling, *Mechanical Behavior of Materials*, 2nd ed., Prentice Hall, Upper Saddle River, NJ, p. 364 (1999)

V. Emamian, M. Kaveh, A. H. Tewfik, "Acoustic emission classification for failure prediction due to mechanical fatigue," Proceeding of SPIE conference on Sensory Phenomena and Measurement Instrumentation for Smart Structure and Materials", Vol. 3986, p. 78-84, New Port Beach, March 6-8, 2000.

J. L. Ford, H. P. Patel, and J. L. Turner, "Interlaminar shear effects in cord-rubber composites," Fiber Science and Technology, Vol. 17, p.255 (1982)

T. J. Fowler, “Acoustic Emission Testing of Fiber Reinforced Plastics,” Preprint 3092, American Society of Civil Engineers, New York (1977)

T. J. Fowler, “Acoustic Emission Testing of Fiber Reinforced Plastics,” Proceedings Paper 15021, J. Technical Council, ASCE, 105(TC2), p. 281-289 (1979)

T. J. Fowler, “Acoustic Emission Testing of Chemical Process Industry Vessels,” Progress in Acoustic Emission II, Japanese Society for Nondestructive Inspection, Tokyo, p. 421-449 (1984)

T. J. Fowler and E. Gray, “Development of an Acoustic Emission Test for Equipment,” Preprint 3583, American Society of Civil Engineers, New York (1979)

J. M. Funt, "Dynamic Testing and Reinforcement of Rubber", Rubber Chemistry and Technology, Vol. 61, p842 (1987)

A. N. Gent, "Strength of elastomers," in Science of Technology of Rubber edited by F. R. Eirich, Chapter 10, Academic Press, New York, NY (1978)

A. N. Gent, "Detachment of an elastic matrix from a rigid spherical inclusion," Journal of Materials Science, Vol. 15, p.2884 (1980)

A. N. Gent, "Failure of cord-rubber composites by pull-out or transverse fracture," Journal of Materials Science, Vol. 16, p.949 (1981)

A. N. Gent and S. M. Lai, "Interfacial bonding, energy dissipation and strength," Proc. of the 145th Spring Technical Meeting of Rubber Division, Amer. Chemical Society, Chicago, IL, Paper D (1994)

A. N. Gent, P. B. Lindley, and A. G. Thomas, "Cut growth and fatigue of rubbers - I. The relationship between cut growth and fatigue," Journal of Applied Polymer Science, Vol. 8, p.455 (1964)

S. Ghaffari and J. Awerbuch, "On the Correlation between Acoustic Emission and Progression of Matrix Splitting in a Unidirectional Graphite/Epoxy Composite", Acoustic Emission: Current Practice and Future Direction, ASTM STP 1077. American Society for Testing and Materials, Philadelphia, PA (1991)

I. Ghorbel, D. Valentin, M. C. Yrieix and J. Grattier, "The Influence of Matrix Rheological Properties on Acoustic Emission and Damage Accumulation in GRP Tubes", Composite Science and Technology, Vol. 41, p.221 (1991)

V. E. Gough, "Structure of the Pneumatic Tire" in Mechanics of Pneumatic Tires edited by S. K. Clark, U.S. Department of Transportation, Washington D.C. (1982)

A. J. Gray and J. Summerscales, "Acoustic Emission from Cord-Reinforced Rubber", Proc. of 3rd European Conf. on Nondestructive Testing, Firenze, Italy (1984)

H. T. Hahn and R. Y. Kim, "Proof Testing of Composite Materials", Journal of Composite Materials, Vol. 9, p.297 (1975)

M. A. Hamstad, "A Review: Acoustic Emission, A Tool for Composite-Materials Studies," Exper. Mech., Vol. 26, p.7–13 (1986)

M. A. Hamstad, "A Discussion of the Basic Understanding of the Felicity Effect in Fiber Composites," Journal of Acoustic Emission, Vol. 5, No. 2, p. 95-102 (1986)

B. Harris, F. J. Guild and C. R. Brown, "Accumulation of Damage in GRP Laminates", Journal of Physics D: Applied Physics, Vol. 12, p.1385 (1979)

A. L. Highsmith and K. L. Reifsnider, "Stiffness-Reduction Mechanisms in Composite Laminates", ASTM STP #775 "Damage in Composite Materials", American Soc. for Testing and Materials, Philadelphia, PA, p.103 (1982)

Y. S. Huang and O. H. Yeoh, "Crack Initiation and Propagation in Model Cord-Rubber Composites", Rubber Chemistry and Technology, Vol. 62, No.4, p.709 (1989)

D. Hull and L. Golaski, " Acoustic Emission Produced during Failure of Glass Polyester Filament Wound Pipe, Raport Serii Preprinty Nr. 8, Politechnika Wroclawska, Instytut Materialozonawstwai I Mechaniki Technicznej, Wroclaw, Poland (1980)

W. Hwang and K. S. Han, "Cumulative Damage Models and Multi-Stress Fatigue Life Prediction", Journal of Composite Materials, Vol. 20, p.125 (1986)

W. Hwang and K. S. Han, "Fatigue of Composites-Fatigue Modulus Concept and Life Prediction", Journal of Composite Materials, Vol. 20, p.154 (1986)

H. Kaczmarek, "Ultrasonic Detection of Damage in CFRPs", Journal of Composite Materials, Vol. 29, No.l, p.59 (1995)

J. Kawamoto, "Fatigue of Rubber Composites", Ph.D. Thesis (Advisor: J. F. Mandell), M. I. T, Cambridge, MA (1988)

A. J. Kinloch and R. J. Young, Fracture Behavior of Polymers. Applied Science Publishers Co., Ripple Road, Barking, Essex, England (1983)

T. Kohonen, "The self-organizing map", Proceedings of IEEE, Vol.78, No. 9, p.1464-1480, September, (1990)

M. Kumar and C. W. Bert, "Experimental Characterization of Mechanical Behavior of Cord-Rubber Composites", Tire Science and Technology, Vol. 10, p.37 (1982)

G. J. Lake, "Application of an energetics approach to fatigue and fracture in elastomers," Proc. of the 145th Spring Technical Meeting of Rubber Division, Amer. Chemical Society, Chicago, IL, Paper A (1994)

G. J. Lake and P. B. Lindley, "The mechanical fatigue limit for rubber," Journal of Applied. Polymer Sci., Vol. 9, p.1233 (1965)

G. J. Lake and A. G. Thomas, "The strength of highly elastic materials," Proc. Royal Soc. London, Vol. A300, p. 108 (1967)

R. F. Lee and J. A. Donovan, "J-lntegral and crack opening displacement as crack initiation criteria in natural rubber in pure shear and tensile specimens," Rubber Chemistry and Technology, Vol. 60, p.674 (1987)

B. L. Lee and P. K. Hippo, "Monitoring of Damage Accumulation for the Prediction of Fatigue Lifetime of Cord-Rubber Composites", Report on 1991 Summer Faculty Research Program, U.S. Department of Air Force, Air Force Office of Scientific Research (1991)

B. L. Lee, B. H. Ku, D. S. Liu, and P. K. Hippo, „Fatigue of Cord-Rubber Composites: II. Strain-Based Failure Criteria," Rubber Chemistry and Technology Vol. 71, p. 866 (1998)

B. L. Lee, D. S. Liu, M. Chawla and P. C. Ulrich, "Fatigue of Cord-rubber Composites", Rubber Chemistry and Technology Vol. 67, No.5, p. 761 (1994)

B. L. Lee, J. P. Medzorian, P. M. Fourspring, G. J. Migut, M. H. Champion, P. M. Wagner and P. C. Ulrich, "Study of fracture behavior of cord-rubber composites for Lab Prediction of Structural Durability of Aircraft Tires", Society of Automotive Engineers Technical Paper Series #901907, p. 1, SAE, Warrendale, PA (1990)

B. L. Lee, J. P. Medzorian, P. K. Hippo, D. S. Liu and P. C. Ulrich, "Fatigue Lifetime Prediction of Angle-Plied Fiber-Reinforced Elastomer Composites as Pneumatic Tire Materials," in ASTM STP #1211, Advances in Fatigue Lifetime Predictive Techniques (2nd Conf.), p. 203, ASTM, Philadelphia, PA (1993)

B. L. Lee, J. A. Smith, J. P. Medzorian, M. Chawla and P. C. Ulrich, "Fracture Behavior of Fiber-Reinforced Elastomer Composites under Fatigue Loading," Proc. of the 9th Int'l Conf. on Composite Materials, Vol. 2, p. 821, Madrid, Spain (1993)

J. Lenain, "General Principles of Acoustic Emission", Dunegan-Endevco Technical Report DE 78-5 (1979)

P. B. Lindley, "Non-Relaxing Crack Growth and Fatigue in a Non-Crystallizing Rubber", Rubber Chemistry and Technology, Vol. 47, p.1253 (1974)

D. S. Liu and B. L. Lee, "Cumulative Fatigue Damage of Angle-Plied Fiber-Reinforced Elastomer Composites and Its Dependence on Minimum Stress", The 3rd Symposium of ASTM Committee E-8 on Advances in Fatigue Lifetime Predictive Technique, May 15-17, 1994, Montreal, Canada.

D. S. Liu and B. L. Lee, "Fatigue and Residual Strength Degradation of Nylon Cord-Reinforced Rubber Composites", The 146th Technical Meeting of the Rubber Division of American Chemical Society, October 11-14, 1994, Pittsburgh, PA.

LOCAN-AT User's Manual", Physical Acoustics Corp. (1988)

A. Y. C. Lou and J. D. Walter, "Interlaminar shear strain measurements in cord-rubber composites", Rubber Chemistry and Technology, Vol. 52, p.792 (1979)

J. F. Mandell, "Monitoring of Marine Rope Fatigue Behavior", Textile Research Journal, Vol. 57, p. 318 (1987)

M. A. Miner, "Cumulative Damage in Fatigue", Journal of Applied Mechanics, p. A-159-64 (1945)

L. Mullins, Rubber Chemistry and Technology, Vol.21, p. 281 (1948)

Data from Goodyear Tech Book for the Chemical Process Industry, The Goodyear Tire & Rubber Co., Chemical Div., Akron, Ohio 44316

R. Page, R. Weertman and M. Roth, "Investigation of Fatigue-Induced Grain Boundary Cavitation by Small Angle Neutron Scattering", Scripta Metallurgica, Vol.14, p. 773 (1980)

H. P. Patel, J. L. Turner and J. D. Walter, "Radial tire cord-rubber composites", Rubber Chemistry and Technology, Vol. 49, p. 1095 (1976)

R. M. V. Pidaparti, H. T. Y. Yang and W. Soedel, "Modeling and Fracture Prediction of Single Ply Cord-Rubber Composites", Journal of Composite Materials, Vol. 26, No.2, p. 152 (1992)

R. B. Pipes and N. J. Pagano, "Interlaminar stresses in composite laminates under uniform axial extension", Journal of Composite Materials, Vol. 4, p.538 (1970)

A. A. Pollock, "Practical Guide to Acoustic Emission Testing", Physical Acoustics Corporation Publication, Princeton, NJ (1988)

P. Popper, C. Miller, D.L. Filkin and W. J. Schaffers, "A Simple Model for Cornering and Belt Edge Separation in Radial Tires", Tire Science and Technology, Vol. 14, No. 1, p. 3 (1986)

M. J. Qwen and R. J. Howe, "The Accumulation of Damage in Glass-Reinforced Plastic under Tensile and Fatigue Loading", Journal of Physics D: Applied Physics, Vol.5, p. 1637 (1972)

A. Rotem, "Effect of Strain Rate on Acoustic Emission from Fibre Composites", Composites, Vol. 9, No. 1, p. 33 (1978)

H. Rothert, B. Nguyen, and R. Gall, "Comparative study on the incorporation of composite material for tyre computation," Composite Structures (Proc. of 2nd Int'l Conf. on Composite Structures), p. 549, Applied Sci. Publ., London (1983)

C. Scala, J. McCardle and S. Bowles, "Acoustic emission monitoring of a fatigue test of an F/A-18 bulkhead", Journal of Acoustic Emission, Vol.10, p. 49-60, (1992)

J. Schijve, "Prediction methods for fatigue crack growth in aircraft material," ASTM STP #700, Fracture Mechanics, p. 3, ASTM, Philadelphia, PA (1979)

J. T. South, "Mechanical Properties and Durability of Natural Rubber Compounds and Composites," Ph.D Dissertation, Virginia Polytechnic Institute and State University, Blacksburg, VA (2001)

J. C. Spanner, Acoustic Emission Techniques and Application, Index Publ. Co., Evanston, IL (1974)

R. G. Stacer, L. C. Yanyo, and F. N. Kelley, "Observations on the tearing of elastomers," Rubber Chemistry and Technology, Vol. 58, p. 421 (1985)

R. G. Stacer, E. D. Von Meerwall and F. N. Kelly, "Time-dependent tearing of carbon black-filled and strain-crystallizing vulcanizates", Rubber Chemistry and Technology, Vol. 58, p. 913 (1985)

D. O. Stalnaker, R. H. Kennedy, and J. L. Ford, "Interlaminar shear strain in a two-ply balanced cord-rubber composites," Experimental Mechanics, Vol. 20, p. 87 (1980)

A. Stevenson, "Fatigue and fracture of rubber in engineering applications," Proc. of the 145th Spring Technical Meeting of Rubber Division, Amer. Chemical Society, Chicago, IL, Paper B (1994)

F. Tabaddor, "Mechanical Properties of Cord-Rubber Composites", Composite Structure, Vol. 3, p. 33 (1985)

T. Tanimoto and S. Amijima, "Progressive Nature of Fatigue Damage of Glass Fiber Reinforced Plastics", Journal of Composite Materials, Vol.9, p. 380 (1975)

H. Tao and F. Gao, “The Behavior of Acoustic Emission from GRP upon Reloading,” Progress in Acoustic Emission, Japanese Society for Nondestructive Inspection, Tokyo, Japan, p. 50-59 (1982)

A. G. Thomas, "Factors Influencing the Strength of Rubbers", Journal of Polymer Science, Symposium, No. 48, p. 145 (1974)

A. G. Thomas and J. M. Whittle, "Tensile Rupture of Rubber", Rubber Chemistry and Technology, Vol. 44, p. 222 (1970)

J. L. Turner and J. L Ford, "Interply Behavior exhibited in Compliant Filamentary Composite Laminates", Rubber Chemistry and Technology Vol. 55, p. 1078 (1982)

G. T. Venkatesan, D. West, K. M. Buckley, A. Tewfik and M. Kaveh, "Automatic fault monitoring using acoustic emissions", ICASSP 97, Vol. 3, p. 1893-1896, Munich, Germany, April 21-24, 1997.

J. J. Vorachek, "Role of Tire Reinforcements on Composite Static and Dynamic Characteristics", ASTM STP #694, p. 180 (1979)

J. D. Walter, "Cord-Rubber Tire Composites: Theory and Applications", Rubber Chemistry and Technology, Vol. 51, p. 524 (1978)

J. D. Walter, "Cord-reinforced rubber" in Mechanics of Pneumatic Tires edited by S. K. Clark, U.S. Department of Transportation, Washington D.C. (1982)

M. Wevers, I. Verpoest, P. De Meester and E. Aernoudt, "Identification of Fatigue Failure Modes in Carbon Fibre Reinforced Composites with the Energy Discriminating Acoustic Emission Method", Acoustic Emission: Current Practice and Future Direction, ASTM STP 1077. American Society for Testing and Materials, Philadelphia, PA (1991)

H. A. Whitworth, "Modeling Stiffness Reduction of Graphite/Epoxy Composite Laminates", Journal of Composite Materials, Vol. 21, p. 362 (1987)

H. A. Whitworth, "Stiffness/Strength Based Fatigue Characterization of Composite Materials", ASME Pressure Vessels Piping Div, Publ. PVP Vol.174, "Composite and Other New Materials for PVP: Design and Analysis Considerations", p. 147 (1989)

J. N. Yang, "Fatigue and Residual Strength Degradation for Graphite/Epoxy Composites under Tension-Compression Cyclic Loadings", Journal of Composite Materials, Vol. 12, p. 19 (1978)

J. N. Yang and M. D. Liu, "Residual Strength Degradation Model and Theory of Periodic Proof Tests", Journal of Composite Materials, Vol. 11, p. 176 (1977)

0. H. Yeoh, "Model studies of failure phenomena in tires," Proc. of the 145th Spring Technical Meeting of Rubber Division, Amer. Chemical Society, Chicago, IL, Paper C (1994)

VITA

Jaehoon Song

Jaehoon Song was born on February 29, 1964 to Han-Soon Cho and Cheol-Hun Song in Daejon, Korea. After graduating from Nam-Daejon High School, he enrolled at Seoul National University in March, 1983. He completed his B.S. degree in Mechanical Design and Production Engineering in February of 1987. After that, he entered Daewoo Electronics Ltd. Co. and worked at Hermetic Compressor Research Lab. and Quality & Reliability Lab. as a research engineer from January 1987 to July 1998. While he was working at Daewoo Electronics, the company supported his graduate studies at Korea Advanced Institute of Science and Technology (KAIST) and he completed his M.S. degree in Automation and Design Engineering in February of 1996. In the fall of 1998, Jaehoon enrolled in the graduate program at the Pennsylvania State University.